JPL D-11400, Rev. E

Earth Observing System

MISR

Multi-angle
Imaging
Spectro-
Radiometer

Level 2 Aerosol Retrieval Algorithm Theoretical Basis

David J. Diner[1]
Wedad A. Abdou[1]
Thomas P. Ackerman[2]
Kathleen Crean[1]
Howard R. Gordon[3]
Ralph A. Kahn[1]
John V. Martonchik[1]
Stuart McMuldroch[1]
Susan R. Paradise[1]
Bernard Pinty[4]
Michel M. Verstraete[4]
Menghua Wang[3]
Robert A. West[1]

[1]Jet Propulsion Laboratory, California Institute of Technology
[2]Pacific Northwest National Laboratory
[3]University of Miami
[4]Joint Research Centre

JPL

Jet Propulsion Laboratory
California Institute of Technology

April 10, 2001

JPL D-11400, Rev. E

Multi-angle Imaging SpectroRadiometer (MISR)

Level 2 Aerosol Retrieval Algorithm Theoretical Basis

Approval:

David J. Diner
MISR Principal Investigator

The MISR web site should be consulted to determine the latest released version
of this document (http://www-misr.jpl.nasa.gov).
Approval signatures are on file with the MISR Project.

JPL

Jet Propulsion Laboratory
California Institute of Technology

TABLE OF CONTENTS

iv

GLOSSARY OF ACRONYMS

A

ACP (Aerosol Climatology Product)
AGP (Ancillary Geographic Product)
APOP (Aerosol Physical and Optical Properties)
ARP (Ancillary Radiometric Product)
ARVI (Atmospherically-Resistant Vegetation Index)
ASAS (Advanced Solid-state Array Spectroradiometer)
ASL (Above Sea Level)
ASTER (Advanced Spaceborne Thermal Emission and Reflectance radiometer)
ATB (Algorithm Theoretical Basis)
AU (Astronomical Unit)
AVHRR (Advanced Very High Resolution Radiometer)

B

BRF (Bidirectional Reflectance Factor)

C

CCD (Charge-Coupled Device)

D

DAAC (Distributed Active Archive Center)
DAO (Data Assimilation Office)
DDV (Dense Dark Vegetation)

E

ECS (EOSDIS Core System)
EOF (Empirical Orthogonal Function)
EOS (Earth Observing System)
EOSDIS (Earth Observing System Data and Information System)

F

FOV (Field-of-View)

G

GDQI (Geometric Data Quality Indicator)
GEMI (Global Environmental Monitoring Index)

H

HC (High Confidence)

I

IAMAP (International Association for Meteorology and Atmospheric Physics)
IFOV (Instantaneous Field Of View)

J

JPL (Jet Propulsion Laboratory)

L

LC (Low Confidence)

M

MISR (Multi-angle Imaging SpectroRadiometer)
MODIS (Moderate Resolution Imaging Spectroradiometer)

N

NDVI (Normalized Difference Vegetation Index)
NOAA (National Oceanic and Atmospheric Administration)

P

ppmv (parts per million by volume)

R

RCCM (Radiometric Camera-by-camera Cloud Mask)
RDQI (Radiometric Data Quality Indicator)
RH (Relative Humidity)
RMS (Root-Mean-Square)
RT (Radiative Transfer)

S

SAGE (Stratospheric Aerosol and Gas Experiment)
SCF (Science Computing Facility)
SDCM (Stereoscopically Derived Cloud Mask)
SDP (Science Data Production)
SMART (Simulated MISR Ancillary Radiative Transfer)
SOM (Space Oblique Mercator)

T

TASC (Terrestrial Atmosphere and Surface Climatology)

W

WCP (World Climate Programme)
WGS (World Geodetic System)
WMO (World Meteorological Organization)

1. INTRODUCTION

1.1 PURPOSE

This Algorithm Theoretical Basis (ATB) document describes the algorithms used to retrieve the aerosol parameters of the MISR Level 2 Aerosol/Surface Product. These parameters are summarized in Table 1. In particular, this document identifies sources of input data, both MISR and non-MISR, which are required for aerosol retrieval; provides the physical theory and mathematical background underlying the use of this information in the retrievals; includes implementation details; and describes assumptions and limitations of the adopted approach. It is used by the MISR Science Data System Team to establish requirements and functionality of the data processing software.

Table 1: Aerosol parameters in the Level 2 Aerosol/Surface Product

Parameter name	Units	Horizontal Sampling (Coverage)	Comments
Aerosol optical depths	none	17.6 km (Global)	• For each candidate aerosol compositional model used in the retrieval • Reported at 558 nm
Compositional model identifiers	none	17.6 km (Global)	• For candidate models used in the retrieval • References Aerosol Climatology Product
Best estimates of aerosol optical depth	none	17.6 km (Global)	• Determined from retrieval and computing both mean and median of best-fitting model(s) • Reported at 558 nm
Retrieval quality indicators	varies	17.6 km (Global)	• Retrieval applicability, algorithm type, retrieval residuals, parameter uncertainties, summary statistics, and other quality assessment indicators
Ancillary meteorological and atmospheric data	varies	17.6 km (Global)	• Includes ozone optical depth, wind speed, and ambient pressure assumed in the retrieval, and source of data

The MISR Aerosol/Surface Product will be generated routinely during the EOS mission as new images are acquired. Certain information required to interpret the Aerosol/Surface Product, such as properties of the aerosol particles used to generate the compositional models used during the retrievals, the relative abundances of the components in the mixtures, and a geographical/seasonal climatological likelihood estimator for each mixture, is incorporated in the Aerosol Climatology Product (ACP). These products will be deliverable to the EOS user community through the Distributed Active Archive Center (DAAC), but are generated at the MISR Science Computing Facility (SCF), with the possibility of being updated during the mission. The contents and theoretical basis of the ACP parameters are provided in *[M-11]*.

1.2 SCOPE

This document covers the algorithm theoretical basis for the aerosol parameters of the Aerosol/Surface Product which are to be routinely retrieved at the DAAC. Specialized products or parameters are not discussed. Current development and prototyping efforts may result in modifications to parts of certain algorithms. Only the algorithms which will be implemented at the DAAC for routine processing will be preserved in the final release of this document.

Chapter 1 describes the purpose and scope of the document. Chapter 2 provides a brief overview. The processing concept and algorithm description are presented in Chapter 3. Chapter 4 summarizes assumptions and limitations. References for publications cited in the text are given in Chapter 5. Literature references are indicated by a number in italicized square brackets, e.g., *[1]*.

1.3 MISR DOCUMENTS

Reference to MISR Project or reference documents is indicated by a number in italicized square brackets as follows, e.g., *[M-1]*. The MISR web site (http://www-misr.jpl.nasa.gov) should be consulted to determine the latest released version of each of these documents.

[M-1] Experiment Overview, JPL D-13407.

[M-2] Level 1 Radiance Scaling and Conditioning Algorithm Theoretical Basis, JPL D-11507.

[M-3] Level 1 Georectification and Registration Algorithm Theoretical Basis, JPL D-11532.

[M-4] Level 1 Cloud Detection Algorithm Theoretical Basis, JPL D-13397.

[M-5] Level 1 In-flight Radiometric Calibration and Characterization Algorithm Theoretical Basis, JPL D-13398.

[M-6] Level 1 Ancillary Geographic Product Algorithm Theoretical Basis, JPL D-13400.

[M-7] Level 1 In-flight Geometric Calibration Algorithm Theoretical Basis, JPL D-13399.

[M-8] Level 2 Cloud Detection and Classification Algorithm Theoretical Basis, JPL D-11399.

[M-9] Level 2 Top-of-Atmosphere Albedo Algorithm Theoretical Basis, JPL D-13401.

[M-10] Level 2 Surface Retrieval Algorithm Theoretical Basis, JPL D-11401.

[M-11] Level 2 Ancillary Products and Datasets Algorithm Theoretical Basis, JPL D-13402.

[M-12] Science Data Validation Algorithm Theoretical Basis, JPL D-13403.

[M-13] In-flight Radiometric Calibration and Characterization Plan, JPL D-13315.

[M-14] In-flight Geometric Calibration Plan, JPL D-13228.

[M-15] Science Data Validation Plan, JPL D-12626.

[M-16] Science Data Processing Sizing Estimates, JPL D-12569.

[M-17] Science Data Quality Indicators, JPL D-13496.

1.4 REVISIONS

The original version of this document was dated February 23, 1994. Revision A was released December 1, 1994. Revision B was released August 15, 1996. Revision C was released December 3, 1997. Revision D was released December 2, 1999. This version is Revision E. Changes from Rev. D are indicated through the use of change bars, as shown at the left.

2. EXPERIMENT OVERVIEW

2.1 OBJECTIVES OF MISR AEROSOL RETRIEVALS

Aerosols are solid or liquid airborne particulates of various compositions, frequently found in stratified layers. Generally, they are defined as atmospheric particles with sizes between about 0.1 μm and 10 μm, though the sizes of condensation nuclei are typically about 0.01 μm. Under normal conditions, most of the atmospheric aerosol resides in the troposphere. Natural sources (e.g., dust storms, desert and soil erosion, biogenic emissions, forest and grassland fires, and sea spray) account for about 90% of this aerosol, with the rest resulting from anthropogenic activity *[51]*. The background tropospheric aerosol is temporally and spatially variable.

The overall objectives of the MISR aerosol retrievals are:

(1) To study, on a global basis, the magnitude and natural variability in space and time of sunlight absorption and scattering by aerosols in the Earth's atmosphere, particularly tropospheric aerosols, and to determine their effect on climate;

(2) To improve our knowledge of the sources, sinks, and global budgets of aerosols;

(3) To provide atmospheric correction inputs for surface imaging data acquired by MISR and other instruments (e.g., MODIS and ASTER) that are simultaneously viewing the same portion of the Earth, for the purpose of making better quantitative estimates of surface reflectance.

A scientific background on each of these objectives, a historical perspective on aerosol retrievals using remote sensing, the unique contributions of MISR, and a scientific rationale for the aerosol parameter contents of the MISR Aerosol/Surface Product are presented in *[M-1]*.

2.2 INSTRUMENT CHARACTERISTICS

The MISR instrument consists of nine pushbroom cameras. It is capable of global coverage every nine days, and flies in a 705-km descending polar orbit. The cameras are arranged with one camera pointing toward the nadir (designated An), one bank of four cameras pointing in the forward direction (designated Af, Bf, Cf, and Df in order of increasing off-nadir angle), and one bank of four cameras pointing in the aftward direction (using the same convention but designated Aa, Ba, Ca, and Da). Images are acquired with nominal view angles, relative to the surface reference ellipsoid, of 0°, 26.1°, 45.6°, 60.0°, and 70.5° for An, Af/Aa, Bf/Ba, Cf/Ca, and Df/Da, respectively. Each camera uses four Charge-Coupled Device (CCD) line arrays in a single focal plane. The line arrays consist of 1504 photoactive pixels plus 16 light-shielded pixels per array, each 21 μm by 18 μm. Each line array is filtered to provide one of four MISR spectral bands. The spectral band shapes are approximately gaussian and centered at 446, 558, 672, and 866 nm.

MISR contains 36 parallel signal chains corresponding to the four spectral bands in each of the nine cameras. The overlap swath width of the MISR imaging data (that is, the swath seen in common by all nine cameras) is 360 km, which provides global multi-angle coverage of the entire Earth in 9 days at the equator, and 2 days near the poles. The crosstrack IFOV and spacing between centers of each pixel (i.e., the sample spacing) is 275 m for all of the off-nadir cameras, and 250 m for the nadir camera. Downtrack IFOV's depend on view angle, ranging from 214 m in the nadir to 707 m at the most oblique angle. Sample spacing in the downtrack direction is 275 m in all cameras. The instrument is capable of buffering the data to provide 4 sample x 4 line, 2 sample x 2 line, or 1 sample x 4 line averages, in addition to the mode in which pixels are sent with no averaging. The averaging capability is individually selectable within each of the 36 channels, and there are several observational modes of the MISR instrument. The MISR Aerosol/Surface Product is generated from Global Mode data. Global Mode refers to continuous operation with no limitation on swath length. Global coverage in a particular spectral band of one camera is provided by operating the corresponding signal chain continuously in a selected resolution mode. Any choice of averaging modes among the nine cameras that is consistent with the instrument power and data rate allocation is suitable for Global Mode. Current plans are to operate the instrument in the 4 x 4 averaging mode (1.1-km sampling) with selected channels operated in 1 x 1 or 1 x 4 mode. Use of higher resolution data benefits the aerosol retrievals by providing better cloud discrimination than would be achievable with the lower resolution data alone, and by providing retrieval constraints over heterogeneous land.

Additional background on the instrument design is provided in *[M-1]*.

2.3   AEROSOL RETRIEVAL STRATEGY

In order to constrain the MISR aerosol retrievals, it is advantageous to make reasonable use of what is known about the types of aerosols that are found in the troposphere. In general, tropospheric aerosols fall into a small number of compositional categories, which include sea spray, sulfate/nitrate, mineral dust, biogenic particles (also referred to as carbonaceous particles), and urban soot (also referred to as black carbon particles). Approximate size ranges, and the proclivity of each particle type to adsorb water under increasing relative humidity are also known. Therefore, the MISR team has chosen an approach in which the physical and chemical (and therefore optical) properties of candidate aerosols are completely prescribed. The advantages of this approach, in contrast to a purely "generic" representation in terms of effective single scattering albedo, effective size distribution, and effective phase function, are that it potentially enables identification of aerosol sources and provides the means of extending aerosol properties retrieved at the MISR wavelengths to other spectral regions, which will be useful for comparisons with other sensors and for model validation. To this end, a review of published aerosol climatologies was performed (including *[2]*, *[26]*, *[45]*, *[53]* and many others). Aerosol attributes typical of natural conditions as described in these references (such as compositional and size classes) are adopted in the MISR retrievals. However, other attributes, such as aerosol amount and specific spatial and temporal dis-

5

tributions, are not assumed.

A summary of the MISR aerosol retrieval strategy is as follows: Based on the data contained in the ACP, forward radiative transfer calculations are performed to provide various components of the atmospheric radiation field in the 36 MISR channels. These are contained in the Simulated MISR Ancillary Radiative Transfer (SMART) Dataset and supplemented by calculations performed during the retrievals at the DAAC. During routine processing, these calculations will be binned into models that are observationally distinguishable by MISR. The pre-calculated results will be used in conjunction with the MISR observations to determine those models that provide good fits to the data, and to retrieve aerosol optical depth. Three retrieval pathways, one over water and two over land, are utilized. A summary of the various retrieval strategies is shown in Figure 1, and additional background is provided below. For each of the three retrieval paths, optical depth constraints, such as the maximum allowable optical depth, based on the darkest radiance observed in the scene, are calculated.

DARK WATER	DENSE DARK VEGETATION	HETEROGENEOUS LAND
Wind speed → SMART data; Derive optical depth constraints → SMART data, MISR data; SMART data → Minimize residuals ← MISR data; Minimize residuals → Aerosol model	Derive optical depth constraints → SMART data; Veg. index ← MISR data; SMART data → Calculate surface field → Minimize residuals ← MISR data; Minimize residuals → Aerosol model	Derive optical depth constraints → SMART data, MISR data, Average; SMART data/MISR data → Subtract → Angular shape; MISR data/Average → Subtract → Angular shape EOF's; Angular shape & Angular shape EOF's → Minimize residuals → Aerosol model
Uses MISR 672, 866 nm bands. Requires wind speed to establish glitter and whitecap reflectance.	Uses MISR 446, 672 nm bands. Requires use of standard DDV bidirectional reflectance model.	Uses selected MISR bands. Does not require surface bidirectional reflectance or albedo assumptions, but surface must have spatial contrasts.

Figure 1. MISR aerosol retrieval strategies

2.3.1 Aerosol retrievals over dark water

Because of the reflectance uniformity of the large water bodies (e.g., the ocean), and the fact that deep water bodies are essentially black at red and near-infrared wavelengths, considerable progress has been made in development of algorithms to retrieve aerosol properties over dark water. Under the assumption of an aerosol model (i.e., specification of particle size distribution, particle shape, and complex refractive index), it is possible using radiative transfer (RT) theory to derive a one-to-one relationship between observed radiance and aerosol optical depth. Such modeling has been applied to the retrieval of aerosol concentration from Landsat *[8]*, *[14]* and NOAA AVHRR *[15]*, *[27]*, *[42]*, *[46]*, *[47]*. Substantial improvements in the retrieval of aerosol over ocean and other dark water bodies are possible with MISR. Multi-angle radiances, which are governed strongly by the shape of the aerosol scattering phase functions, provide additional information with which to refine the aerosol model used in the retrieval of optical depth.

2.3.2 Aerosol retrievals over land

The retrieval of aerosol optical depth over land from space is considerably less well developed than the dark water case because of the higher brightness and heterogeneity of the land surface. The simplest means of determining the atmospheric contribution to the satellite signal is to make an assumption about the surface reflectivity or albedo. Locations where the surface boundary condition is believed to be reasonably well understood are areas covered by Dense Dark Vegetation (DDV). A method based on imaging over DDV has been investigated *[19]* and forms the basis of the MODIS aerosol retrieval over land *[25]*. The low reflectance of dense vegetation in the visible portion of the spectrum is used in conjunction with an aerosol model to retrieve optical depth. This approach is similar to the method used for retrievals over dark water. For DDV, the angular reflectance shape of the surface boundary condition is specified, and the absolute reflectance is allowed to vary as a free parameter (within certain limits). Therefore, MISR can provide enhancements to single-view-angle approaches to aerosol retrievals over DDV, as is planned for dark water.

Since dense vegetation is found only over a portion of the land surface, other methods are required to extend the aerosol retrieval spatial coverage. Separability of the surface-leaving and atmosphere-leaving signals over terrain with heterogeneous surface reflectance is the objective of several methods developed by the MISR team *[5]*, *[6]*, *[28]*, *[29]*, *[31]*. The heterogeneous land algorithm differs from the dark water and DDV retrieval methods in that it does not use the observed radiances directly, but instead uses the presence of spatial contrasts to derive an Empirical Orthogonal Function (EOF) representation of the angular variation of the scene reflectance, which is then used to estimate the scene path radiance (the radiance field reflected from the atmosphere without interacting with the surface). This is used in turn to determine the best-fitting aerosol models.

3. ALGORITHM DESCRIPTION

3.1 PROCESSING OUTLINE

3.1.1 Processing flow

Processing flow concepts are shown diagrammatically throughout the document. The convention for the various elements displayed in these diagrams is shown in Figure 2.
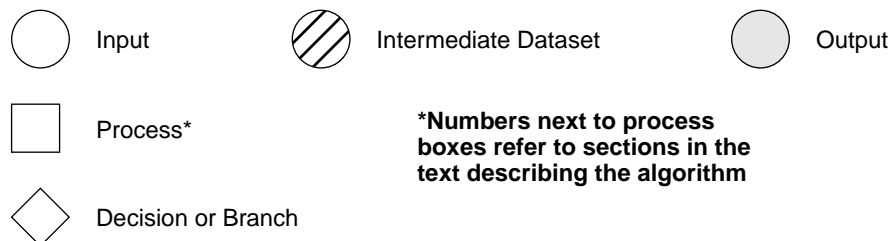
Figure 2. Conventions used in processing flow diagrams

The aerosol retrieval process is assisted by establishment of three ancillary datasets that are generated at the MISR SCF and then delivered to the DAAC. Further details are provided in *[M-11]*. These datasets are:

(1) The Terrestrial Atmosphere and Surface Climatology (TASC) Dataset, which provides baseline meteorological and ozone fields to be used as defaults if real-time or near-real-time inputs for these variables are unavailable.

(2) The Aerosol Climatology Product (ACP), which consists of three component parts: an aerosol physical and optical properties file containing microphysical and scattering characteristics of a set of aerosol types upon which the retrievals are based; an aerosol mixture file, which specifies the mixtures of pure aerosol types which comprise candidate models to be used during the retrievals and information about the mixtures required during the retrievals; and an aerosol "clim-likely" file which provides a geographical and seasonal measure of climatological likelihood of each mixture.

(3) The Simulated MISR Ancillary Radiative Transfer (SMART) Dataset, which contains components of the radiation fields used to generate the model top-of-atmosphere equivalent reflectances to which the MISR observations are compared during the retrievals and is generated by performing radiative transfer calculations on stratified atmospheric models containing the aerosols found in the ACP. The calculations contained in the SMART Dataset include two surface boundary condition cases: (1) oceans or large dark water bodies, and (2) spectrally black surface, which is used in the retrievals over land.

The remaining elements of the retrieval occur during routine processing at the DAAC. The MISR aerosol retrieval approach depends upon (1) whether the viewed region contains dark water or land; (2) whether the surface contains samples of dense, dark vegetation; and (3) on environ-

mental conditions, such as whether the land surface is heterogeneous or homogeneous in reflectance. The output of the aerosol retrieval process is then used to generate the surface parameters which are also part of the Aerosol/Surface Product. At the present time, aerosol retrievals are not implemented for non-heterogeneous land areas. A retrieval flag indicates which path was used for each set of measurements.

Figure 3 outlines the concept for the "Stage 1" DAAC processing in which the data within each 17.6-km region upon which the aerosol retrieval is potentially to be performed are screened using regional filters, averaged to the appropriate spatial resolutions required for the retrievals, normalized to an Earth-Sun distance of 1 AU, converted to equivalent reflectances, corrected for spectral out-of-band leakage, corrected for ozone absorption, and then screened using subregional filters. All subregions which are unusable according to any of these criteria are eliminated. Processing of a region proceeds only if a sufficient number of subregions and camera views survive these tests. Ancillary meteorological and atmospheric parameters required for the retrievals are also calculated in Stage 1.

Figure 4 is a schematic representation of the conceptual "Stage 2" retrieval processing path to be followed at the DAAC. In Stage 2, the processing path is determined and the aerosol retrieval algorithm to be used is identified according to the following hierarchy: (1) The minimum equivalent reflectances in the most oblique camera views that survived Stage 1 processing are identified for the purpose of putting an upper bound on aerosol optical depth; (2) The dark water algorithm is selected if the region is identified as open ocean or the interior of a large inland water body; (3) A search for DDV subregions is made and the appropriate algorithm is selected if any are found; (4) If no DDV subregions are found, the heterogeneous land algorithm pathway is selected and if sufficient contrast is present the necessary inputs are calculated; (5) Over land, if the above paths do not lead to a viable algorithm (e.g., if the scene consists of a homogenous, bright land target), various default approaches are attempted in order to establish a regional aerosol optical depth and the Algorithm Type Flag is set accordingly.

Figure 5 is a schematic representation of the conceptual "Stage 3" retrieval processing path to be followed at the DAAC. In Stage 3, the actual retrievals are performed, according to the algorithm type and pre-determined calculations provided by Stage 2.
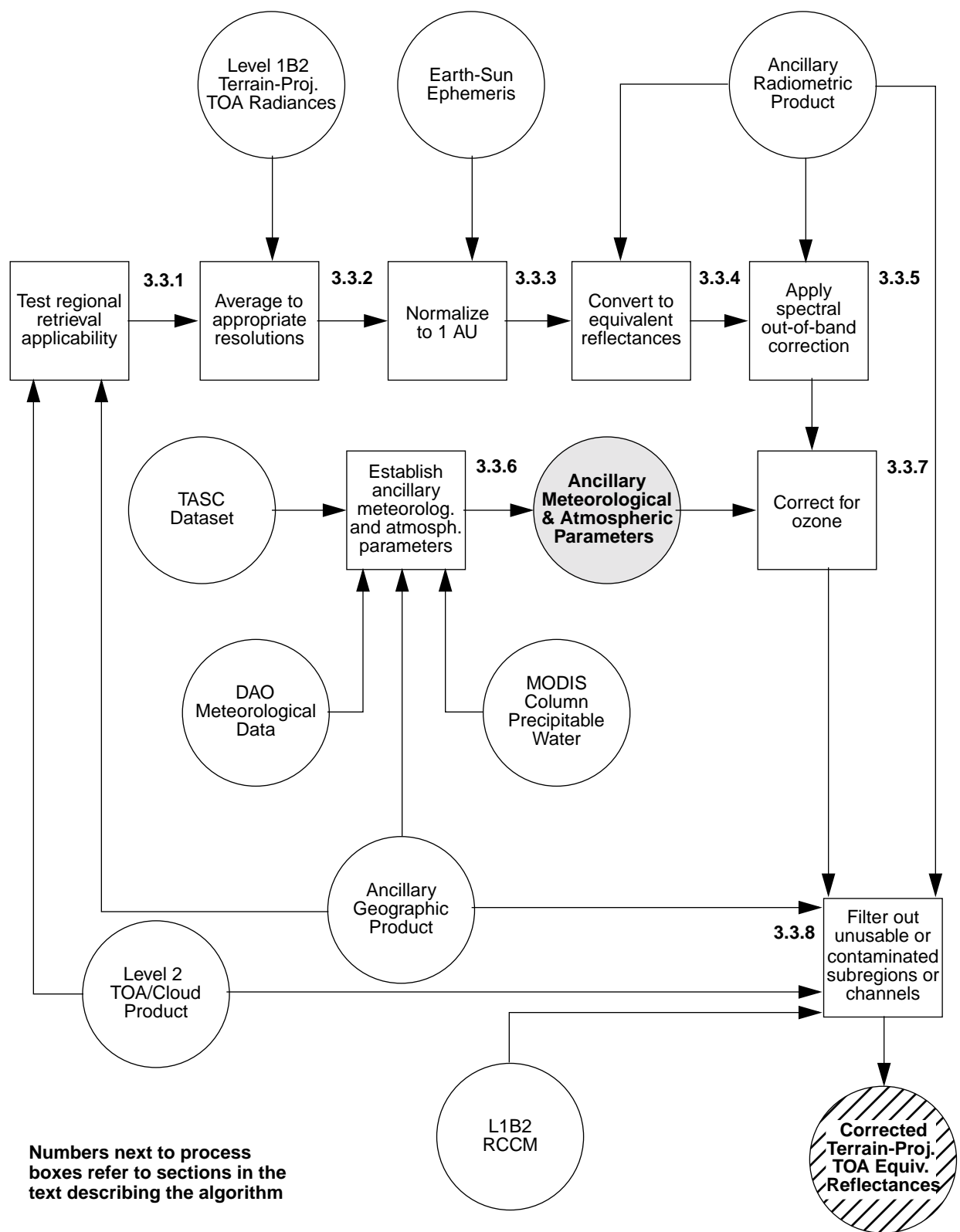
Figure 3. Stage 1 retrieval processing concept
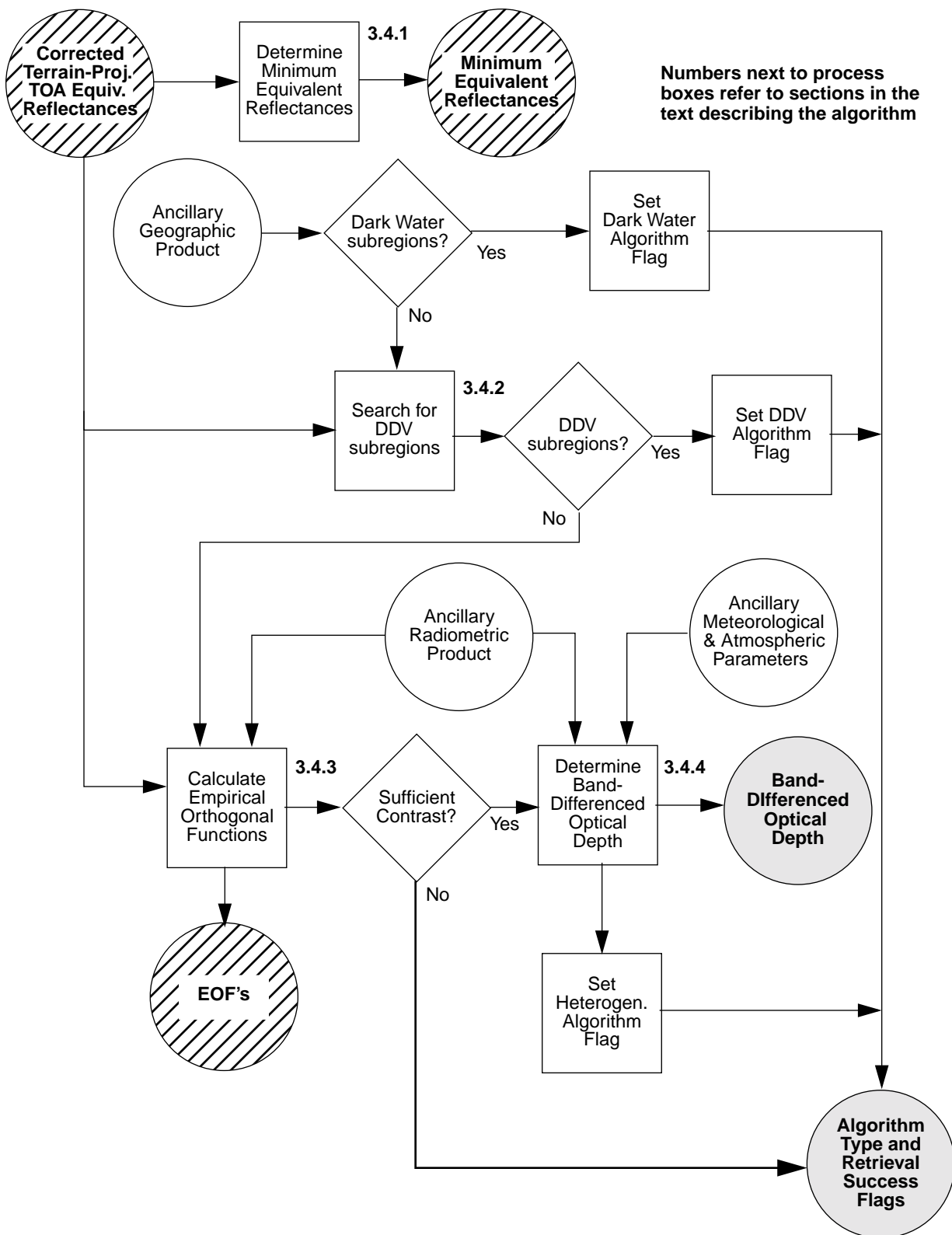
Figure 4. Stage 2 retrieval processing concept

Corrected Terrain-Proj. TOA Equiv. Reflectances

Establish equivalent reflectances for retrieval **3.5.1**

Establish aerosol models **3.5.2**

Aerosol Climatology Product

Repeat for all appropriate aerosol models

Determine model TOA equivalent reflectances **3.5.3**

SMART Dataset

Minimum Equivalent Reflectances

EOF's

Calculate optical depth upper bound **3.5.4**

Algorithm Type Flag

Optical Depth Upper Bounds

Compute residual **3.5.5**

Aerosol Retrieval Residuals

Ancillary Radiometric Product

Compute optical depth and uncertainty **3.5.6**

Aerosol Model Identifiers

Ancillary Meteorological & Atmospheric Parameters

Aerosol Optical Depths and Uncertainties

Establish optical depth defaults **3.5.7**

Numbers next to process boxes refer to sections in the text describing the algorithm

Calculate best estimate optical depths **3.5.8**

Best Estimate Optical Depths

Figure 5. Stage 3 retrieval processing concept

12

3.1.2 Data staging and management

Aerosol retrievals are performed on 17.6-km regions, and for those regions containing land a surface retrieval is performed before the entire process shifts to the next region. In order to make the process efficient from a data staging standpoint, and to allow establishment of default optical depths over land, the manner in which the regions are stepped through is important.

A domain is defined to be a 70.4 km x 70.4 km area, that is, a 4 x 4 array of regions. Because the SMART Dataset is large, minimal re-staging of data is desirable. Parameters within SMART depend on view and illumination geometry. Therefore, regional geometric parameters are averaged over each domain, and SMART parameters corresponding to the domain-averaged geometry are used. Thus, all regions within a given domain are processed before moving on to the next domain and its associated set of regions.

Additionally, in order to maximize land surface retrieval coverage, default aerosol optical depths (and an associated aerosol model) are established when the land aerosol retrieval process fails to find a suitable model in a particular region. The method for setting these defaults is discussed in §3.5.7. Because some defaults use he average optical depth for the previously-processed domain, it is desirable for successive domains to be spatially contiguous. Within each MISR 563.2 km x 140.8 km data block, there are 8 domains cross-track and 2 along-track. As a swath of data is processed, the order of domain processing follows the serpentine pattern shown in Figure 6. There is no preferred order for processing of regions within a domain.
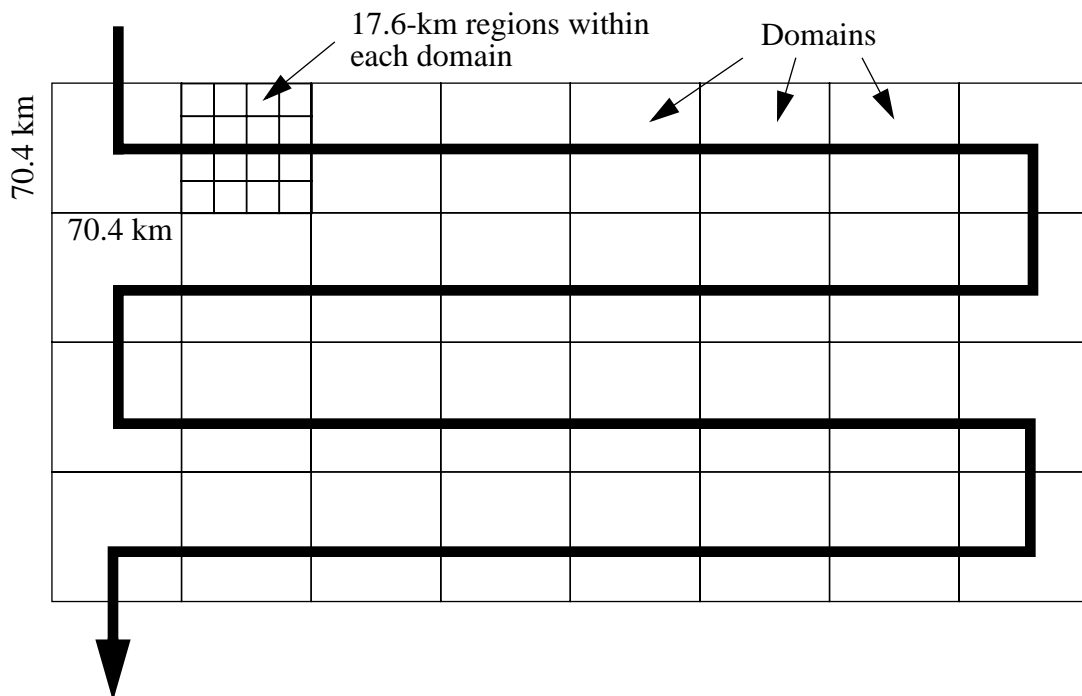
Figure 6. Pattern for stepping through domains

3.2 ALGORITHM INPUT

3.2.1 MISR data

Required inputs for the aerosol retrieval to be obtained from other parts of the MISR data system are summarized in Table 2 (see also Figures 3 - 5). Further information on each of the inputs is provided below.

Table 2: Aerosol/Surface Product inputs (MISR data) used for aerosol retrievals

Input data	Source of data	Reference
Terrain-projected TOA radiances	Level 1B2 Geo-rectified Radiance Product	*[M-3]*
Ellipsoid-projected TOA radiances	Level 1B2 Geo-rectified Radiance Product	*[M-3]*
Data Quality Indicators and Data Flags	Level 1B2 Geo-rectified Radiance Product	*[M-3]*
Ellipsoid-referenced geometric parameters	Level 1B2 Geo-rectified Radiance Product	*[M-3]*
Radiometric Camera-by-camera Cloud Mask (RCCM)	Level 1B2 Geo-rectified Radiance Product	*[M-4]*
Stereoscopically Derived Cloud Mask (SDCM)	Level 2 TOA/Cloud Product	*[M-8]*
Cloud Shadow Mask	Level 2 TOA/Cloud Product	*[M-8]*
Topographic Shadow Mask	Level 2 TOA/Cloud Product	*[M-8]*
Regional cloud fraction	Level 2 TOA/Cloud Product	*[M-8]*
Land/water flags	Ancillary Geographic Product	*[M-6]*
Regional elevation data	Ancillary Geographic Product	*[M-6]*
Instrument measurement uncertainties and signal-to-noise ratios	Ancillary Radiometric Product	*[M-5]*
Spectral out-of-band correction matrix	Ancillary Radiometric Product	*[M-5]*
Band-weighted exo-atmospheric solar irradiances	Ancillary Radiometric Product	*[M-5]*
Standardized solar-weighted band center wavelengths	Ancillary Radiometric Product	*[M-5]*
Pure aerosol optical properties	Aerosol Climatology Product	*[M-11]*
Aerosol mixture model specifications	Aerosol Climatology Product	*[M-11]*
Model TOA equivalent reflectances and radiative transfer parameters	SMART Dataset	*[M-11]*

3.2.1.1 Terrain-projected TOA radiances

The terrain-projected TOA radiance parameter is derived at Level 1B2 and consists of geolo-

cated, registered, and calibrated radiances in all 36 channels of the instrument projected onto the surface terrain. A resampling process is required in order to implement this projection, and the effects of surface topography are taken into account. Terrain-projected radiances have not had any atmospheric correction applied and include both surface and atmospheric contributions to the signal. The data are resampled onto a Space Oblique Mercator grid. Note that the input from Level 1B2 consists of 16-bit integer words. Conversion of these integers to floating point values corresponding to radiances in the appropriate units (W m^{-2} sr^{-1} μm^{-1}) is accomplished by applying a multiplicative scale factor obtained from the Ancillary Radiometric Product (ARP).

3.2.1.2   Ellipsoid-projected TOA radiances

Over oceans, the surface is assumed to correspond to the WGS84 ellipsoid. For this purpose, terrain-projected and ellipsoid-projected radiances are equivalent. To avoid duplication, these are stored in only one of the projected radiance parameter sets (the ellipsoid projection) generated during Level 1B2 processing. Thus, to access radiances over ocean, this parameter set must be ingested. Again, the data are encoded as 16-bit integers, which must be converted to radiances by the appropriate scaling, as discussed above.

3.2.1.3   Data Quality Indicators and Data Flags

A Radiometric Data Quality Indicator (RDQI) will be associated with each projected radiance provided by Level 1B2. This indicator will provide a representation of the radiometric quality of the input radiances used to generate values reported in the Geo-rectified Radiance Product. Because of the data resampling required at Level 1B2, each projected radiance represents a bilinear interpolation of four surrounding radiances obtained from the MISR images. The radiances in the imagery will be coded with a quality indicator specifying the reliability level of the radiometry on a pixel-by-pixel basis. From these, a scaled value will be produced at Level 1B2. The RDQI's take on values of 0 - 3, as follows:

RDQI = 0: Radiometric accuracy meets all specifications

RDQI = 1: Radiometric accuracy is sufficient for certain applications but some specifications are violated (see *[M-2]* and *[M-3]*)

RDQI = 2: Radiance value is available but of insufficient accuracy to be used in Level 2 retrievals

RDQI = 3: Radiance value is unavailable.

Thus, higher quality data are associated with smaller values of RDQI.

In addition to the RDQI's, radiances reported in Level 1B2 will be encoded to provide Data Flag information, for example, to indicate that a particular point on the Space Oblique Mercator (SOM) grid was topographically obscured from view by a particular camera.

Finally, MISR data will have an associated Geometric Data Quality Indicator (GDQI). The GDQI will provide a measure of how much image matching was used to insure high-quality image registration, relative to a pure reliance on spacecraft-supplied navigation.

3.2.1.4 Ellipsoid-referenced geometric parameters

These are calculated at Level 1B2, and provide view zenith and azimuth angles as well as solar zenith and azimuth angles.

3.2.1.5 Radiometric Camera-by-camera Cloud Mask (RCCM)

This is obtained from the MISR Level 1B2 Geo-rectified Radiance Product. It is used as a default cloud mask if the Stereoscopically Derived Cloud Mask (SDCM) from the TOA/Cloud Product is unavailable. In the event the RCCM is used, an aerosol retrieval is attempted only on those samples for which there is high confidence of no cloud cover as determined from this mask. The RCCM also contains a mask to eliminate regions contaminated by sun glitter, derived on the basis that a particular view direction may be within a certain cone angle of the direction corresponding to specular reflection.

3.2.1.6 Stereoscopically Derived Cloud Mask (SDCM)

The confidence levels associated with the retrieval of stereoscopic heights within the TOA/Cloud Product are used to generate a Stereoscopically Derived Cloud Mask. The algorithm for generating the SDCM within the TOA/Cloud retrievals incorporates the RCCM. Thus, if the SDCM is available, it is not necessary to use the RCCM, that is, the RCCM is used only as a default.

3.2.1.7 Cloud Shadow Mask

A Cloud Shadow Mask is provided by the TOA/Cloud Product on 1.1-km centers. It is derived by projecting the stereoscopically-derived cloud altitudes, along the line of sight of the solar illumination vector, to the surface terrain. It is used to eliminate from aerosol retrievals those subregions that are contaminated by cloud shadow, as these subregions violate the radiative transfer assumptions inherent in the retrievals.

3.2.1.8 Topographic Shadow Mask

A Topographic Shadow Mask is provided by the TOA/Cloud Product on 1.1-km centers. It is derived in a similar manner as the Cloud Shadow Mask. It is used to eliminate from aerosol retrievals those subregions that are contaminated by topographic shadow.

3.2.1.9   Regional cloud fraction

This information is provided for 17.6-km regions by the TOA/Cloud Product. If the cloud fraction exceeds a certain amount, the region is bypassed as far as aerosol retrievals are concerned.

3.2.1.10   Land/water flags

These are obtained on 1.1-km centers from the Ancillary Geographic Product (AGP). This product is generated at the MISR SCF and stored at the DAAC. The land/water flag includes an indicator of water regions where application of the dark water aerosol retrieval algorithm is appropriate.

3.2.1.11   Regional elevation data

These inputs consist of the mean surface elevation and standard deviation of surface elevation over 17.6-km regions, relative to the WGS84 reference ellipsoid. These data are obtained from the AGP.

3.2.1.12   Spectral out-of-band correction matrix

As described in §3.3.5, a spectral out-of-band correction is applied to MISR data to compensate for larger than desired energy outside the nominal in-band region of the spectral filters. This correction requires the use of a 4 x 4 matrix. The elements of this matrix are stored in the ARP.

3.2.1.13   Instrument measurement uncertainties and signal-to-noise ratios

These are required in order to determine the goodness-of-fit of various aerosol models to the MISR observations, to evaluate the angle-to-angle smoothness of the data, and to determine the level of scene contrast. They are obtained from the Ancillary Radiometric Product (ARP). This product is updated routinely at the MISR SCF and stored at the DAAC. Measurement uncertainties provide statistical estimates of potential systematic errors in absolute, as well as relative (e.g., camera-to-camera, band-to-band, and pixel-to-pixel), radiometry. Signal-to-noise ratios provide a measure of random noise.

3.2.1.14   Band-weighted exo-atmospheric solar irradiances

These are used to convert top-of-atmosphere radiances to equivalent reflectances. They are obtained from the ARP. There are several types of band-weighted exo-atmospheric solar irradiances, E_0, contained in the ARP, distinguished by how the spectrally-varying irradiances $E_{0\lambda}$ are weighted by the spectral response of the MISR cameras. During Level 1 processing of MISR data, a correction to the observed radiances is made to account for variations in the in-band spectral response from pixel-to-pixel and camera-to-camera. As a result, the conversion of radiances to

equivalent reflectances required for aerosol retrievals make use of the parameters designated $E_{0,b}^{std}$ in the ARP (*[M-2]*, *[M-5]*) where the superscript *std* indicates weighting by a standardized spectral response over the total spectral range for which the cameras have measurable sensitivity, and the subscript *b* indicates that a value of this parameter is provided for each of the 4 instrument spectral bands.

3.2.1.15 Standardized solar-weighted band center wavelengths

These parameters, denoted $\lambda_{m,\,solar,\,b}^{std,\,in-band}$, are the central wavelengths determined from a moments analysis, for each band, of the standardized in-band spectral response curve weighted by the exo-atmospheric solar irradiance spectrum. They are used as the band center wavelengths for the purpose of calculating Rayleigh scattering optical depth.

3.2.1.16 Pure aerosol optical properties

The aerosol prescriptions which form the basis of the MISR retrievals are stored in the Aerosol Climatology Product (ACP). One portion of this product contains physical properties (e.g., size distribution, index of refraction, density, and tendency to adsorb water), based upon current knowledge, and effective optical properties calculated using Mie theory for spherical particles, and ellipsoid approximations/geometric optics for non-spherical cases *[36]*. Each of these aerosols is considered "pure", that is, of a single chemical composition and unimodal size distribution. Because the MISR cloud screens may not completely eliminate cirrus or ground fog, a "typical" thin cirrus cloud model *[33]*, *[37]*, *[48]* and a "near-surface fog" model are included in the ACP. The optical properties of thin cirrus (optical depth ≤ 0.1) are believed to be easier to model than those for thicker cloud. In particular, thin cirrus tends to have small (tens of microns), randomly-oriented, monodisperse fractal crystals. For thicker cirrus, these simplifying characteristics are likely to be invalid, and an admixture of liquid water droplets may also be present, even at very low temperatures *[44]*. Lacking a community consensus on thick cirrus phase functions at this time, however, our strategy will be to use the thin cirrus model, and to treat with caution those retrievals which return a cirrus optical depth > 0.1. Cirrus scattering models and screens are expected to be improved by MISR and MODIS; based on EOS results, the present strategy will be revised accordingly.

Aerosol properties are presented, where appropriate, for a range of relative humidities. All aerosols are modeled using either log-normal or power law size distributions, except the cirrus size distribution which is approximated from cirrostratus observations. All aerosol particles are assumed to be spherical, except for mineral dust, which is modeled as randomly oriented prolate and oblate spheroids, and thin cirrus, which is modeled as equidimensional, randomly oriented hexagonal prisms.

The contents of the ACP, the theoretical basis behind its generation, and the treatment of the variation of particle sizes and optical properties with relative humidity, are described in *[M-11]*.

3.2.1.17 Aerosol mixture model specifications

During routine aerosol retrievals at the DAAC, it is necessary to establish the mixtures of pure aerosols included in the ACP that will be compared to the MISR observations. For each region of the globe, an additional portion of the ACP defines those mixtures, for each of the retrieval pathways that may occur (i.e., dark water, DDV, or heterogeneous land), providing the component pure aerosol model identifiers, and the relative abundances of each component, defined in terms of fraction of total optical depth. In addition, this part of the ACP contains information required during the retrievals, such as optical depth spectral scaling factors and single-scattering albedos of the aerosol mixtures. Finally, the "clim-likely" part of the ACP assigns a likelihood value to each of the selected aerosol models, based on reasonable climatological expectations. Details are provided in *[M-11]*.

3.2.1.18 Model TOA equivalent reflectances and radiative transfer parameters

Using the optical properties of the aerosol models in the ACP, forward radiative transfer calculations are performed at the MISR SCF to calculate components of the top-of-atmosphere equivalent reflectance field, other top- and bottom-of-atmosphere radiometric parameters, and diffuse and total atmospheric transmittance. These are calculated for a variety of view and illumination geometries, corresponding to the range of values relevant to the MISR experiment. The results, for discrete values of total aerosol optical depth, and surface type, comprise the Simulated MISR Ancillary Radiative Transfer (SMART) Dataset.

We assume a multiple-layer, horizontally homogeneous atmosphere plus dark water surface model in generating the SMART Dataset. The Rayleigh scattering part of the atmosphere is assumed to be present in all the layers. For a given aerosol model, consisting of either tropospheric aerosol, stratospheric aerosol, or cirrus cloud, the altitude limits and scale height of the aerosol layer are specified. Atmospheric water vapor is modeled as being confined to the lowest layers. All layers are not simultaneously populated (e.g., the pure cirrus model contains no tropospheric aerosol). A purely absorbing layer consisting of ozone is assumed to overlie all of the scattering layers, but is not included in the forward calculations; rather, a correction is made during the retrieval process (see §3.3.7).

For the aerosol retrievals over homogenous land regions identified as being covered by Dense Dark Vegetation, and for the retrievals over heterogeneous land surfaces, the radiation fields from the SMART Dataset are those corresponding to a black surface, and the effects of surface reflectance are accounted for during the actual retrievals. Over dark water, the pre-calculated radiation fields in the SMART Dataset provide an additional component assuming a surface model that accounts for Fresnel reflection and the effects of wind speed on sun glint and whitecaps.

Top-of-atmosphere equivalent reflectances, which form the basis for the MISR aerosol re-

trievals, are calculated using the doubling/adding method of solving the radiative transfer equation for plane-parallel geometry. These calculations are performed for the pure aerosol types contained in the ACP over a range of optical depths. The minor water vapor absorption affecting the MISR band 4 radiances is included in the forward calculations. In general, the radiance L leaving the top of the atmosphere can be written as

$$
\begin{aligned}
L_{x,y}(-\mu, \mu_0, \phi - \phi_0) \; = \; & L^{atm}(-\mu, \mu_0, \phi - \phi_0) + \\
& + \exp(-\tau/\mu) \cdot \frac{1}{\pi} \int_0^1 \int_0^{2\pi} R_{x,y}^{surf}(-\mu, \mu', \phi - \phi') L_{x,y}^{inc}(\mu', \mu_0, \phi' - \phi_0) \mu' d\mu' d\phi' + \\
& + \frac{1}{\pi} \int_0^1 \int_0^{2\pi} \int_0^1 \int_0^{2\pi} T_{x,y}(-\mu, -\mu'', \phi - \phi'') \otimes R_{x,y}^{surf}(-\mu'', \mu', \phi'' - \phi') L_{x,y}^{inc}(\mu', \mu_0, \phi' - \phi_0) \mu' d\mu'' d\phi'' d\mu' d\phi'
\end{aligned}
$$

$$(1)$$

where x, y are the image spatial coordinates in a Cartesian coordinate system in which $+z$ points toward the center of the Earth and is normal to the surface ellipsoid (not the local topographically-defined surface orientation), $+x$ points toward the north pole, θ and θ_0 are the view and Sun angles with respect to the $+z$ axis, $\mu = |\cos \theta|$, $\mu_0 = |\cos \theta_0|$, ϕ_0 is the azimuthal angle of the solar illumination vector, and ϕ is the azimuthal angle of a vector pointing toward the MISR instrument, also in the ellipsoid reference system. These definitions lead to the convention of using $-\mu$ and μ for upwelling and downwelling radiation respectively. The properties of the atmosphere are assumed to be horizontally homogeneous. On the right-hand-side of Eq. (1), ^{atm} is the radiance field scattered by the atmosphere to space without interacting with the surface (i.e., the path radiance), τ is the optical depth of the total atmosphere, $^{inc}_{x,y}$ is the direct and diffuse downward radiance field incident on the surface, T is the upward diffuse transmittance, and $R_{x,y}^{surf}$ is the spatially variable surface bidirectional reflectance factor (BRF). The BRF of a surface target is defined as the bidirectional reflectance distribution function of the target ratioed to the bidirectional reflectance distribution function from a non-absorbing lambertian surface *[39]*.

In the general three-dimensional solution to the radiative transfer problem with a horizontally uniform atmosphere over a spatially varying and flat surface, the transmittance $T_{x,y}$ can be thought of as a point-spread function and with the convolution operation $\otimes$ describes the blurring effect of the atmosphere on the surface reflectance $R_{x,y}^{surf}$ *[4]*. When the image spatial resolution is comparable to the atmospheric scattering scale height (defined by the vertical distribution of the aerosols and/or Rayleigh scattering molecules), Eq. (1) reduces to the standard one-dimensional radiative transfer regime, and T is effectively a delta function in the spatial coordinates. In this case, Eq. (1) simplifies to:

$$L_{x,y}(-\mu, \mu_0, \phi - \phi_0) = L^{atm}(-\mu, \mu_0, \phi - \phi_0) +$$

$$+ \exp(-\tau/\mu) \cdot \frac{1}{\pi} \int_0^1 \int_0^{2\pi} R_{x,y}^{surf}(-\mu, \mu', \phi - \phi') L_{x,y}^{inc}(\mu', \mu_0, \phi' - \phi_0) \mu' d\mu' d\phi' +$$

$$+ \frac{1}{\pi} \int_0^1 \int_0^{2\pi} \int_0^1 \int_0^{2\pi} T(-\mu, -\mu'', \phi - \phi'') R_{x,y}^{surf}(-\mu'', \mu', \phi'' - \phi') L_{x,y}^{inc}(\mu', \mu_0, \phi' - \phi_0) \mu' d\mu'' d\phi'' d\mu' d\phi'$$

$$(2)$$

As described in §2.2, MISR data will be acquired in various averaging modes. The 3-D radiative transfer regime is appropriate for the high-resolution channels (1 x 1 or 1 x 4) and the 1-D regime is appropriate for 4 x 4-averaged samples. A further simplification of Eq. (2) occurs over surfaces which are uniform in reflectance. For such cases, Eq. (2) is simplified by eliminating the *x, y* subscripts from the equation. Finally, in the case where the surface is black, only the path radiance term survives.

Since polarization of scattered light can affect the radiances measured by MISR, the effects of polarization are incorporated by correcting radiances in our scalar calculations by subtracting the contribution due to the Rayleigh scattering, including its interaction with the surface and then adding back this contribution as calculated with a vector code. The interaction of the polarized Rayleigh scattering from the atmosphere and the polarizing Fresnel reflection from the dark water surface is important for radiance calculations, and our correction takes this into account.

The ACP contains the optical properties of pure particles upon which the MISR retrievals are based, and the SMART Dataset contains radiometric quantities for these pure aerosols. During routine retrievals at the DAAC, mixtures of these aerosols will be compared to the MISR observations. Mixing ratios are specified on a quantized grid. Sensitivity studies are being performed to determine which mixtures are distinguishable by the MISR instrument under the illumination and viewing conditions of the EOS orbit. Models which are observationally indistinguishable to within the measurement uncertainties of MISR will be binned together, thus limiting the number of distinct combinations. When complete, the results will dictate the various mixtures to be used in the retrieval process, yielding a substantial improvement over previous satellite-based retrievals of tropospheric aerosols. Modified linear mixing rules are used to generate the required radiometric properties of these mixtures. The relevant equations are provided in §3.5.3. The modified linear mixing equations described there require splitting the path radiance component of the TOA equivalent reflectance field into its single- and multiple-scattered components.

Additional details on SMART Dataset contents and generation are provided in *[M-11]*.

3.2.2 Non-MISR data

Required inputs for the aerosol retrieval to be obtained from non-MISR sources are summarized in Table 3. Further information on each of the inputs is provided below.

Table 3: Aerosol/Surface Product inputs (non-MISR data) used for aerosol retrievals

Input data	Source of data
Earth-Sun ephemeris	SDP Toolkit
Stratospheric aerosol optical depth and size distribution parameters	SAGE III (if available)
Column ozone abundance	EOS Data Assimilation Office (DAO) or climatological values in the TASC Dataset
Meteorological variables (column precipitable water, surface pressure, surface temperature, temperature profile, geopotential height profile, near-surface wind speed)	EOS Data Assimilation Office (DAO), climatological values in the TASC Dataset, or MODIS Level 2

3.2.2.1 Earth-Sun ephemeris

This is used to obtain the Earth-Sun distance, such that observed radiances can be normalized to the standard distance of 1 AU. The source is the Science Data Production (SDP) Toolkit, which is generated by the EOSDIS Core System (ECS) contractor.

3.2.2.2 Stratospheric aerosol optical depth and size distribution parameters

The MISR retrievals are based on a variety of tropospheric models as well as a stratospheric aerosol model. If SAGE III data are available at the time of the EOS-AM1 mission, we will report the integrated optical depth measurements as part of the MISR Aerosol/Surface Product, in order to provide a post-retrieval constraint.

3.2.2.3 Column ozone abundance

The sensitivity of the MISR instrument to ozone is great enough to warrant applying a correction. Near-real-time values for ozone abundance from the EOS Data Assimilation Office (DAO) will be used. If these are unavailable, climatological values obtained from the TASC Dataset will usually suffice to a high degree of accuracy.

3.2.2.4 Meteorological variables

The following meteorological variables are used in the MISR aerosol retrievals. They will be obtained from DAO or MODIS Level 2 data. In the event that real-time meteorological fields

are unavailable, the MISR aerosol retrieval will rely on climatological values provided in the TASC Dataset (see *[M-11]*). Although real-time data are preferable, the climatological values for these fields will meet our minimum requirements for accuracy in all but extreme cases. The use of each parameter in the retrieval process is briefly described.

3.2.2.4.1   Column precipitable water

Column precipitable water is not planned to be used to constrain the aerosol retrievals. However, it will be reported with the Aerosol/Surface product and may be used at a later time. It is possible that this parameter may be obtained from MODIS.

3.2.2.4.2   Relative humidity

A vertical relative humidity (RH)profile on a standard set of pressure levels will be obtained from DAO. At present, these data will not be used to constrain the aerosol retrievals; however, like the column precipitable water these data will be reported in the Aerosol/Surface product.

3.2.2.4.3   Surface pressure

The surface pressure will be used to establish the amount of Rayleigh scattering to include in the models used during the retrievals.

3.2.2.4.4   Surface temperature and temperature profile

The temperature profile is used to obtain the ratio of temperature at a given altitude to the surface temperature. This ratio, and the surface temperature, are used in the calculation of pressure at an arbitrary altitude above sea level. The temperature profile stored in the TASC Dataset is given as a function of altitude above sea level, z. The profile obtained from DAO is obtained as a function of pressure. It is converted to a temperature vs. height profile by using the DAO-provided geopotential height vs. pressure profile.

3.2.2.4.5   Geopotential height profile

Geopotential height as a function of pressure is obtained from the DAO, in units of meters. We make the assumption that geopotential and geometric height are equal.

3.2.2.4.6   Near-surface atmospheric wind speed

In conjunction with a model of the effect of wind on water surface roughness, this parameter is used in the calculation of the TOA radiance field over dark water and for the purpose of identifying portions of each camera's FOV that may be contaminated by glitter, and for determining the

lower boundary condition for dark water aerosol retrievals.

3.3 THEORETICAL DESCRIPTION: STAGE 1 RETRIEVAL PROCESSING

Figure 3 shows those processes which occur at the DAAC involving processing of the data prior to actual aerosol retrievals (referred to as Stage 1). In the following sections, the physical basis of these processes is described, and a mathematical description of the algorithm which is used to implement each process is presented.

3.3.1 Test regional retrieval applicability

3.3.1.1 Physics of the problem

Several tests will be applied to determine the suitability of using each sample observed in each of the MISR instrument channels for aerosol retrieval. The purpose of this step is to determine whether a particular 17.6 km x 17.6 km region is suitable for performing an aerosol retrieval.

3.3.1.2 Mathematical description of the algorithm

3.3.1.2.1 *Regional solar zenith angle test*

A region is deemed unacceptable for aerosol retrieval if the cosine of the solar zenith angle, μ_0, is < 0.2. The reason for this limitation is that plane-parallel radiative transfer theory is assumed for the retrievals, and this assumption breaks down for very oblique illumination angles.

3.3.1.2.2 *Regional topographic complexity test*

A region is classified as topographically complex, and unsuitable for aerosol retrieval, if the standard deviation of the regional surface elevation exceeds 250 m.

3.3.1.2.3 *Regional cloudiness test*

To determine if a region is too cloudy for aerosol retrieval, we use two parameters: $\tilde{F}_{\text{CloudHC}}$ and $\tilde{F}_{\text{CloudLC}}$. These parameters are obtained from the TOA/Cloud Product, and are defined to be the fractional area of the 17.6-km region that contains cloud with high confidence and low confidence, respectively, including information from both the Radiometric Camera-by-camera Cloud Mask and the Stereoscopically-Derived Cloud Mask, but excluding information from the Angular Signature Cloud Mask. For further discussion, see *[M-8]*.

If the TOA/Cloud Product is not available, the nearest available RCCM to nadir (in order of preference: An, Af, Aa, Bf, Ba, etc...) from Level 1B2 is used as a backup. In this case, we set $\tilde{F}_{\text{CloudHC}}$ equal to the fraction of the 16 x 16 array of 1.1-km subregions within the region that is

classified by this RCCM as CloudHC, and set $\tilde{F}_{\text{CloudLC}}$ equal to the fraction of the 16 x 16 array of 1.1-km subregions within the region that is classified by the RCCM as CloudLC.

The region is classified as too cloudy for aerosol retrieval if $\tilde{F}_{\text{CloudHC}}$ or $\tilde{F}_{\text{CloudLC}}$ exceed specified threshold values. Currently, we set these thresholds to 100%, effectively causing this regional test to be bypassed. Analysis of actual data will be performed to establish the appropriate thresholds. Other screens will nevertheless be applied on a subregional basis (see, e.g., §3.3.8.2.6, §3.3.8.2.7, §3.3.8.2.9, and §3.3.8.2.10).

3.3.1.2.4 *Sufficient data test*

There are other reasons why a region may be determined to be unsuitable for aerosol retrieval. For example, application of the subregion-by-subregion and channel-by-channel tests (see §3.3.8) may eliminate so much data that when an attempt is made to apply a particular retrieval algorithm, there is an insufficient number of surviving subregions or channels. Another example is the heterogeneous land algorithm, which may determine that insufficient contrast was present. As opposed to the regional topographic complexity or regional cloudiness tests, these evaluations cannot be made until further processing has been accomplished.

3.3.2 Average subregion radiances

3.3.2.1 Physics of the problem

Radiances provided by the MISR Level 1B2 Geo-rectified Radiance Product are in the same averaging mode in each channel as the data were acquired on orbit. For certain channels, these data need to be averaged to coarser resolution in order to apply the aerosol retrieval algorithm (e.g., red band data acquired at 275-m sampling need to be averaged 4 lines x 4 samples in order to generate a 1.1-km input).

3.3.2.2 Mathematical description of the algorithm

Averaging over all applicable samples is used as required to generate samples with the appropriate resolution for each algorithm. Thus, the output average radiance is given by:

$$L_{av} = \frac{\sum\limits_{i,j} w(i,j)L(i,j)}{\sum\limits_{i,j} w(i,j)} \tag{3}$$

where $L(i,j)$ is the radiance for the $(i,j)^{\text{th}}$ sample, and the corresponding weight, $w(i,j)$, is equal to 1 if the RDQI for the sample is $\leq \text{RDQI}_1$; otherwise $w(i,j) = 0$. We set $\text{RDQI}_1 = 1$.

An RDQI value, RDQI_{av}, is also assigned to L_{av}. Its calculation takes into account the individual RDQI's as well as what proportion of the total number of 1x1 samples that make up the subregion, N, contain valid data. In generating a 1x4 (275 m cross-track x 1.1 km along-track) subregion from 1x1 data, for example, $N = 4$, and in generating a 4x4 (1.1 km cross-track x 1.1 km along-track) subregion, $N = 16$. We define

$$\text{RDQI}_{av} = nearest\ integer\left\{\frac{1}{N}\sum_{i,\,j}\text{RDQI}'(i,\,j)\right\} \tag{3a}$$

where $\text{RDQI}'(i,\,j) = \text{RDQI}(i,\,j)$ if $\text{RDQI}(i,\,j) \leq \text{RDQI}_1$; otherwise $\text{RDQI}'(i,\,j) = \text{RDQI}_2$. We set $\text{RDQI}_2 = 3$.

In the event that $\text{RDQI}_{av} = 3$, L_{av} is set to a flag value indicating "missing data". However, if $\text{RDQI}_{av} = 3$ and any of the $L(i,\,j)$ is a flag value indicating "topographically obscured", L_{av} is also set to the "topographically obscured" flag value.

3.3.3   Normalize to Earth-Sun distance of 1 AU

3.3.3.1   Physics of the problem

The equivalent reflectances in the SMART Dataset are generated assuming a standard Earth-Sun distance of 1 AU. Because of the slight eccentricity of the Earth's orbit, MISR observations must be normalized to this distance before comparisons with the SMART Dataset can be made.

3.3.3.2   Mathematical description of the algorithm

Letting d be the Earth-Sun distance in AU, the normalization is simply made by multiplying the observed MISR radiances by d^2.

3.3.4   Convert to equivalent reflectances

3.3.4.1   Physics of the problem

Top-of-atmosphere (TOA) radiometric information contained in the SMART Dataset and other ancillary sources are provided in the form of equivalent reflectances. In order to compare MISR measurements with the data from these sources, MISR radiances, L, must be converted to equivalent reflectances, ρ. Equivalent reflectance conceptually represents an arbitrary radiance level in terms of the particular value of reflectance of an exo-atmospheric lambertian target, illuminated by the Sun at normal incidence, that would yield the same radiance at the sensor. For example, a perfectly reflecting lambertian target illuminated by overhead Sun has a true reflectance and an equivalent reflectance of 1.0 at all view angles. If the same target were illuminated at a solar

incidence angle of 60°, its true reflectance is still 1.0, but $\rho = 0.5$ (cos 60° × 1.0) at all view angles.

3.3.4.2 Mathematical description of the algorithm

The conversion of radiance to equivalent reflectance is given by:

$$\rho \;=\; \pi L / E^{std}_{0,\,b} \qquad\qquad (4)$$

where L is the radiance within a given sample in band b as provided by the Level 1B2 product, and $E^{std}_{0,\,b}$ is the band-weighted spectral exo-atmospheric solar irradiance for band b as defined in §3.2.1.14.

3.3.5 Apply spectral out-of-band correction

3.3.5.1 Physics of the problem

During pre-flight camera testing, it was discovered that the amount of out-of-band light is larger than called for in the spectral response specification by about a factor of three. For scenes of different spectral content than the Spectralon panels against which the MISR cameras are calibrated in flight, small radiometric errors result from the fact that the out-of-band integrated response is typically about 3% of the integrated in-band response. Thus, compensation for this phenomenon is desirable for the aerosol and surface retrievals, as the information contained in the ancillary datasets (ACP and SMART) assume that the radiation is essentially monochromatic at the MISR band-center wavelengths (an exception is the water vapor content of band 4 within the SMART Dataset, which is integrated over the instrument's spectral response). The correction approach requires co-registration of the four MISR bands in order to obtain an estimate of the scene spectrum. For these reasons, the correction is implemented at this stage of MISR systematic data processing.

3.3.5.2 Mathematical description of the algorithm

The correction algorithm is applied to each subregion to be used in the MISR aerosol and/or surface retrievals. It requires a value of equivalent reflectance at each of the four MISR wavelengths. If less than the full complement of four bands is available, linear interpolation is used, or if this is not feasible, the equivalent reflectance is set equal to the value in the closest available band. This assignment of missing equivalent reflectances is done only for the purpose of applying this algorithm, and only the bands in which actual MISR data are available are used in subsequent processing. The correction algorithm is implemented by applying the following equation:

$$
\begin{bmatrix} \rho_1 \\ \rho_2 \\ \rho_3 \\ \rho_4 \end{bmatrix}_{corrected} = M \begin{bmatrix} \rho_1 \\ \rho_2 \\ \rho_3 \\ \rho_4 \end{bmatrix} \tag{5}
$$

where the corrected equivalent reflectances are obtained from the uncorrected values by multiplying a column vector of the uncorrected values by M, a 4 x 4 correction matrix. Because this is a small correction, the matrix M is dominated by its diagonal elements. The derivation underlying Eq. (5) assumes that the actual scene spectrum can be approximated, for the purposes of this correction, by a piecewise linear function constrained by the MISR observations and knowledge of the actual spectral response of the cameras (determined from pre-flight spectral calibration), the ideal spectral response, and solar irradiance spectrum (see *[M-5]*). The elements of M are stored in the ARP.

If application of Eq. (5) results in any of the corrected equivalent reflectances becoming negative, this correction is skipped and the uncorrected equivalent reflectances are used.

3.3.6   Establish ancillary meteorological and atmospheric parameters

3.3.6.1   Physics of the problem

The ancillary atmospheric parameters required for the aerosol retrievals are the ambient pressure, the column ozone abundance, and the near-surface wind speed. The mean terrain altitude of the 17.6-km region, z, is obtained from the AGP. The ambient pressure at this altitude, P_z, is derived by assuming hydrostatic equilibrium and a constant temperature lapse rate. This pressure is required for the determination of Rayleigh scattering optical depth and for establishing the pressure to which the inputs from the SMART Dataset are interpolated. Column ozone abundance does not include any correction for terrain altitude, as all terrain heights are beneath the bulk of the ozone. Near-surface wind speed is used only in the dark water retrievals. Column precipitable water is also ingested and reported with the product, although it is not currently used in the retrievals.

3.3.6.2   Mathematical description of the algorithm

If DAO data are available, pressure at height z, P_z is calculated by assuming that geometric and geopotential height are equal and linearly interpolating the $z(P)$ profile to the regional mean terrain altitude. If TASC climatological data are used, P_z is given by:

$$
P_z = P_s \cdot F(z, z_0) \tag{6}
$$

where P_s is the surface pressure in hPa, z_0 is the mean altitude of the grid cell in the TASC Dataset,

28

and $F(z,z_0)$ is a function to correct for the difference in the average altitude of the 17.6-km region (z) and the average altitude of the TASC grid cell (z_0), and is given by

$$F(z, z_0) = \exp\left[\frac{-c(z - z_0)}{T_s}\right] \quad \text{for } 0.99 \leq t \leq 1.01$$

$$F(z, z_0) = t^{\left[\frac{c(z - z_0)}{T_s(1 - t)}\right]} \quad \text{otherwise} \tag{7}$$

where t is the ratio of the atmospheric temperature at altitude z to the surface air temperature, expressed in Kelvins, and is obtained by linearly interpolating the temperature profile to altitude z, c is a constant equal to 34 K km^{-1}, and T_s is the surface air temperature.

Near-surface wind is provided by the DAO, and as a default, by the TASC Dataset, as vector components U and V in m/sec. For the dark water aerosol retrieval, scalar wind speed W is required, and is calculated from

$$W = \sqrt{U^2 + V^2} \tag{7a}$$

3.3.7 Correct for ozone absorption

3.3.7.1 Physics of the problem

Top-of-the-atmosphere (TOA) equivalent reflectances obtained by MISR include a small effect due to ozone absorption. The ratio of column extinction optical depth due to ozone, relative to that due to Rayleigh scattering, for each of the MISR bands, has been calculated according to:

$$R_i = \frac{\int \tau_{ozone}(\lambda) f_i(\lambda) d\lambda}{\int \tau_{Rayleigh}(\lambda) f_i(\lambda) d\lambda} \tag{8}$$

where R_i is the ratio for filter i, f_i is the filter response at wavelength λ, and τ_{ozone} and $\tau_{Rayleigh}$ are the wavelength-dependent ozone and Rayleigh optical depths. Climatological global averaged ozone values are around 300 Dobson units, and range from a high of 460 near the Arctic Circle in northern spring to 180 in the Antarctic ozone "hole" in southern spring [52]. For 300, 400, and 450 Dobson unit ozone columns, in a 1000 mb atmosphere at 193 K, the results for the MISR bands are shown in Table 4.

29

Table 4: Ozone optical depths relative to Rayleigh optical depths in the MISR spectral bands

Band	R_i (300 Dobsons)	R_i (400 Dobsons)	R_i (450 Dobsons)	$\tau_{Rayleigh}$
1	0.00541	0.00746	0.00824	0.236
2	0.336	0.447	0.504	0.094
3	0.347	0.464	0.521	0.044
4	0.0738	0.0971	0.112	0.016

The final column in Table 4 gives the Rayleigh extinction optical depth at band center, for each MISR band. From this table, an upper bound on the ozone optical depth in MISR bands 2 and 3 is about 0.5 of the Rayleigh contribution, requiring correction. An accuracy of about 20 Dobson units in the column abundance is needed for these corrections, suggesting that climatology values will be adequate for all but the most extreme ozone events. Upper bounds on the ozone extinction are 10% of the Rayleigh contribution in band 4, and 1% in band 1. For comparison, aerosol extinction optical depths of interest to the MISR experiment are about 0.05 or greater.

Since the majority of the ozone resides in the stratosphere, correction of the MISR equivalent reflectances for ozone absorption is accomplished by assuming that sunlight is directly attenuated only, by an amount depending on the ozone amount and the sun-camera geometry.

3.3.7.2   Mathematical description of the algorithm

For the MISR aerosol retrieval, column abundance of ozone (in Dobsons) will be converted to ozone optical depth in each of the MISR channels, and used as input to the TOA equivalent reflectance correction. The ozone climatology provided by the TASC Dataset is given in Dobson units directly. However, ozone abundance provided by the DAO is input as parts per million by volume (ppmv) and a conversion to Dobsons is required.

When available, the following data are input from the DAO: A_{ozone}, the ozone abundance in ppmv; h, the geopotential height in meters; and air temperature, T (K). Each of these is reported at a specified set of pressure levels. At a given pressure level i,

$$n_i(air) = \frac{P_i}{kT_i} \tag{8a}$$

where P_i is pressure in N/m^2 (1 mbar = 1 hPa = 100 N/m^2), n_i (air) is the total number of molecules

of air in a unit volume, k is Boltzmann's constant, 1.381×10^{-23} J/deg/molecule, and T_i is the air temperature. The number of ozone molecules per unit volume at this pressure level is

$$n_i(ozone) = A_{ozone, i} n_i(air) \times 10^{-6} \qquad (8b)$$

The total number of ozone molecules per unit area in a column is determined by integrating the $n_i(ozone)$ profile. Since $n_i(ozone)$ is calculated only at a limited number of pressure levels, this integration is best performed by first converting the ordinate from pressure to altitude, calculating the number of molecules per unit volume in each height interval, and summing over all height intervals (the altitude of each pressure level is calculated from the geopotential vs. pressure profile since geopotential is roughly equivalent to altitude for values less than ~80 km). Therefore:

$$N_{ozone} = \sum_{i=1}^{L-1} \frac{(h_{i+1} - h_i)}{2} [n_i(ozone) + n_{i+1}(ozone)] \qquad (8c)$$

where N_{ozone} is the total number of ozone molecules per unit area, h_i is the altitude of the ith level in meters, and L is the total number of levels. Converting this to Dobson units, D_{ozone}:

$$D_{ozone} = \frac{N_{ozone} k T_{STP}}{P_{STP}} \times 10^5 \qquad (8d)$$

where T_{STP} and P_{STP} are the standard temperature and pressure, respectively, with $T_{STP} = 288$ K and $P_{STP} = 1.01325 \times 10^5$ N/m^2.

The relationship between column ozone optical depth, τ_{ozone}, and ozone abundance, D_{ozone}, is

$$\tau_{ozone}(\lambda) = c_\lambda D_{ozone} \qquad (9)$$

where c_λ is equal to 4.26×10^{-6}, 1.05×10^{-4}, 5.09×10^{-5}, and 3.94×10^{-6}, respectively, for bands 1 through 4.

The ozone correction is straightforward to implement, since ozone only absorbs light, and is written:

$$[\rho(-\mu, \mu_0, \phi - \phi_0)]_{ozone\ corrected} = \rho(-\mu, \mu_0, \phi - \phi_0) \cdot \exp\left[\tau_{ozone}\left(\frac{1}{\mu} + \frac{1}{\mu_0}\right)\right] \qquad (10)$$

3.3.8   Filter out unusable or contaminated subregions or channels

3.3.8.1   Physics of the problem

In this step, aerosol retrieval applicability is tested on a subregional (1.1 km x 1.1 km), camera-by-camera, or channel-by-channel basis. The following tests are done in sequential fashion. If a particular subregion or channel is found to be unusable or contaminated according to a certain test, the remaining tests are not performed. A retrieval applicability mask, consisting of a 16 x 16 array corresponding to each of the subregions within a 17.6-km x 17.6-km region, is generated for each of the 36 channels of MISR, and contains a flag indicating either that retrieval is acceptable or the name of the test which resulted in an unusable or contaminated designation.

3.3.8.2   Mathematical description of the algorithm

3.3.8.2.1   Missing data test

Any subregion and channel for which there is an indication of missing data is flagged as unsuitable for aerosol retrieval.

3.3.8.2.2   Topographic obscuration test

Any subregion equivalent reflectance corresponding to an input radiance that has been encoded to indicate that the surface view is obscured by topography is considered unacceptable for aerosol retrieval in that camera.

3.3.8.2.3   Glitter contamination test

A glitter contamination mask is included in the RCCM. If a particular subregion is classified as anything other than Land in the AGP, and also flagged as glitter contaminated at a particular view angle, all bands at that angle are deemed unsuitable for aerosol retrieval. For subregions classified as Land, the glitter mask is not applied. Although there may be spatially unresolved water bodies within the subregion, snow or ice may be present, or there may have been recent rainfall giving rise to sun glint, the angle-to-angle smoothness test (see §3.3.8.2.9) is used to detect and filter out the affected subregions. This strategy preserves as much data as possible for utilization in the aerosol retrievals while ensuring that unsuitable data are screened.

3.3.8.2.4   Topographic shadow test

Any subregion which is flagged by the Topographic Shadow Mask as shadowed due to topographic interference with direct solar illumination is unacceptable for aerosol retrieval in all channels. If the Topographic Shadow Mask is not available, this step is skipped. However, the Quality Assessment parameters associated with aerosol retrieval will indicate whether the Topo-

graphic Shadow Mask was available during processing.

3.3.8.2.5 *Topographic complexity evaluation*

Subregions of topographic complexity are defined to be those for which the root-mean-square (RMS) elevation variation exceeds 250 m, or for which the average slope exceeds 20°, as determined from the AGP. In this event, all channels are unacceptable for aerosol retrieval.

3.3.8.2.6 *Cloud masking*

Mathematical details of the RCCM are provided in *[M-4]*, and details of the SDCM are provided in *[M-8]*. The logic shown in Table 5 is used in determining whether a given camera view of a subregion is cloud contaminated, as determined by the inputs from both the RCCM at the given camera angle and the SDCM (HC refers to High Confidence and LC refers to Low Confidence). The bottom line of the table is used in the event that the SDCM is not available during processing, and only the RCCM is available from Level 1B2. Note that both the RCCM and SDCM are provided on 1.1-km centers. The Quality Assessment parameters associated with aerosol retrieval will indicate which cloud masks were available during processing.

Table 5: Cloud mask decision matrix (Yes=use that camera in subsequent processing)

		Radiometric Camera-by-camera Cloud Mask (RCCM)				
		CloudHC	CloudLC	ClearLC	ClearHC	Not Available
Stereo-scopically Derived Cloud Mask (SDCM)	CloudHC	No	No	No	No	No
	CloudLC	No	No	No	No	No
	NearSurface	No	No	Yes	Yes	No
	Clear	Yes	Yes	Yes	Yes	No
	Not Available	No	No	Yes	Yes	No

3.3.8.2.7 *Cloud shadow masking*

A Cloud Shadow Mask is provided by the Level 2 TOA/Cloud Product *[M-8]*. It classifies each 1.1-km subregion as Cloud Shadowed with High Confidence (CloudShadowHC), Cloud Shadowed with Low Confidence (CloudShadowLC), or Cloud Shadow Free. If either of the first two classifications is assigned to a subregion, that subregion is eliminated from use in aerosol retrieval. If the Cloud Shadow Mask is not available, this step is skipped. However, the Quality Assessment parameters associated with aerosol retrieval will indicate whether the Cloud Shadow Mask was available during processing.

33

3.3.8.2.8   Data quality evaluation

Only subregions and channels for which the Radiometric Data Quality Indicator is $\leq$ a threshold RDQI value $RDQI_3$ are deemed acceptable for aerosol retrieval. $RDQI_3$ is presently set to 0. Geometric Data Quality Indicators from Level 1B2 are reported as part of the Aerosol/Surface Product but are not used to reject regions for processing.

3.3.8.2.9   Angle-to-angle smoothness evaluation

This is a test to insure that the equivalent reflectance field is "smooth" as a function of angle. Clouds, glitter, or other effects which have escaped detection using other methods may be amenable to detection using this test. It is applied to each spectral band separately, and to the forward + nadir camera set independently of the aftward + nadir camera set. Failure of the smoothness test for either set causes the subregion, in the spectral band being examined, to be eliminated from aerosol processing (but *not* from surface processing).

The presence of rainbows in the scattering phase function of an atmospheric aerosol can cause the angular variation of equivalent reflectance to not be smooth. Currently, cameras which are "rainbow-influenced" are simply flagged as such.

The algorithm works as follows for each camera set (forward + nadir or aftward + nadir). For the available cameras in each set, we calculate the scattering angle, Ω, defined by

$$\cos\Omega = -\mu\mu_0 + (1 - \mu^2)^{\frac{1}{2}}(1 - \mu_0^2)^{\frac{1}{2}}\cos(\phi - \phi_0) \tag{11}$$

Any camera for which Ω is in the range Ω_1 to Ω_2 is then flagged as "rainbow-influenced"; if Ω is not in this range the camera is "rainbow-free". We set $\Omega_1 = 110°$ and $\Omega_2 = 160°$ if the AGP indicates that the subregion is suitable for dark water retrieval; otherwise, we set $\Omega_1 = 180°$ and $\Omega_2 = 0°$ (this choice results in no "rainbow-influenced" flagging when viewing non-dark-water).

We then count the number of available cameras in the set which have not been eliminated by previous tests. If this number is < 4, this test is skipped for that camera set.

If there are either 4 or 5 available cameras, the subregion equivalent reflectances are then fit to a polynomial with one less degrees of freedom than the number of cameras, that is, a quadratic polynomial in the case of 4 cameras and a cubic polynomial in the case of 5 cameras. Let $\rho_{poly,k}$ be the polynomial fit value of equivalent reflectance for camera k, and let $\rho_{MISR,k}$ be the corresponding measured value. Now calculate the parameter

$$\chi^2_{smooth} = \frac{1}{N_c} \cdot \sum_{k=1}^{N_c} \frac{(\rho_{MISR,\,k} - \rho_{poly,\,k})^2}{\sigma^2_{cam,\,k}} \tag{12}$$

where N_c is the number of cameras in the set (i.e., 4 or 5) and $\sigma_{cam,k}$ is the relative camera-to-camera radiometric uncertainty in $\rho_{MISR,k}$.

The value of $\sigma_{cam,k}$ is obtained by using calibration uncertainty information provided in the MISR Ancillary Radiometric Product (see *[M-5]*). These data are provided at a standard set of equivalent reflectances (nominally 15 values), for each channel (band and camera combination) of the instrument. Specifically, we make use of:

(1) ε_{cam_sys}, the systematic component of the camera-to-camera relative radiometric uncertainty, expressed in percent, at the tabulated set of equivalent reflectance levels and in the appropriate channel;

(2) SNR_{am}, the signal-to-noise ratio at the tabulated set of equivalent reflectance levels and in the appropriate channel, for the averaging mode $am = 4x4$.

Now, to calculate $\sigma_{cam,\,k}$ corresponding to equivalent reflectance $\rho = \rho_{MISR,\,k}$, we first linearly interpolate the tabulated values of ε_{cam_sys} and SNR_{4x4} to this equivalent reflectance. Denoting these interpolated values $\varepsilon_{cam\_sys}(\rho_{MISR,k})$ and $SNR_{4x4}(\rho_{MISR,k})$, we then have

$$\sigma^2_{cam,\,k} = \rho^2_{MISR,\,k} \left\{ \left(\frac{\varepsilon_{cam\_sys}(\rho_{MISR,\,k})}{100} \right)^2 + \left(\frac{1}{SNR_{4x4}(\rho_{MISR,\,k})} \right)^2 \right\} \tag{12a}$$

If a value of χ^2_{smooth} is obtained for either the forward + nadir or aftward + nadir set (or both), and if either of these values exceeds 4, the subregion is considered unacceptable for aerosol retrieval, for the wavelength band which is being examined.

3.3.8.2.10 Angle-to-angle correlation evaluation

The angle-to-angle correlation mask is designed to detect features which result in poor correlation of the equivalent reflectance spatial distribution from one view angle to another, e.g. a cloud within a subregion that may have been missed by the RCCM or SDCM. This algorithm is unique in that it makes use of the 4 x 4 arrays of 275-m red band equivalent reflectances in each 1.1-km subregion which has survived previous tests. Poor correlation results in subregions being eliminated from aerosol processing, but *not* from surface processing.

The first step is to generate a camera-averaged "template" 4 x 4 image from the 275-m red band data for subregions which have not been eliminated by previous tests. The equivalent reflec-

tance of pixel *i, j* in the template image, $\rho_t(i, j)$, is calculated to be a data quality-weighted average of the equivalent reflectances of all cameras, where the RDQI corresponds to each 275-m sample. That is, we calculate:

$$\rho_t(i, j) = \frac{\sum\limits_{k} w_k(i, j)\rho_k(i, j)}{\sum\limits_{k} w_k(i, j)} \tag{13}$$

where the sum over *k* refers to the available cameras, $\rho_k(i, j)$ is the equivalent reflectance in pixel *i, j* for the kth camera, and $w_k(i, j) = 1$ if the RDQI associated with $\rho_k(i, j)$ is $\leq RDQI_4$; otherwise $w_k(i, j) = 0$. If the denominator in Eq. (13) is zero, that is, all cameras have $RDQI > RDQI_4$ in a particular pixel, the value of $\rho_t(i, j)$ is undefined. This does not matter because in the following steps of the algorithm, pixels for which the $RDQI > RDQI_4$ are not included. We presently set $RDQI_4 = 1$.

We now compute the correlation between the 4 x 4 subregion image of each camera to the template image. For each camera, the variance and covariance are calculated as follows:

$$\sigma_k^2 = \langle \rho_k^2 \rangle - \langle \rho_k \rangle^2$$

$$\sigma_t^2 = \langle \rho_t^2 \rangle - \langle \rho_t \rangle^2$$

$$\sigma_{kt}^2 = \langle \rho_k \rho_t \rangle - \langle \rho_k \rangle \langle \rho_t \rangle \tag{14}$$

where the subscript *k* refers to camera *k*, the subscript *t* refers to the template, and the angle brackets indicate a spatial average, computed over the 4 x 4 array of pixels. A straight (unweighted) average is calculated; however, the averaging includes only those pixels for which $RDQI \leq RDQI_4$. Then, the square of the normalized cross-correlation is calculated as follows:

$$C = \frac{\sigma_{kt}^2 \cdot |\sigma_{kt}^2|}{\sigma_k^2 \cdot \sigma_t^2} \tag{15}$$

Note that the sign of the covariance between the two windows is preserved in Eq. (15). If there is a high correlation between the equivalent reflectance distribution between the camera *k* and the template, *C* will take on values close to 1. Anti-correlation results in negative values of *C*. The criterion for accepting a camera in the subsequent retrievals is that the value of *C* must exceed a threshold value C_{thresh}. This threshold value is currently set to 0.25 based on experience with this algorithm using in-flight data. If the test fails for any camera, the entire subregion is eliminated.

Note that if the denominator of Eq. (15) is zero or close enough to zero to cause a computational problem (this can occur if the equivalent reflectances distributions are uniform), the correlation test is considered to be passed for the affected cameras.

3.4 THEORETICAL DESCRIPTION: STAGE 2 RETRIEVAL PROCESSING

Figure 4 shows those processes which occur at the DAAC prior to the actual aerosol retrievals, in which the processing pathway is chosen dependent on the scene content (referred to as Stage 2). As a first step, input from the Ancillary Geographic Product is used to check the suitability of subregions for application of the dark water retrieval algorithm. If at least one such subregion has passed through the contamination filters in Stage 1, the dark water algorithm is used. Otherwise, a test for the presence of DDV will be initiated, using a vegetation index calculated from TOA equivalent reflectances. Values above a certain threshold will provide a reasonable indicator of the presence of DDV. If no suitable DDV samples are found, the heterogeneous land path is chosen. The latter path is dependent on the presence of a sufficient amount of spatial contrast in the scene. This is evaluated during application of the algorithm by checking the magnitudes of the eigenvalues. If insufficient contrast is present, the region is flagged as unsuitable for further retrieval processing.

In the following sections, the physical basis of the processes which occur during Stage 2 processing is described, and a mathematical description of the algorithm which is used to implement each process is presented.

3.4.1 Determine minimum equivalent reflectances

3.4.1.1 Physics of the problem

The purpose of this process is to constrain the upper bound of spectral optical depth. For each 17.6 km square region composed of 1.1-km samples, the first step is to find the smallest observed equivalent reflectance for each spectral band at each camera angle. The darkest samples in the region will be used to constrain the maximum allowable amount (in terms of optical depth) of a given type of aerosol; a greater amount of that type of aerosol would require the physical impossibility of negative surface reflectivities in order to reproduce the observed TOA equivalent reflectance (see §3.5.4). Knowledge of the minimum spectral equivalent reflectances obviously provides a useful constraint on later steps in the aerosol retrieval process and the resulting maximum optical depths are themselves valuable indicators of maximum aerosol amount and are archived as part of the retrieval product.

3.4.1.2 Mathematical description of the algorithm

The algorithm finds the minimum equivalent reflectances in the four spectral bands at each camera angle in a region of 16 x 16 samples, each 1.1 km in size, ignoring contaminated samples.

Simple inequality tests are used.

3.4.2 Search for Dense Dark Vegetation (DDV) subregions

3.4.2.1 Physics of the problem

This algorithm has not been implemented. Processing currently proceeds directly to the heterogeneous land algorithm for non-dark water areas.

The identification of DDV samples within a given land region can be accomplished by comparing its computed vegetation index to a threshold value. A common vegetation index, the Normalized Difference Vegetation Index (NDVI) can be defined for MISR wavelengths as

$$\text{NDVI} = \frac{\rho_4 - \rho_3}{\rho_4 + \rho_3} \tag{16}$$

where ρ_4 is the near-infrared equivalent reflectance (band 4) and ρ_3 is the red equivalent reflectance (band 3). In general the two wavelengths straddle the photosynthetic absorption edge so that ρ_3 is significantly smaller than ρ_4 for DDV. Therefore, if the two equivalent reflectances are measured in the absence of atmospheric effects, e.g., at ground level, the NDVI is close to unity for dense, dark vegetation (DDV). Here, DDV is defined such that any direct ground reflectance is completely obscured by the vegetation and that the strong photosynthetic absorption at the red wavelength guarantees a very low reflectance compared to the near-infrared.

If the equivalent reflectance measurements ρ_4 and ρ_3 are made from a spacecraft instead of at ground level, then the inevitable atmospheric contamination of both equivalent reflectances will modify the value of the NDVI when compared to the ground level value. The atmosphere-contaminated NDVI for a given DDV site is generally smaller than the corresponding ground level NDVI, due mainly to the atmospheric path radiance contribution to the measured equivalent reflectance at the red wavelength. In general, NDVI will decrease as view zenith angle increases for DDV, due to the increased atmospheric contribution. This characteristic forms the basis of an algorithm to estimate the value of NDVI that would have been observed in the absence of the atmosphere. Martonchik [30] showed that when NDVI is plotted as a function of $1/\mu$, where μ is the cosine of the view zenith angle, and the curves are extrapolated to the hypothetical geometry $1/\mu = 0$, the extrapolated NDVI values are in good agreement with the values obtained in the absence of atmospheric contamination. These studies were based on simulations using measured surface-level directional reflectances in the red and near-infrared [21], [23], coupled with radiative transfer calculations for a variety of aerosol optical depths and scattering functions. This extrapolated NDVI, in conjunction with a threshold value, will be used as the means of detecting DDV samples. Relative to other atmospherically-insensitive indices such as ARVI (Atmospherically Resistant Vegetation Index) [20] which also includes a measurement at a blue wavelength, and the Global Environmental Mon-

itoring Index, GEMI *[40]*, which is derived from non-linear combinations of red and near-infrared equivalent reflectances, the extrapolated NDVI is based upon the definition of the index as used routinely by the surface community, thus providing a historical continuity.

3.4.2.2 Mathematical description of the algorithm

Beginning with Eq. (2), it can be shown in a mathematically formal sense (e.g., through the method of successive orders of scattering) that

$$\lim_{1/\mu \to 0} \rho^{atm} \to 0$$

$$\lim_{1/\mu \to 0} T \to 0 \tag{17}$$

where ρ^{atm} is the atmospheric path equivalent reflectance and, therefore

$$\lim_{1/\mu \to 0} \rho_\lambda = \lim_{1/\mu \to 0} \frac{1}{\pi} \int_0^1 \int_0^{2\pi} R^{surf}(-\mu, \mu', \phi - \phi') \rho^{inc}(\mu', \mu_0, \phi' - \phi_0) \mu' d\mu' d\phi' = \lim_{1/\mu \to 0} \rho_\lambda^{surf} \tag{18}$$

where we have replaced radiances by equivalent reflectances. Using Eq. (18), we then can re-express Eq. (16) as

$$\lim_{1/\mu \to 0} \text{NDVI} = \lim_{1/\mu \to 0} \frac{\rho_4^{surf} - \rho_3^{surf}}{\rho_4^{surf} + \rho_3^{surf}} = \lim_{1/\mu \to 0} \frac{\rho_4 - \rho_3}{\rho_4 + \rho_3} \tag{19}$$

in which the surface-leaving equivalent reflectances are replaced by TOA equivalent reflectances.

Since μ is physically restricted to values less than or equal to unity ($\mu = 1$ implies a nadir view), there can be no physical measurement of NDVI (or ρ) corresponding to $1/\mu = 0$. It is, however, possible (and practical) to extrapolate the measured NDVI to its value in the limit as $1/\mu$ approaches 0. Equation (19) implies that the NDVI derived from TOA equivalent reflectances have the same value in the limit as $1/\mu$ approaches 0 as those derived from surface-leaving radiances. Furthermore, for lambertian surfaces the value of surface NDVI is independent of μ, and for near-nadir geometries a near-view angle-independence is representative of natural surfaces as well. Thus, the value of extrapolated NDVI (i.e., NDVI at $1/\mu = 0$), obtained from TOA equivalent reflectances, is basically independent of the atmospheric condition including aerosol properties. For further details, see Martonchik *[30]*.

In practice, the extrapolation to $1/\mu = 0$ is performed by fitting a quadratic in NDVI vs. $1/\mu$.

A quadratic is fit to all forward cameras (including the nadir camera) with acceptable data, and the slope of the fit at $1/\mu = 1$ is then used to linearly extrapolate to $1/\mu = 0$. This requires valid data in bands 3 and 4, in at least three forward cameras. A quadratic fit is also done for all aftward cameras (including the nadir camera) with acceptable data, and the linear extrapolated to $1/\mu = 0$ is done. This requires valid data in bands 3 and 4, in at least three aftward cameras. If extrapolated NDVI values are obtained for both the forward and the aftward camera sets, then the two values are averaged, to get a final extrapolated NDVI value. If only one is obtained, this one value is used. Then, the samples which are classified as DDV are those for which the final extrapolated NDVI is > NDVI$_{thresh}$. The adopted value for the threshold, NDVI$_{thresh}$, is 0.75.

3.4.3   Calculate empirical orthogonal functions (heterogeneous land)

3.4.3.1   Physics of the problem

The concept behind this step of the heterogeneous land aerosol retrieval is to constrain the angular shape of the surface-leaving radiation field *[28]*. The constraints to be derived at this stage of the processing take the form of empirical orthogonal functions (EOF's), determined from an analysis of the angular shape characteristics of the TOA equivalent reflectances of the various heterogeneous samples in the region for which the retrieval is being done. The heterogeneous land retrieval algorithm then uses these EOF's to represent the sample-averaged surface-leaving reflectances for the region. Since the sample-averaged TOA equivalent reflectance is dependent on both the sample-averaged surface-leaving reflectance and the atmospheric path radiance this processing step serves as a precursor to the solution for the best-fitting aerosol model, described below. This section also describes the procedure used to establish whether there is sufficient spatial contrast in the scene to proceed with the heterogeneous land algorithm.

3.4.3.2   Mathematical description of the algorithm

Regions 17.6 km x 17.6 km in size (i.e., 16 x 16 1.1-km samples) are analyzed under the assumption that 1-D radiation transfer, described by Eq. (2), is valid. The EOF's required to implement the heterogeneous land aerosol retrieval are the eigenvectors associated with the real, symmetric scatter matrix constructed from reduced sample equivalent reflectances, defined to be sample TOA equivalent reflectances minus the sample-averaged TOA equivalent reflectance. This subtraction removes the atmospheric path radiance, which is assumed to be the same for each sample in the region. The construction of the EOF's is done on each spectral band individually. Calculation of the EOF's and application of the subsequent retrieval algorithm is done for all available bands for which certain conditions are met. For each band individually we require:

(1) That the subregions used in the retrieval must be viewed in common by all available cameras, and that the common number of subregions is ≥ 64;

(2) That all subregions used in the retrieval must be viewed by at least two forward-looking cameras, of which at least one is Cf or Df and of which at least one is Af or Bf, and at least two aftward-looking cameras, of which at least one is Ca or Da and of which at least one is Aa or Ba.

If these conditions are met, these subregions and cameras are used in the EOF calculation and in the retrieval. However, if the common number of subregions is < 64 for all of the available cameras, drop all available D cameras, and check to see that requirement (2) is still satisfied, and that requirement (1) is now satisfied. If so, these subregions and cameras are used in the EOF calculation and retrieval. Otherwise, this band is not used. Note that in applying the above logic, it is allowable for a different set of subregions and cameras to be selected for band i than are used in band j.

First, compute each reduced sample equivalent reflectance at location x, y for each camera view angle,

$$J_{x, y}(\mu, \mu_0, \phi - \phi_0) = \rho_{x, y}(\mu, \mu_0, \phi - \phi_0) - \rho_{bias}(\mu, \mu_0, \phi - \phi_0) \tag{20}$$

where ρ_{bias} denotes an offset equivalent reflectance, which is established to be the minimum value over all the samples in the region, for each channel individually. Each $J_{x, y}$ then is a sample-dependent linear combination of the spatially variable component of the TOA sample equivalent reflectance, called surface functions [see Eq. (70)]. The scatter matrix [41] then is defined as

$$C_{ij} = \frac{1}{N_{sub}} \sum_{x, y} J_{x, y, i} \cdot J_{x, y, j} \tag{21}$$

where the indices i and j are used to denote the viewing geometry and N_{sub} is the number of summed-up subregions. The scatter matrix is a N_{cam} x N_{cam} element array, where N_{cam} is the number of available cameras (nominally, 9) in the particular spectral band being analyzed, with μ_i, ϕ_i defining the view geometry of MISR camera i. The eigenvectors of C are solutions to the eigenvector equation given by

$$\sum_{j = 1}^{N_{cam}} C_{ij} \cdot f_{j, n} = \lambda_n \cdot f_{i, n} \tag{22}$$

where λ_n is the eigenvalue (real and positive) of $f_{i, n}$. In general there will be N_{cam} eigenvalue and eigenvector solutions with the N_{cam}-element eigenvectors forming an orthonormal set, i.e.,

$$\sum_{i=1}^{N_{cam}} f_{i,n} \cdot f_{i,m} = \delta_{nm} \tag{23}$$

where δ_{nm} is the Kronecker delta. Thus, every N_{cam}-element vector $J_{x,y}$ can be expanded in terms of this orthonormal set as

$$J_{x,y,i} = \sum_{n=1}^{N_{cam}} A_n{}^{x,y} \cdot f_{i,n} \tag{24}$$

where $A_n{}^{x,y}$ are the principal components,

$$A_n{}^{x,y} = \sum_{i=1}^{N_{cam}} J_{x,y,i} \cdot f_{i,n} \tag{25}$$

obtained by applying the orthonormality condition of Eq. (23) to Eq. (24).

The eigenvectors are ordered according to the magnitude of the corresponding eigenvalues, i.e., $\lambda_1 > \lambda_2 > ... > \lambda_{N_{cam}}$. The set of vectors f is the optimum basis function set to represent the vectors $J_{x,y}$ in the sense that if only the $N < N_{cam}$ eigenvectors are used in the expansion, then the resulting error e is a minimum when compared to the error using first N vectors from a different vector basis function set. The error is defined as

$$e = \frac{1}{N_{sub}} \sum_{x,y} \sum_{i=1}^{N_{cam}} \left(J_{x,y,i} - \sum_{n=1}^{N} A_n{}^{x,y} \cdot f_{i,n} \right)^2$$

$$= \frac{1}{N_{sub}} \sum_{x,y} \sum_{i=1}^{N_{cam}} \left(\sum_{n=N+1}^{N_{cam}} A_n{}^{x,y} \cdot f_{i,n} \right)^2 = \sum_{n=N+1}^{N_{cam}} \lambda_n \tag{26}$$

This basis function set should also be the optimum orthonormal set to expand the sample-averaged TOA equivalent reflectance minus the atmospheric path term since all reduced equivalent reflectances are composed of the same surface functions as expressed in Eq. (70). Further discussion, and a demonstration of this technique using Advanced Solid-state Array Spectroradiometer (ASAS) aircraft data is given in *[31]*.

To determine if there is sufficient contrast among the subregions used in the retrieval, the following procedure is used. Since it follows from Eq. (26) that

$$\frac{1}{N_{sub}}\sum_{x,y}\sum_{i=1}^{N_{cam}}[J_{x,y,i}]^2 = \frac{1}{N_{sub}}\sum_{i=1}^{N_{cam}}\sum_{x,y}[J_{x,y,i}]^2 = \sum_{n=1}^{N_{cam}}\lambda_n \qquad (27)$$

where $J_{x,y,i}$ is defined by Eq. (20), then if $J_{x,y,i}$ consists of random noise only, (i.e., $J_{x,y,i} = n_{x,y,i}$, such that the region is homogeneous in equivalent reflectance), then

$$\sum_{i=1}^{N_{cam}}\sigma_{noise,i}^2 = \sum_{n=1}^{N_{cam}}\lambda_n \qquad (28)$$

where N_{sub} is the number of subregions being used and

$$\sigma_{noise,i}^2 = \frac{1}{N_{sub}}\sum_{x,y}[n_{x,y,i}]^2 \qquad (29)$$

Now, if we let the random component of the noise in the average equivalent reflectance $\langle\rho_i\rangle$ in camera i be given by

$$\sigma_{noise,i} = \frac{\langle\rho_i\rangle}{SNR_i} \qquad (30)$$

where SNR_i is the signal-to-noise ratio in camera i at equivalent reflectance level $\langle\rho_i\rangle$, then there is sufficient scene contrast above the level of instrument noise if

$$\frac{\displaystyle\sum_{n=1}^{N_{cam}}\lambda_n}{\displaystyle\sum_{i=1}^{N_{cam}}\sigma_{noise,i}^2} \geq T \qquad (31)$$

where T is a threshold value for adequate contrast above the level of the noise. We set T to 5. If Eq. (31) is not satisfied, the heterogeneous land aerosol retrieval algorithm is not applied.

The value of $\sigma_{noise,i}$ to be used in Eq. (31) is determined by reading the table of SNR_{am} from the ARP for averaging mode $am = 4x4$, at the nominal 15 values of equivalent reflectance level, and in the appropriate channel. The SNR is then interpolated linearly to obtain a value at $\langle\rho_i\rangle$, and Eq. (30) is applied.

43

3.4.4   Determine band-differenced optical depth (heterogeneous land)

3.4.4.1   Physics of the problem

This algorithm is not currently implemented.

This step provides a constraint on the spectral variation of aerosol optical depth (and aerosol type) using the high resolution equivalent reflectances corrected for ozone optical depth. The basis of this approach is that at sub-kilometer resolution, over regions of heterogeneous reflectance, 3-D radiative transfer theory applies [i.e., Eq. (1)]. The radiance field reaching MISR consists of several components, and only the component which corresponds to surface-leaving radiances attenuated by the angle-dependent direct atmospheric transmittance will contain spatial contrasts. That is, over these spatial scales diffusely scattered upwelling radiation will be horizontally uniform. This means that differences in TOA equivalent reflectances from adjacent samples depend only on the direct field, and contain the product of the angular dependence of the surface reflectance difference and the atmospheric transmittance, the latter term described by Beer's law. Ratioing these differences at two wavelengths where the angular shape of the surface reflectances are expected to be similar then permits solution for the difference in optical depth between the two wavelengths. Subtracting off the Rayleigh portion leaves the column aerosol contribution. This method will be applied to the 1 x 1 and 1 x 4-averaged samples occurring within each 17.6 km x 17.6 km region.

3.4.4.2   Mathematical description of the algorithm

This algorithm is described in *[6]* and is based on the 3-D radiative transfer regime which is appropriate for high resolution data, and is to be applied in the crosstrack direction to unaveraged and 1 x 4-averaged data. We now define the surface hemispherical directional reflectance factor, r:

$$r_{x,y}(-\mu, \mu_0, \phi - \phi_0) = \frac{1}{E(\mu_0)} \int_0^1 \int_0^{2\pi} R_{x,y}^{surf}(-\mu, \mu', \phi - \phi') L^{inc}(\mu', \mu_0, \phi' - \phi_0)\mu' d\mu' d\phi' \qquad (32)$$

where E is the surface irradiance. Finally, we define the top-of-atmosphere bidirectional reflectance factor R by $R = \pi L/(\mu_0 E_0)$, where E_0 is the exo-atmospheric solar irradiance. Taking differences of adjacent pixels in the crosstrack direction, applying the assumption that at sub-kilometer resolution the first and third terms on the right-hand-side of Eq. (1) are either spatially uniform or slowly varying, and using Eq. (32):

$$R_{x, y+1}(\mu, \mu_0, \phi-\phi_0) - R_{x, y}(\mu, \mu_0, \phi-\phi_0) = \hat{R}_{x, y}(\mu, \mu_0, \phi-\phi_0)$$

$$= \frac{E(\mu_0)}{\mu_0 E_0}\hat{r}_{x, y}(-\mu, \mu_0, \phi-\phi_0)\exp(-\tau/\mu) \tag{33}$$

where the caretted symbols indicate pixel differences. Considering Eq. (33) at two wavelengths, λ and λ_0, and taking the ratio, we have

$$\frac{\hat{R}_{x, y, \lambda}}{\hat{R}_{x, y, \lambda_0}} = \exp(-\Delta\tau/\mu) \cdot \frac{[E(\mu_0)/E_0]_\lambda}{[E(\mu_0)/E_0]_{\lambda_0}} \cdot \frac{\hat{r}_{x, y, \lambda}(-\mu, \mu_0, \phi-\phi_0)}{\hat{r}_{x, y, \lambda_0}(-\mu, \mu_0, \phi-\phi_0)} \tag{34}$$

where $\Delta\tau = \tau(\lambda) - \tau(\lambda_0)$. If the surface reflectances (both angular shape and spatial pattern) are highly correlated, the ratio of the reflectance factor fields can be modeled as a constant, independent of spatial location and view angle, in which case Eq. (34) simplifies to

$$\hat{R}_{x, y, \lambda} = a \cdot \exp(-\Delta\tau/\mu)\hat{R}_{x, y, \lambda_0} \tag{35}$$

Hence, $a \cdot \exp(-\Delta\tau/\mu)$ is the slope, s, of the line formed by plotting $\hat{R}_{x, y, \lambda}$ against $\hat{R}_{x, y, \lambda_0}$. In order to apply this algorithm, we require that the cross correlation coefficient, C, exceeds a threshold value, C_{thresh}. The cross correlation coefficient is defined in Eqs. (14) and (15), except that we use $\hat{R}_{x, y, \lambda}$ and $\hat{R}_{x, y, \lambda_0}$ rather than ρ_k and ρ_t in the calculation of the variances and covariances. We require $C_{thresh} \geq 0.95$. Additionally, we require $s > 0$. If either of these conditions is violated, this algorithm is not implemented.

After finding s, we can solve for $\Delta\tau$, the y-intercept of the line:

$$-\mu\ln(s) = \Delta\tau - \mu\ln(a) \tag{36}$$

Applying this method to MISR bands 1 and 3 yields a value of $\Delta\tau$ which is determined by the aerosol type and amount.

Testing this theory on ASAS aircraft data, we find that the relation predicted by Eq. (36) is not exactly linear, and also shows some difference between the forward and aftward views. This leads us to conclude that the assumption made in Eq. (35), that the ratio of the surface reflectances from the two different wavelengths is a constant, is not strictly true. To account for this, suppose that instead of being a constant, the ratio of the reflectances were a low-order polynomial in μ, $P(\mu)$, again independent of spatial position. Then Eq. (36) becomes:

$$-\mu\ln(s) = \Delta\tau - \mu\ln[P(\mu)] \tag{37}$$

45

with the right-hand side approaching $\Delta\tau$ as $\mu \to 0$. Equation (37) should become more nearly linear for μ close to 0. Therefore, instead of fitting a single straight line simultaneously to all angles, we use only the data at the two highest view angles (i.e., smallest values of μ), independently for the forward and aftward branches. These extrapolations provide upper and lower bounds on $\Delta\tau$ and we interpret the difference as a measure of the uncertainty in $\Delta\tau$ derived using this approach.

Note that the value of $\Delta\tau$ determined using the above method refers to the spectral difference in column optical depth, which includes all scatterers and absorbers in the column, with the exception of ozone, for which a correction has been made prior to this processing step. Thus, it is necessary to subtract from $\Delta\tau$ the value corresponding to Rayleigh scattering in order to obtain a value corresponding to the spectral optical depth difference for the column aerosol. That is, we report the aerosol component of the band-differenced optical depth from

$$\Delta\tau_a = \Delta\tau - \Delta\tau_R \tag{38}$$

where $\Delta\tau_R = \tau_R(\lambda) - \tau_R(\lambda_0)$, and the Rayleigh optical depth at each of the two wavelengths is calculated according to Eq. (21) of *[M-11]*. The wavelengths used are the $\lambda_{m,\,solar,\,b}^{std,\,in-band}$ values for bands 1 and 3 obtained from the ARP.

In summary, the algorithm works as follows:

(1) Beginning with the Df camera, take differences of the BRF's in adjacent pixels in the crosstrack direction to form the set $\hat{R}_{x,\,y,\,1}$ and $\hat{R}_{x,\,y,\,3}$ for bands 1 and 3, respectively. Eliminate any values for which either of the BRF's in the adjacent pixel differences have RDQI > RDQI$_5$. We set RDQI$_5$ = 0.

(2) Retain only those values of $\hat{R}_{x,\,y,\,1}$ and $\hat{R}_{x,\,y,\,3}$ that correspond to the same spatial locations. Since the algorithm is applied to MISR data in 1x4 summing mode, there will be at most 63 difference values for each of 16 rows within a 17.6-km region. If the number of values of $\hat{R}_{x,\,y,\,1}$ and $\hat{R}_{x,\,y,\,3}$ to be correlated is less than 100, do not continue further with this algorithm.

(3) Repeat steps (1) and (2) for the Cf, Da, and Ca cameras. If the amount of available data in any of these four cameras falls below the threshold established in step (2), this algorithm is not applied.

(4) Establish the four slope values s_{Df}, s_{Cf}, s_{Da}, and s_{Ca} by regressing $\hat{R}_{x,\,y,\,1}$ (on the ordinate) against $\hat{R}_{x,\,y,\,3}$ (on the abscissa) at each angle. If any of the regressions do not satisfy the correlation coefficient threshold test, do not proceed further with the algorithm.

(5) Apply Eq. (36) to s_{Df} and s_{Cf} to obtain a value of $\Delta\tau_{forward} = \tau_1 - \tau_3$ corresponding to the forward cameras.

(6) Apply Eq. (36) to s_{Da} and s_{Ca} to obtain a value of $\Delta\tau_{aftward} = \tau_1 - \tau_3$ corresponding to the aftward cameras.

(7) Remove the Rayleigh contribution from the optical depth difference estimates.

(8) Report the resulting bounds on $\Delta\tau_a$ in the Aerosol/Surface Product.

Although this algorithm is not presently envisioned to be used as a constraint on the retrievals during routine processing, it will provide useful information as part of post-retrieval data analysis in helping to distinguish between different aerosol models which, based on the criteria applied during the retrievals, were equally viable candidates in fitting the MISR observations.

3.5 THEORETICAL DESCRIPTION: STAGE 3 RETRIEVAL PROCESSING

During this stage, aerosol retrievals are performed for the various 17.6-km x 17.6-km regions. Retrievals consist of determining the "goodness of fit" of a set of aerosol models to the MISR observations, based on a set of criteria described below. The set of candidate models is established by referencing the Aerosol Climatology Product, and each in turn is compared with the MISR data. The processing steps described in §3.5.3 through §3.5.8 are repeated for each aerosol model to be tested during the retrieval. The retrieval results, including goodness-of-fit parameters and other retrieval flags, will be reported in the Aerosol/Surface Product for all candidate models. However, only those models for which the goodness-of-fit parameters satisfy pre-established criteria are deemed "successful" retrievals. Whether a single model or multiple models provide suitable fits to the data depends on the ambient atmospheric conditions, the view and solar geometry, and the completeness of the ACP and SMART databases. Among the successful models, the minimum and maximum optical depths provide a measure of uncertainty of the "best estimate" optical depth reported in the Aerosol/Surface Product.

During retrievals, MISR band 2 (green) is used as a reference band. This means that when stepping through various values of optical depth to find the best-fitting value for a particular aerosol model, the band 2 optical depth is the independent variable. Optical depths in the other MISR bands are appropriately scaled, using the spectral extinction cross sections of the models contained in the ACP. Band 2 is used because its effective wavelength (558 nm) is closest to the reference wavelength commonly used by the aerosol community. After retrievals are performed, optical depth results are reported for this band. The user may convert the reported optical depths to other bands by making use of the spectral extinction cross section data contained in the ACP.

3.5.1 Establish equivalent reflectances for retrieval

3.5.1.1 Physics of the problem

This step involves establishing the equivalent reflectances corresponding to the MISR observations that will be used during the retrievals. The methodology depends on the retrieval pathway

chosen in Stage 2. The dark water and DDV situations are handled similarly, whereas the hetero-geneous land case involves a different strategy. This is because in applying the retrieval algorithms, the equivalent reflectances from all suitable dark water or DDV 1.1-km subregions are combined together (by taking a median), whereas for heterogeneous land the mean (calculated during the process of establishing EOF's) are used.

3.5.1.2   Mathematical description of the algorithm

3.5.1.2.1   *Dark water*

This retrieval pathway uses all available cameras in bands 3 and 4. For a given channel, all subregion equivalent reflectances which have survived the contamination screens are used to find the minimum equivalent reflectance for that channel, as described in §3.4.1. As many channels out of the maximum possible value of 18 (2 bands x 9 angles) which have a minimum equivalent reflectance associated with them are used in the retrieval. The minimum allowable number of channels is 1.

3.5.1.2.2   *Dense dark vegetation*

The same approach is used for DDV as is used for dark water, except that bands 1 and 3 are used. The minimum allowable number of channels is 2.

3.5.1.2.3   *Heterogeneous land*

For the heterogeneous land retrieval algorithm, the retrieval incorporates a selectable set of bands and the common subregions between cameras as determined in §3.4.3 for the calculation of the EOF's. Using those criteria, and requiring a minimum of one spectral band, the minimum allowable number of channels in order to perform a retrieval is 4. A spatial average of the subregion equivalent reflectances within each camera and band is needed by the algorithm.

3.5.2   Establish aerosol models

The aerosol models to be compared with MISR observations during the retrievals consist of tropospheric models generated from mixtures of the pure particles contained in the ACP, plus fog, cirrus, and a stratospheric aerosol. The ACP also defines which mixtures are to be used for each of the aerosol retrieval pathways (dark water, DDV, heterogeneous land). Each tropospheric mixture contains up to three pure particles, and the relative abundances are specified in the ACP. Tropospheric aerosols are divided into marine and continental, and each of these two groupings is subdivided into four categories: clean, industrial, carbonaceous (biomass burning), and dusty. All maritime mixtures contain accumulation mode 1 sulfate and accumulation mode sea salt plus a third component which is either coarse mode sea salt, black carbon (soot), carbonaceous (biomass burn-

ing) aerosol, or accumulation mode mineral dust. All continental mixtures contain accumulation mode 1 sulfate and accumulation mode mineral dust plus a third component which is either black carbon (soot), carbonaceous (biomass burning) aerosol, or coarse mode mineral dust.

Relative abundances of the components are defined in the ACP in terms of fraction of total optical depth (*not* by numbers of particles). Since these relative abundances are wavelength and relative humidity dependent, due to the dependence of extinction cross section on wavelength and RH, the ACP provides the fractional optical depth mixing ratios at each relative humidity and wavelength. The ACP also provides information on which mixtures are to be used in conjunction with each aerosol retrieval pathway.

3.5.3   Determine model TOA equivalent reflectances

3.5.3.1   Physics of the problem

This section describes how the model TOA equivalent reflectances used as the basis of the aerosol retrievals are calculated. A principal input to this process is the SMART Dataset, which contains information on a standard optical depth grid. This grid is identical in all four MISR bands. The model TOA equivalent reflectances described in this section are calculated at each wavelength used in the retrievals on this optical depth grid. Once this set of values has been established, they will then be interpolated to a finer optical depth grid for the purpose of computing the residuals between the model and observed TOA equivalent reflectances as a function of optical depth, in order to find the optical depth that minimizes these residuals for each aerosol model. This interpolation and the calculation of the residuals are described later, in §3.5.5.

3.5.3.1.1   *Dark water*

For aerosol models consisting of the pure particles contained in the ACP, components of the TOA equivalent reflectances are obtained from the SMART Dataset, with the surface component provided using an assumed wind-speed-driven glitter and whitecap model. It is then required to interpolate the data in the SMART Dataset to the correct observing and illumination geometry.

For aerosols comprised of mixtures of several pure particle types, calculations based on the SMART Dataset input are required to establish the TOA equivalent reflectances. These are obtained during the retrievals, using a modified form of linear mixing theory. Standard linear mixing states that TOA equivalent reflectance for a mixture of particles having a particular total optical depth can be approximated by summing the TOA equivalent reflectances for the individual aerosol components, evaluated at the total optical depth value, but weighted in the summation by that component's relative abundance (as a fraction of the total extinction optical depth). This approximation is exact in the single-scattering limit, and works well for multiple scattering mixtures of conservatively and mildly absorbing particles. However, when a component is highly absorbing, the linear

49

mixing approximation consistently overestimates the TOA equivalent reflectances. To account for this, a new method has been developed, which generalizes linear mixing to include absorbing particles.

3.5.3.1.2   Dense dark vegetation

Because of the low reflectance (a few percent) of DDV in the visible portion of the spectrum, Kaufman and Sendra *[19]* suggested the use of such surfaces as a controlled background for aerosol retrievals. Because of the multi-angle imaging strategy of MISR, an extension of this approach is required, in which not only the surface albedo, but shape of the bidirectional reflectance distribution function is specified.

Retrievals over surfaces identified as containing DDV require calculation of the TOA equivalent reflectances corresponding to an assumed surface bidirectional reflectance model. The radiative transfer calculations required to account for reflectance from the surface and scattering between the atmosphere and surface are performed during the retrieval processing. It is well established that vegetated surfaces reflect radiation anisotropically. The angular shape of the radiation field depends on the optical properties of the scatterers (leaves, stems) as well as on the geometric structure. A number of approaches have been taken to develop models of the surface anisotropy, including physically-based as well as empirical methods (see *[49]* for references). For the purposes of the MISR aerosol retrieval, the model is to be used solely as a lower boundary condition for the radiative transfer calculations, and it is immaterial for this application whether a physical or empirical representation is used, as long as the model is an accurate representation of DDV angular reflectance.

Once the required radiative transfer calculations are performed, the steps involving interpolation and mixing of aerosols follow a similar methodology as for the dark water case.

3.5.3.1.3   Heterogeneous land

The heterogeneous land retrieval approach makes use of the black surface radiation fields provided in the SMART Dataset, interpolated to the appropriate geometries. Modified linear mixing theory is used to generate aerosol mixtures.

3.5.3.2   Mathematical description of the algorithm

3.5.3.2.1   Pure aerosol TOA equivalent reflectance calculations

As described above, the required pure aerosol TOA equivalent reflectances for the dark water and heterogeneous land retrieval pathways are obtained from the SMART Dataset. In the DDV case, additional radiative transfer calculations must be performed.

The model used to describe the DDV surface bidirectional reflectance factor is that of Rahman et al. *[43]*:

$$R^{surf}(-\mu, \mu_0, \phi - \phi_0) = r_0[\mu_0\mu(\mu + \mu_0)]^{k-1} \cdot \frac{(1 - g^2)}{[1 + g^2 - 2g\cos\Omega]^{3/2}} \cdot \left[1 + \frac{1 - r_{0,hot}}{1 + G}\right] \quad (39)$$

where Ω is the scattering angle, defined by Eq. (11) and the geometric factor G is given by

$$G = \left\{\left(\frac{1}{\mu^2} - 1\right) + \left(\frac{1}{\mu_0^2} - 1\right) + 2\left[\sqrt{\left(\frac{1}{\mu^2} - 1\right)\left(\frac{1}{\mu_0^2} - 1\right)}\right]\cos(\phi - \phi_0)\right\}^{\frac{1}{2}} \quad (40)$$

Note that the definition of G differs slightly from *[43]* due to the different conventions in the definition of $\phi - \phi_0$ that we use, and that we cast the equations in terms of scattering angle, whereas *[43]* uses phase angle. The three adjustable parameters in Eq. (39) are the variables r_0, k, and g. The last term on the right hand side of Eq. (39) is included to model the "hot spot" for vegetation canopies, i.e., the brightness increase which occurs near scattering angles of 180° (backscatter); the value of r_0 included in this term, denoted $r_{0,hot}$, is set to the fixed value of 0.015. For DDV retrievals, the variables k and g are pre-specified, whereas r_0 is permitted to vary (within limits) along with the optical depth of each aerosol model. Thus, it is convenient to let

$$R^{surf}(-\mu, \mu_0, \phi - \phi_0) = r_0\hat{R}^{surf}(-\mu, \mu_0, \phi - \phi_0) \quad (41)$$

where $\hat{R}^{surf}$ represents a normalized BRF that describes the angular shape. Based on fits of Eq. (39) to measured *[3]*, *[21]*, *[22]*, *[23]*, *[24]* and synthetic *[12]*, *[38]* reflectance factor data sets, Engelsen et al. *[7]* recommend values for k and g of 0.5 and -0.2, respectively, with an associated variance for each of about 0.02.

To make the radiative transfer equations rapid and efficient, we assume that the surface BRF given by Eq. (39) is expandable in a Fourier series in the cosine of $\phi - \phi_0$ and that only the first two terms of this expansion contribute significantly to the radiation field diffusely transmitted from the surface to space (although the full functional form is used for directly transmitted light). Let

$$\alpha = 4\int_0^1\int_0^1 \hat{R}_0^{surf}(-\mu', \mu)\mu'\mu d\mu' d\mu \quad (42)$$

$$A(-\mu) = 2\int_0^1 \hat{R}_0^{surf}(-\mu, \mu')\mu' d\mu' \quad (43)$$

51

$$\hat{R}_0^{surf}(-\mu, \mu') = \frac{1}{2\pi} \int_0^{2\pi} \hat{R}^{surf}(-\mu', \mu, \phi' - \phi)d\phi' \tag{44}$$

In addition, we define

$$\hat{R}_1^{surf}(-\mu, \mu') = \frac{1}{\pi} \int_0^{2\pi} \hat{R}^{surf}(-\mu', \mu, \phi' - \phi)\cos(\phi' - \phi)d\phi' \tag{45}$$

We also assume that the diffuse atmospheric transmittance is expandable in a Fourier series, and only the first two terms of the expansion are retained. The mathematical representation is:

$$T(-\mu', -\mu, \phi' - \phi) \cong T_0(-\mu', -\mu) + T_1(-\mu', -\mu)\cos(\phi' - \phi) \tag{46}$$

These two terms for upward diffuse transmittance, which are functions of view and illumination zenith angles, are contained in the SMART Dataset, separated into their single- and multiple-scattered components. This distinction is used in the surface retrievals *[M-10]*. For the purpose of the aerosol retrievals, the single- and multiple-scattered components are simply added together:

$$T_0(-\mu', -\mu) = T_{0, ss}(-\mu', -\mu) + T_{0, ms}(-\mu', -\mu)$$

$$T_1(-\mu', -\mu) = T_{1, ss}(-\mu', -\mu) + T_{1, ms}(-\mu', -\mu) \tag{47}$$

Given the above definitions, the quantities α, A, $\hat{R}_0^{surf}$, and $\hat{R}_1^{surf}$ are calculated once the surface BRF is specified, that is, once k and g are established in Eq. (39). The following functions are then generated for each pure aerosol model to be used as part of the retrievals:

$$f_0(-\mu, -\mu_0) = 2\pi \int_0^1 \hat{R}_0^{surf}(-\mu, \mu')T_0(-\mu_0, -\mu')d\mu' \tag{48}$$

$$f_1(-\mu, -\mu_0) = \pi \int_0^1 \hat{R}_1^{surf}(-\mu, \mu')T_1(-\mu_0, -\mu')d\mu' \tag{49}$$

$$g_0(-\mu, -\mu_0) = 2\pi \int_0^1 T_0(-\mu, -\mu')\hat{R}_0^{surf}(-\mu_0, \mu')d\mu' \tag{50}$$

$$g_1(-\mu, -\mu_0) = \pi \int_0^1 T_1(-\mu, -\mu') \hat{R}_1^{surf}(-\mu_0, \mu') d\mu' \tag{51}$$

$$h_0(-\mu, -\mu_0) = 2\pi \int_0^1 T_0(-\mu, -\mu') f_0(-\mu', -\mu_0) d\mu' \tag{52}$$

$$h_1(-\mu, -\mu_0) = \pi \int_0^1 T_1(-\mu, -\mu') f_1(-\mu', -\mu_0) d\mu' \tag{53}$$

$$a_0(-\mu) = 2\pi \int_0^1 T_0(-\mu, -\mu') A(-\mu') d\mu' \tag{54}$$

Finally, the component of the TOA equivalent reflectance for the DDV case which includes reflections from the surface is given by

$$\rho_{surf}(-\mu, \mu_0, \phi - \phi_0) = r_0[\hat{\rho}(-\mu, \mu_0, \phi - \phi_0)] \tag{55}$$

i.e., a term which is linearly multiplied by r_0. To get the total TOA equivalent reflectance, the term in Eq. (55) must be added to the field corresponding to a black surface (the path radiance term).

To obtain an expression for $\hat{\rho}$, let e_b^{dir} and e_b^{diff} be the direct and diffuse components of the downwelling irradiance at the bottom of the atmosphere, assuming a black surface, normalized to the exo-atmospheric solar irradiance. The quantity e_b^{dir} is calculated from

$$e_b^{dir}(\mu_0) = \mu_0 e^{-\tau/\mu_0} \tag{56}$$

and e_b^{diff} is obtained from the SMART Dataset by summing the single- and multiple-scattered parts, i.e.,

$$e_b^{diff}(\mu_0) = e_{b,ss}^{diff}(\mu_0) + e_{b,ms}^{diff}(\mu_0) \tag{57}$$

Then, we have that

$$\hat{\rho}(-\mu, \mu_0, \phi - \phi_0) = e^{-\tau/\mu} e_b^{dir}(\mu_0) \hat{R}^{surf}(-\mu, \mu_0, \phi - \phi_0) +$$

$$+ \mu_0 e^{-\tau/\mu} f_0(-\mu, -\mu_0) + \mu_0 e^{-\tau/\mu} f_1(-\mu, -\mu_0) \cos(\phi - \phi_0) +$$

$$+ \mu_0 e^{-\tau/\mu_0} g_0(-\mu, -\mu_0) + \mu_0 e^{-\tau/\mu_0} g_1(-\mu, -\mu_0) \cos(\phi - \phi_0) +$$

$$+ \mu_0 h_0(-\mu, -\mu_0) + \mu_0 h_1(-\mu, -\mu_0) \cos(\phi - \phi_0) +$$

$$+ \frac{\{r_0\}\alpha s}{1 - \{r_0\}\alpha s} [e_b^{dir}(\mu_0) + e_b^{diff}(\mu_0)] \cdot [e^{-\tau/\mu} A(-\mu) + a_0(-\mu)]$$

$$(58)$$

where s is the bottom-of-atmosphere bihemispherical albedo, obtained by summing its single- and multiple-scattered components contained in the SMART Dataset. Note that the last term depends on r_0 and therefore, Eq. (55) is not strictly linear in r_0. Linearity, however, is desirable in order to make the retrievals computationally efficient. Fortunately, since the product of r_0 and s is small, the last term of Eq. (58) can be reasonably approximated by specifying a fixed value for r_0. The fixed value r_0 that is used for this purpose, denoted $\{r_0\}$, is 0.015.

3.5.3.2.2 *Nearest neighbor and interpolative assignments of parameter values*

Each region over which aerosol retrievals are performed will have a set of μ and ϕ - ϕ_0 values associated with each camera, and a single value of μ_0. For DDV retrievals, the calculations described in §3.5.3.2.1 are used to provide TOA equivalent reflectances according to Eq. (55) at these geometries directly. For dark water and heterogeneous land, multiple-scattered TOA equivalent reflectances are provided in the SMART Dataset on a predetermined geometric grid, and interpolation is necessary. The equivalent reflectance fields in the SMART Dataset are provided on a grid in μ, μ_0, and Ω, rather than μ, μ_0, and ϕ - ϕ_0. This is done so that the grid in Ω can be tailored to provide fine enough sampling in the rainbow region, where the single-scattering phase functions of large, spherical particles vary considerably. The same μ, μ_0, and Ω grid is used for all aerosol types. Because of the one-to-one correspondence between ϕ - ϕ_0 and Ω, expressed by Eq. (11), quadratic interpolation of the SMART equivalent reflectances over each of the variables μ, μ_0, and Ω provides the required data at the values of μ, μ_0, and ϕ - ϕ_0 required for a given camera.

Additional assignments of parameter values to be used in the retrievals are performed as follows:

(1) For dark water retrievals, use SMART equivalent reflectances for the wind speed which is closest to the ambient wind speed.

(2) For all retrievals, use SMART-provided quantities, which are provided at two values of atmospheric pressure, and linearly interpolate to the ambient surface pressure at the mean terrain altitude of the 17.6-km region.

3.5.3.2.3 *Aerosol mixture TOA equivalent reflectance calculations*

The retrieval process requires determination of equivalent reflectance of aerosol mixtures in terms of the equivalent reflectances of the pure particles comprising the mixture. In principle, the most exact way to do this is to perform the appropriate radiative transfer calculations for the aerosol mixture and store the results in the SMART Dataset. However, in order to provide operational flexibility in case it is determined that a different set of mixtures should be used, and to minimize the required storage space for the SMART Dataset, an approximation which requires knowledge of only the pure particle optical properties and equivalent reflectances is utilized.

The approximation used is a generalization of the linear mixing approach. For a given total optical depth τ of an aerosol mixture containing n components, standard linear mixing states that:

$$\rho_{mixture}(-\mu, \mu_0, \phi - \phi_0; \tau) = \sum_n f_n \rho_n(-\mu, \mu_0, \phi - \phi_0; \tau) \tag{59}$$

where $\rho_{mixture}$ is the TOA equivalent reflectance for the aerosol mixture, ρ_n is the TOA equivalent reflectance for the nth aerosol component, and f_n is the relative abundance of the nth aerosol component. Note that the equivalent reflectances for each aerosol component contain all contributions due to Rayleigh scattering or other atmospheric constituents common to each of the pure aerosol cases. Equation (59) is exact in the single scattering limit, but significantly overestimates the TOA equivalent reflectances when one or more of the aerosol components is highly absorbing. The following equation provides a much better approximation:

$$\rho_{mixture}(-\mu, \mu_0, \phi - \phi_0; \tau) =$$

$$\rho_{R,ms}^{black}(-\mu, \mu_0, \phi - \phi_0; \tau_R) +$$

$$+ \sum_n f_n \rho_{n,ss}^{black}(-\mu, \mu_0, \phi - \phi_0; \tau) +$$

$$+ \sum_n f_n \frac{\varpi_{mix}}{\varpi_n} e^{-\tau|\varpi_{mix} - \varpi_n|} [\rho_{n,ms}^{black}(-\mu, \mu_0, \phi - \phi_0; \tau) - \rho_{R,ms}^{black}(-\mu, \mu_0, \phi - \phi_0; \tau_R)] +$$

$$+ \sum_n f_n \rho_{n,surf}(-\mu, \mu_0, \phi - \phi_0; \tau) \tag{60}$$

where $\rho_{n,ss}^{black}$ is the TOA equivalent reflectance resulting from single-scattered radiation over a

black surface (including the contributions from both Rayleigh scattering and aerosol particle n), $\rho_{n,ms}^{black}$ is the multiple-scattered field under the same conditions, $\rho_{R,ms}^{black}$ is the pure Rayleigh multiple-scattered field over a black surface, τ_R is the Rayleigh optical depth, ϖ_n is the single scattering albedo of the nth pure aerosol component (obtained from the ACP), ϖ_{mix} is the single scattering albedo for the mixture (also obtained from the ACP), and $\rho_{n,surf}$ is the component of the TOA radiation field involving interactions with the surface, for aerosol particle n. For the dark water retrievals, $\rho_{n,surf}$ is obtained from the SMART Dataset, and for DDV retrievals, $\rho_{n,surf}$ is equal to $r_0 \hat{\rho}_n$, [see Eqs. (55) and (58)].

As mentioned previously, the terms in Eq. (60) which are obtained from the SMART Dataset are stored there as functions of μ, μ_0, and Ω for practical reasons. However, we make use of the correspondence between Ω and ϕ - ϕ_0 in showing the terms in Eq. (60) as explicit functions of μ, μ_0, and ϕ - ϕ_0.

Equation (60) preserves the standard linear mixing formulation for single-scattered radiation and for radiation which has interacted with the surface. It reduces the magnitude of the multiple-scattered field in the path radiance field when absorbing aerosols are present. Application of this modified linear mixing equation to the path radiance has been tested for all combinations of aerosols contained in the ACP, and provides accurate results for all cases up to total aerosol optical depths of at least 2.

3.5.4   Determine optical depth upper bound

3.5.4.1   Physics of the problem

This step is performed for each candidate aerosol model. The algorithm to determine the upper bound on optical depth is the same whether the region is dark water, DDV, or heterogeneous land. It uses the TOA equivalent reflectances assuming a black surface in a straightforward manner to find the optical depth of the particular model being tested that corresponds to the minimum equivalent reflectances calculated during the Stage 2 processing.

3.5.4.2   Mathematical description of the algorithm

The optical depth upper bound is computed as follows:

(1) For each camera that is available for retrieval, and for each available band within a given camera, take the model black surface TOA equivalent reflectances as a function of optical depth. Quadratically interpolate these values to find the optical depth in each of the available bands that corresponds to the observed minimum equivalent reflectance (found in §3.4.1) in the same band;

(2) Use the optical depth scaling factors for the given aerosol model, provided by the ACP, to scale the optical depths in bands 1, 3, and 4 to band 2;

(3) Repeat steps (1) and (2) for all cameras;

(4) Given the set of optical depths determined from the above steps (maximum of 36 values), the optical depth upper bound is established as the minimum value in this set.

3.5.5   Compute residuals as a function of optical depth

The computation of residuals differs depending on the surface type. The following sections describe the physics of the problem for each surface type, followed by a mathematical description of the algorithm. Scenes for which the surface reflectance is not dark water or heterogeneous land [as defined by the Eq. (31)] are not currently being dealt with.

The residuals derived below are defined to be functions of optical depth in MISR band 2 (558 nm) as the independent variable. For a particular aerosol model, the best-fitting optical depth is the one that minimizes the parameters χ^2_{abs} for dark water and DDV, and χ^2_{hetero} for heterogeneous land. These parameters, defined below, provide measures of the residuals between the model and observed TOA equivalent reflectances. In order to find the optical depth that minimizes these residuals, we compute them as a function of optical depth on a fine grid. The model TOA equivalent reflectances calculated in §3.5.3 are established at optical depth values corresponding to the grid contained in the SMART Dataset. We use quadratic interpolation to determine equivalent reflectances at optical depths on a finer grid, to insure that the value that minimizes the residuals is not missed.

After the best-fitting optical depth for each aerosol model is found, additional residuals, known as χ^2_{geom} and χ^2_{spec}, are calculated for the dark water and DDV retrievals, and a final parameter, χ^2_{maxdev}, is calculated for the dark water case. These additional parameters are used as discriminants of the goodness-of-fit of a particular aerosol model to the MISR observations. They are evaluated at the best-fitting optical depth by interpolating the equivalent reflectances determined in §3.5.3 on the SMART Dataset optical depth grid to this value and performing the requisite calculations.

It is important to note that the mathematical definitions of the residuals include summations over wavelength of various model terms, such as equivalent reflectances. Thus, while stepping through the fine grid of optical depth values in the reference band (band 2), it is necessary to determine the optical depth at the other MISR wavelengths at which the model terms included in the summations are to be calculated. Because optical depth depends on wavelength, and this dependence varies from one aerosol model to another, spectral scaling factors provided by the ACP are used to determine the appropriately scaled optical depths in bands 1, 3, and 4.

3.5.5.1   Physics of the problem

3.5.5.1.1   Dark water

Having specified surface wind speed, and given the view/solar geometry corresponding to a particular measurement, the TOA equivalent reflectances in the 672 nm and 866 nm MISR channels are determined at each camera angle for each of the aerosol compositional mixture/size distribution models to be tested. The predicted equivalent reflectances for each model and optical depth value are compared with the actual MISR observations and various residuals between them are calculated. A single retrieval will be performed over a 17.6 km x 17.6 km region, using MISR minimum equivalent reflectances as described in §3.4.1.

3.5.5.1.2   Dense dark vegetation

For subregions within a region determined to be DDV, the retrieval process is very similar to the dark water case with several exceptions:

(1) Vegetation will be darkest in the 446 and 672 nm bands;

(2) The angular shape of the bidirectional reflectance distribution function for dense vegetation canopies must be assumed as the surface boundary condition;

(3) The absolute reflectance of the surface is treated as a free parameter, whereas in the dark water case the surface model specifies both the angular shape of the surface reflectance as well as its absolute value;

(4) The observations may occur over terrain which is above sea level, so the altitude must be taken into account in determining the Rayleigh scattering optical depth.

Given these inputs, predicted TOA equivalent reflectances are determined for each aerosol compositional model being considered. Again, residuals between the model and observed equivalent reflectances are returned for each aerosol case. A poor fit of the model to the observations could arise from an inadequate model of the surface bidirectional reflectance as well as a deficiency in the aerosol mixture models. Experience with actual MISR data will be necessary to determine the needed model improvements.

3.5.5.1.3   Heterogeneous land

Finding the residuals for heterogeneous land requires a different strategy than used for the dark water and DDV cases. The goodness-of-fit criterion to be applied is that the angular shape of the sample-averaged TOA equivalent reflectance (from all available samples in a 17.6 km x 17.6 km region) minus the atmospheric path term (the component of the radiation field which is back-scattered to space without interacting with the surface) must be similar in a least squares sense to a linear combination of EOF's (fewer than nine), generated from the TOA equivalent reflectances

only (see §3.4.3.2). It can be shown that if all samples within the region have the same angular shape of their bidirectional reflectance factors, or BRF's, (albeit different albedos in order to provide surface contrast), this criterion can be satisfied exactly if the "correct" aerosol model is assumed. The basis of this MISR retrieval algorithm is to assume that the same goodness-of-fit criterion holds even in the more realistic case where both albedo and bidirectional reflectance vary from sample to sample. The effectiveness of this method under this generalized case was demonstrated theoretically *[28]* and the algorithm was used in the analysis of ASAS airborne, multi-angle imagery *[29]*.

3.5.5.2   Mathematical description of the algorithm

3.5.5.2.1   Dark water

The criterion to be used to find the best-fitting optical depth is minimization of the reduced χ^2_{abs} parameter, calculated as a function of optical depth as follows:

$$\chi^2_{abs}(\tau) = \frac{\sum_l \left[\sum_{j=1}^{9} w_j \cdot v(l, j) \cdot \frac{[\rho_{MISR}(l, j) - \rho_{model}(l, j)]^2}{\sigma^2_{abs}(l, j)} \right]}{\sum_l \left[\sum_{j=1}^{9} w_j \cdot v(l, j) \right]} \tag{61}$$

where ρ_{MISR} are MISR equivalent reflectances, computed by taking the median over the subregions in the 17.6 km x 17.6 km region which passed through all screens, ρ_{model} are the model TOA equivalent reflectances for the aerosol mixture, and σ_{abs} is the absolute radiometric uncertainty in ρ_{MISR}. The sum over j corresponds to the cameras and the sum over l corresponds to wavelength, and for dark water includes only bands 3 and 4, the wavelengths at which the dark water surface is assumed to have negligible reflectance. The parameter $v(l, j) = 1$ if a valid value of $\rho_{MISR}(l,j)$ exists; otherwise $v(l, j) = 0$. Eq. (61) also contains weighting factors w_j. For the dark water retrievals, the w_j's are the inverse of the cosine of the view angle of camera j, providing a greater weighting of the more oblique cameras to take advantage of the longer atmospheric slant path.

The value of σ_{abs} is obtained as follows:

$$\sigma_{abs} = 0.05\rho_{MISR} \tag{61a}$$

Once χ^2_{abs} has been minimized as described in §3.5.6.2, its absolute value establishes whether the candidate aerosol model provides a good fit to the measurements. In theory, a value of $\chi^2 \leq$ 1 indicates a good fit. However, to allow for unmodeled sources of uncertainty, we raise the threshold; currently a value of 4 is used. Furthermore, additional parameters are used to determine the

goodness of fit of the particular aerosol model to the MISR data. These additional parameters are defined as follows, and are calculated using the optical depth determined from the minimization of χ^2_{abs} (see §3.5.6.2). One is the angular shape normalized to a reference camera (*refcam*), which emphasizes camera-to-camera geometric differences:

$$\chi^2_{geom}(\tau) = \frac{\sum\limits_l \left[\sum\limits_{j=1,\, j \neq refcam}^{9} w_j \cdot v'(l,j) \cdot \dfrac{\left(\dfrac{\rho_{MISR}(l,j)}{\rho_{MISR}(l,refcam)} - \dfrac{\rho_{model}(l,j)}{\rho_{model}(l,refcam)} \right)^2}{\sigma^2_{geom}(l,j)} \right]}{\sum\limits_l \left[\sum\limits_{j=1,\, j \neq refcam}^{9} w_j \cdot v'(l,j) \right]}$$
(62)

where σ_{geom} (a dimensionless quantity) is given by:

$$\sigma_{geom}(l,j) = 0.05 \frac{\rho_{MISR}(l,j)}{\rho_{MISR}(l,refcam)}$$
(63)

The reference camera is preferentially An; however if this camera is not available (e.g., due to glitter) Af is used; if this is unavailable Aa is used; if this is unavailable Bf is used; and if this is unavailable Ba is used. If none of these are available then χ^2_{geom} is set to 0 causing this test to be bypassed. The parameter $v'(l,j) = 1$ if valid values of $\rho_{MISR}(l,j)$ and $\rho_{MISR}(l,refcam)$ exist; otherwise $v(l,j) = 0$. For dark water, the summation over l in Eq. (62) includes only bands 3 and 4.

Equation deleted   (63a)

Another goodness-of-fit parameter is angular shape of the spectral ratio relative to band 3:

$$\chi^2_{spec}(\tau) = \frac{\sum\limits_{l,\, l \neq 3} \left[\sum\limits_{j=1}^{9} w_j \cdot v''(l,j) \dfrac{\left(\dfrac{\rho_{MISR}(l,j)}{\rho_{MISR}(band3,j)} - \dfrac{\rho_{model}(l,j)}{\rho_{model}(band3,j)} \right)^2}{\sigma^2_{spec}(l,j)} \right]}{\sum\limits_{l,\, l \neq 3} \left[\sum\limits_{j=1}^{9} w_j \cdot v''(l,j) \right]}$$
(64)

where $v''(l,j) = 1$ if valid values of $\rho_{MISR}(l,j)$ and $\rho_{MISR}(band3,j)$ exist; otherwise $v''(l,j) = 0$. For dark water, the summation over l in Eq. (64) includes only band 4. We also have that

$$\sigma_{spec}(l, j) = 0.05 \frac{\rho_{MISR}(l, j)}{\rho_{MISR}(band3, j)} \tag{65}$$

Equation deleted (65a)

The advantage of defining metrics such as those given in Eqs. (62) and (64) is that the instrument relative accuracies are higher than the absolute accuracy, thus providing potentially greater sensitivity. Simulations have shown that χ^2_{geom} tends to be more sensitive to particle size than to composition, whereas χ^2_{spec} tends to depend more on both particle size and composition.

Finally, we define a maximum deviation parameter:

$$\chi^2_{maxdev}(\tau) = \underset{l, j}{Max} \left\{ \frac{[\rho_{MISR}(l, j) - \rho_{model}(l, j)]^2}{\sigma^2_{abs}(l, j)} \right\} \tag{66}$$

to find the channel at which the observed equivalent reflectance is most different from the model equivalent reflectance.

Successful aerosol models are those for which all four metrics, χ^2_{abs}, χ^2_{geom}, χ^2_{spec}, and χ^2_{maxdev} are ≤ specified threshold values. These thresholds may be adjusted pending further theoretical sensitivity studies and experience with actual MISR data. Currently, the thresholds are 4, 16, 4, and 16, respectively.

3.5.5.2.2 Dense dark vegetation

Similar criteria as for dark water are used here. The equivalent reflectances for all DDV samples are combined together by computing the median for each channel, and these median DDV equivalent reflectances then are compared to the appropriate subset of aerosol/surface models. However, there are several notable differences:

(1) The sum over wavelength corresponds to bands 1 and 3, the wavelengths at which DDV has the lowest reflectance;

(2) The values of the aerosol optical depth, the BRF parameter r_0 in band 1, and the BRF parameter r_0 in band 3 are varied in order to minimize the χ^2_{abs} parameter. The other χ^2 metrics are then calculated for these optimal values of optical depth and surface reflectance;

(3) The σ^2_{abs}, σ^2_{geom}, and σ^2_{spec} are modified to include uncertainty in the assumed shape of the surface bidirectional reflectance distribution function;

(4) The χ^2_{maxdev} test is not used. Again, this is because of uncertainty in the assumed shape of the surface bidirectional reflectance distribution function;

(5) For χ^2_{abs}, χ^2_{geom}, and χ^2_{spec}, the threshold value of χ^2 corresponding to an acceptable fit is taken to be 3.

The latter four differences account for a greater uncertainty in specification of the surface boundary condition relative to the dark water retrieval case.

We now derive the optimal value of r_0 for bands 1 and 3, for a given value of τ, that minimizes χ^2_{abs}. Inserting Eq. (55) into Eq. (60), and letting $\rho^{black}_{mixture}$ be the equivalent reflectance corresponding to the path radiance of the aerosol mixture, determined from the modified linear mixing theory, we have

$$\rho_{mixture}(-\mu, \mu_0, \phi - \phi_0; \tau) = \rho^{black}_{mixture}(-\mu, \mu_0, \phi - \phi_0; \tau) + r_0 \hat{\rho}_{mixture}(-\mu, \mu_0, \phi - \phi_0; \tau) \qquad (67)$$

where

$$\hat{\rho}_{mixture}(-\mu, \mu_0, \phi - \phi_0; \tau) = \sum_n f_n \hat{\rho}_n(-\mu, \mu_0, \phi - \phi_0; \tau) \qquad (68)$$

in which the terms containing surface interaction combine according to standard linear mixing. Then, equating $\rho_{mixture}$ with ρ_{model} in the version of Eq. (61) appropriate for DDV (i.e., summation over bands 1 and 3 rather than 3 and 4), and setting the derivative of χ^2_{abs} with respect to r_0 to zero, the value of r_0 in band l which minimizes χ^2_{abs} for a given value of τ and aerosol mixture is given by

$$\tilde{r}_0(l) = \frac{\displaystyle\sum_{j=1}^{9} \frac{w_j \cdot v(l, j) \cdot [\rho_{MISR}(l, j) - \rho^{black}_{mixture}(l, j)] \hat{\rho}_{mixture}(l, j)}{\sigma^2_{abs}(l, j)}}{\displaystyle\sum_{j=1}^{9} \frac{w_j \cdot v(l, j) \cdot [\hat{\rho}_{mixture}(l, j)]^2}{\sigma^2_{abs}(l, j)}} \qquad (69)$$

where w_j and $v(l, j)$ are defined in the text following Eq. (61). We require that $\tilde{r}_0(l)$ fall within specified limits, namely $0 \le \tilde{r}_0(l) \le 0.03$. If $\tilde{r}_0$ as determined from Eq. (69) < 0, it is replaced by 0, and if it is > 0.03, it is replaced by 0.03. The values of $\tilde{r}_0(l)$ resulting from this process are then used in calculating χ^2_{abs}.

Before χ^2_{abs} and $\tilde{r}_0$ can be determined, σ^2_{abs} in Eqs. (61) and (69) must be modified to include the uncertainty in $\rho_{mixture}$ due to the uncertainties in the surface model parameters k and g.

Assuming no correlation between the measurement and model uncertainties, the modified σ^2_{abs} can be approximated by

$$\sigma^2_{abs}(l, j) \Rightarrow \sigma^2_{abs}(l, j) + [q^2_k(j) + q^2_g(j)]r^2_0\hat{\rho}^2_{mixture}(l, j) \tag{69a}$$

with

$$q^2_k(j) = \sigma^2_k \cdot ln^2[\mu_0\mu_j(\mu_j + \mu_0)]$$

$$q^2_g(j) = \sigma^2_g \cdot \left[\frac{2g}{1 - g^2} + \frac{3[g - \cos\Omega_j]}{1 + g^2 - 2g\cos\Omega_j}\right]^2 \tag{69b}$$

The functions q^2_k and q^2_g were derived for the surface model defined by Eq. (39), with σ^2_k and σ^2_g being the variances associated with the values for k and g, respectively. As stated previously, for DDV k is set to 0.5 and g to -0.2 and the variances σ^2_k and σ^2_g are each set at 0.02. Note that σ^2_{abs} in Eq. (69) now also depends on r_0 via Eq. (69a). This dependence, however, was ignored in the derivation of Eq. (69) since it has minimal impact on the derived value of $\tilde{r}_0$. Therefore, a set value of 0.015 for r_0 is used in the expression for σ^2_{abs}.

Once χ^2_{abs} is determined as a function of τ, the procedure described in §3.5.6 is then used to find the value of τ that minimizes χ^2_{abs}. Using these values of $\tilde{r}_0(1)$, $\tilde{r}_0(3)$, and τ, the metrics χ^2_{abs}, χ^2_{geom}, and χ^2_{spec} are then calculated to determine whether a successful aerosol model has been found.

3.5.5.2.3   Heterogeneous land

The reduced sample equivalent reflectance, $J_{x, y}$, defined by Eq. (20), can be considered to be a linear combination of surface functions, $\rho^{land}_{x, y}$, defined to be the sample-dependent component of the TOA equivalent reflectance, i.e.,

$$\rho^{land}_{x, y}(-\mu, \mu_0, \phi - \phi_0) = \exp(-\tau/\mu)\frac{1}{\pi}\int_0^1\int_0^{2\pi} R^{surf}_{x, y}(-\mu, \mu', \phi - \phi')\rho^{inc}_{x, y}(\mu', \mu_0, \phi' - \phi_0)\mu'd\mu'd\phi'$$

$$+ \frac{1}{\pi}\int_0^1\int_0^{2\pi}\int_0^1\int_0^{2\pi} T(-\mu, -\mu'', \phi - \phi'')R^{surf}_{x, y}(-\mu'', \mu', \phi'' - \phi')\rho^{inc}_{x, y}(\mu', \mu_0, \phi' - \phi_0)\mu'd\mu'd\phi'd\mu''d\phi'' \tag{70}$$

where $\rho^{inc}_{x, y}$ is the equivalent reflectance corresponding to the radiance incident upon the surface.

If a single BRF shape is able to describe the view angle variability of the surface within a region (the individual sample reflectance, however, being variable), then the reduced sample equivalent reflectances are proportional to each other, i.e.,

$$J_{x, y, j} = c' \cdot J_{x', y', j} = c \cdot f_{j, 1} \qquad (71)$$

In this particular case the scatter matrix has rank 1, producing a single EOF, $f_{j, 1}$, which is proportional to $J_{x, y}$. This is a limited form of Eq. (24). If the correct equivalent reflectance corresponding to the atmospheric path radiance, which is the same as the TOA equivalent reflectance for a black surface ρ^{black}, is subtracted from the sample-averaged TOA equivalent reflectance, $\langle \rho_{MISR} \rangle$, then the view angle variability of $\langle \rho_{MISR} \rangle - \rho^{black}$ also must be the same as for the EOF, $f_{j, 1}$. This criterion of angular shape comparison determines the best estimate of the aerosol optical depth by requiring that it produce the minimum χ^2 between $\langle \rho_{MISR} \rangle - \rho^{black}$ and $f_{j, 1}$. This can be written as

$$\chi^2_{hetero}(\tau) = \frac{\displaystyle\sum_{l = 1}^{4} \sum_{j = 1}^{9} v'''(l, j) \cdot \frac{[\langle \rho_{MISR}(l, j) \rangle - \rho^{black}(l, j) - A_1(l) \cdot f_{j, 1}(l)]^2}{\sigma^2_{hetero}(l, j)}}{\displaystyle\sum_{l = 1}^{4} \sum_{j = 1}^{9} v'''(l, j)} \qquad (72)$$

where the summation is over the nine MISR view angles and four wavelengths, $v'''(l, j) = 1$ if a valid value of $\langle \rho_{MISR} \rangle$ exists; otherwise $v'''(l, j) = 0$. The quantity σ^2_{hetero} is the estimated variance of the numerator for the individual summed terms, and A_1 is varied to minimize the summation result in a least squares sense.

When a number of different BRF shapes are represented in the region then Eq. (72) is not rigorously satisfied for the various samples x, y. However, we note that the various $J_{x, y}$ are made up of different linear combinations of surface functions, $\rho^{land}_{x, y}$, and these $J_{x, y}$ are most efficiently decomposed using EOF's, $f_{j, n}$, according to Eq. (24). Since $\langle \rho_{MISR} \rangle - \rho^{black}$ is also a linear combination of surface functions it also is efficiently decomposed using the same EOF's. Therefore Eq. (72) can be generalized to

$$\chi^2_{hetero}(\tau) = \frac{\displaystyle\sum_{l = 1}^{4} \sum_{j = 1}^{9} v'''(l, j) \cdot \frac{\left(\langle \rho_{MISR}(l, j) \rangle - \rho^{black}(l, j) - \displaystyle\sum_{n = 1}^{N(l)} A_n(l) \cdot f_{j, n}(l) \right)^2}{\sigma^2_{hetero}(l)}}{\displaystyle\sum_{l = 1}^{4} \sum_{j = 1}^{9} v'''(l, j)} \qquad (73)$$

where $N(l)$ (the number of eigenvectors used in band $l) < N_{cam}(l)$, where $N_{cam}(l)$ is the number of cameras with valid data in wavelength band l, and is given by

$$N_{cam}(l) = \sum_{j=1}^{9} v'''(l, j) \tag{73a}$$

The expansion coefficients A_n are obtained by applying the orthonormality condition of Eq. (23) to the bracketed expression in Eq. (73), i.e.,

$$A_n(l) = \sum_{j=1}^{9} [\langle \rho_{MISR}(l, j) \rangle - \rho^{black}(l, j)] \cdot f_{j,n}(l) \tag{74}$$

The contribution of an individual eigenvector in describing the angular shape of the surface functions of a given scene is determined by the relative size of its eigenvalue [see §3.4.3.2 and Eq. (26)]. Therefore, only those eigenvectors with eigenvalues greater than or equal to a certain size are used in the summation in Eq. (73). The maximum number of usable eigenvectors in wavelength band l, $N_{max}(l)$, is determined by the condition

$$\sum_{n=1}^{N_{max}(l)-1} \lambda_n < 0.99 \cdot \sum_{n=1}^{N_{cam}(l)} \lambda_n \leq \sum_{n=1}^{N_{max}(l)} \lambda_n, \tag{75}$$

i.e., ignoring those eigenvectors which contribute less than 1% to the angular variability of the image. There is also the constraint that $N_{max}(l)$ must be less than $N_{cam}(l)$, the total number of eigenvectors.

$$\textit{Equation deleted} \tag{75a}$$

We establish

$$\sigma_{hetero}(l, j) = 0.05 \cdot \langle \rho_{MISR}(l, j) \rangle \tag{75b}$$

For each of the candidate aerosol models a χ^2 is then computed for each value of $N(l)$ used in Eq. (73), starting with all $N(l) = 1$ (the first eigenvector only) and incrementing the number of eigenvectors in each wavelength band simultaneously by unity but not letting the number in any given wavelength band exceed $N_{max}(l)$. Varying the model aerosol optical depth, the minimum χ^2 for each combination of $N(l)$ values, denoted χ_N^2, defines an estimate of the optical depth τ_N. The procedure for determining χ_N^2 and τ_N, and the associated uncertainty $\Delta\tau_N$, is described in §3.5.6. The number of different cases established by this procedure is equal to:

$$N_{cases} = \max_{l} \{N_{max}(l)\}$$ (75c)

i.e., the largest value of $N_{max}(l)$ from among the four wavelength bands.

For the aerosol model being evaluated, the reported best-fitting optical depth is then computed from a weighted average of all N_{cases} optical depths:

$$\tau = \frac{\displaystyle\sum_{N=1}^{N_{cases}} \frac{\tau_N}{\chi_N^2}}{\displaystyle\sum_{N=1}^{N_{cases}} \frac{1}{\chi_N^2}}$$ (76)

where the weights are the inverses of the χ_N^2. The formal uncertainty $\Delta\tau$ associated with τ is then expressed as

$$\Delta\tau = \frac{\sqrt{\displaystyle\sum_{N=1}^{N_{cases}} \frac{\Delta\tau_N}{\chi_N^2}}}{\displaystyle\sum_{N=1}^{N_{cases}} \frac{1}{\chi_N^2}}$$ (77)

Finally, the effective χ^2 associated with τ is defined as the weighted average of all of the χ_N^2:

$$\chi_{hetero}^2 = \frac{N_{cases}}{\displaystyle\sum_{N=1}^{N_{cases}} \frac{1}{\chi_N^2}}$$ (78)

We consider successful aerosol models to be those for which $\chi_{hetero}^2 \leq 10$.

3.5.6   Compute aerosol optical depth and uncertainty

3.5.6.1   Physics of the problem

Given the methodology for defining residuals as a function of optical depth for each aerosol model, the best-fitting value of τ for that model is the one which minimizes the appropriate χ^2, i.e., χ_{abs}^2 for the dark water case and DDV cases, and χ_{hetero}^2 for the heterogeneous land case. Because

of the nonlinear dependence on optical depth inherent in the retrievals, there is no analytic method of minimizing the residuals. Instead, the brute force method of stepping through optical depth on a grid is used, starting from the maximum value determined as described in §3.5.4 and working downwards. For the DDV case, the parameters $\tilde{r}_0(1)$ and $\tilde{r}_0(3)$ are determined by least-squares (within specified limits) to minimize χ^2_{abs} for each value of τ on the grid, as described in §3.5.5.2.2. The result of this process is a tabulated set of χ^2 values as a function of τ. This curve is then used to determine a best-fitting τ and its associated formal uncertainty. For the heterogeneous land case, this procedure is followed for each of the N_{max} cases, as described in §3.5.5.2.3, and the final results are obtained by combining the results from each case together.

3.5.6.2 Mathematical description of the algorithm

Given numerical values of χ^2 as a function of τ, the smallest χ^2 and the values on either side of it are used to compute a parabolic fit, represented by the coefficients of the equation

$$\ln(\chi^2) \;=\; A + B\tau + C\tau^2 \tag{79}$$

are determined from the three values of χ^2 vs. τ. The logarithm of χ^2 is used instead of χ^2 to guarantee that the minimum value of χ^2, determined from the fitting procedure, is always positive. Then, the optical depth which minimizes χ^2 is given by

$$\tau \;=\; -\frac{B}{2C} \tag{80}$$

and the uncertainty in τ is given by

$$\Delta\tau \;=\; \sqrt{\frac{ln\left(1 + \dfrac{1}{\chi^2_{min}}\right)}{C}} \tag{81}$$

where χ^2_{min} is the minimum χ^2 at τ.

The χ^2 that are reported correspond to the value of τ determined from Eq. (80), using Eq. (61) in the case of dark water and DDV, and Eq. (73) in the case of heterogeneous land. In the event that the value of τ which minimizes χ^2 is either of the endpoints (i.e., zero or the upper bound), the aerosol optical depth is set to this value and the formal uncertainty is set to a default value that flags this situation and no formal uncertainty is calculated using Eq. (81). This default value of $\Delta\tau$ is 2.0. In the heterogeneous land situation, where multiple estimates of τ are combined together, the use of this default value for $\Delta\tau$ causes these cases to be ignored in the weighting procedure.

3.5.7 Establish optical depth defaults

3.5.7.1 Physics of the problem

We desire to maximize the coverage of land surface retrievals. These retrievals require at least one regional optical depth value and its associated model. If land aerosol processing fails to find a suitable aerosol model that meets the criteria for a successful retrieval, a default aerosol model is established, and a default optical depth is assigned to this model. The default model is chosen from the available Mixture File, and selected to be a model that is believed to represent a "typical" aerosol for land.

3.5.7.2 Mathematical description of the algorithm

The default aerosol model having been specified, the assigned optical depth is established by choosing among the following alternatives.

3.5.7.2.1 *Low optical depth upper bound*

If the optical depth upper bound associated with the default model (see §3.5.4) is ≤ 0.1, the default aerosol optical depth is set to:

$$\tau_{default} = \frac{\tau_{upper\ bound}}{2} \tag{81a}$$

In this case the maximum error on the assigned default optical depth is 0.05.

3.5.7.2.2 *Rayleigh only*

If no previously processed domain has a domain-mean optical depth associated with it (see §3.5.8.2), and the low optical depth upper bound criterion is not met, the default aerosol optical depth is set to:

$$\tau_{default} = 0.0 \tag{81b}$$

3.5.7.2.3 *Previous domain*

If a previously processed domain has a domain-mean optical depth associated with it, and the low optical depth upper bound criterion is not met, the default aerosol optical depth is set to:

$$\tau_{default} = \tau_{previous\ domain\ mean} \tag{81c}$$

This default requires that the previous domain-mean optical depth does not exceed the optical depth upper bound for the default aerosol model within the region currently being processed.

3.5.7.2.4 *Previous domain test with upper bound override*

If a previously processed domain has a domain-mean optical depth associated with it, the low optical depth upper bound criterion is not met, and the previous domain-mean optical depth exceeds the optical depth upper bound for the default aerosol model within the region currently being processed, the default aerosol optical depth is set to:

$$\tau_{default} = \tau_{upper\ bound} - 0.05 \tag{81d}$$

3.5.8 Calculate overall best estimate of aerosol optical depth

3.5.8.1 Physics of the problem

The radiometric performance of the instrument will dictate which aerosol models fit the data to within the instrumental uncertainties. Any model fit which meets the criteria described in §3.5.5.2 is deemed to be a valid fit. Of course, the best situation is that only one of the multiple initial guesses will qualify as a best fit. However, it is possible for more than one model to satisfy the goodness-of-fit criteria. Resolution of the ambiguous nature of this situation will require reference to additional information, such as the climatological likelihood parameters contained in the Aerosol Climatology Product. Finally, it is possible that no model will qualify as fitting the observational data to within the radiometric performance of the instrument. This will be indicative of a failure of the pre-determined models to represent the ambient atmospheric state or some other limitation of the algorithm or instrument performance. Reporting the residual of the fits in the Aerosol/Surface Product will enable flagging these cases. Experience with actual MISR data will be necessary to determine the needed model improvements. An Aerosol Retrieval Success Indicator is established for each region as a simple way of determining (e.g., for subsequent surface retrieval processing) if at least one good fitting model has been found (see *[M-17]*).

Assuming that at least one model meets the goodness-of-fit criteria, and each of these models has an optical depth associated with it as determined according to the algorithm described in §3.5.6, several overall best estimates of aerosol optical depth are calculated, along with measures of the spread in values. When a default optical depth and its single associated model have been established, all of the best-estimate values correspond to this default.

3.5.8.2 Mathematical description of the algorithm

Given a set of n models that satisfy the goodness-of-fit criteria, where $n \geq 1$, and the associated optical depths τ_n for each of these models, the overall best estimates of optical depth are given by

$$\tau_{best,\,1} = Mean(\tau_n)$$

$$\tau_{best,\,2} = Weighted\;mean(\tau_n)$$

$$\tau_{best,\,3} = Median(\tau_n)$$

$$\tau_{best,\,4} = \tilde{\tau}_n \qquad \qquad (82)$$

No weighting is used in the calculation of the straight mean; but the weighted mean uses the inverse of χ^2_{abs} or χ^2_{het} (as appropriate) as the weights. The quantity $\tilde{\tau}_n$ is the optical depth for which χ^2_{abs} or χ^2_{het} (as appropriate) is smallest. Measures of variation are also calculated:

$$\sigma_1 = Standard\;deviation(\tau_n)$$

$$\sigma_2 = Weighted\;standard\,deviation(\tau_n) \qquad (82a)$$

where for the weighted standard deviation the inverse of χ^2_{abs} or χ^2_{het} (as appropriate) are used as the weights.

The quantities in Eqs. (82) and (82a) are calculated for each 17.6 km x 17.6 km region. Additionally, the mean and median are calculated and reported over each 70.4 km x 70.4 km domain. Furthermore, a two-dimensional histogram of the regional τ_n values within a domain is provided, where one dimension is aerosol mixture and the other is optical depth in steps of 0.05.

3.6 PRACTICAL CONSIDERATIONS

3.6.1 Numerical computation considerations

Requirements on processing speed and data storage are described in *[M-16]*.

3.6.2 Configuration of retrievals

An Aerosol Retrieval Configuration File is used to establish the numerical values of adjustable parameters used within the retrievals, e.g., thresholds establishing whether a successful retrieval occurred. This avoids "hard-wiring" specific values into the software. The Aerosol/Surface Product will contain information indicating what version of the configuration file was used. The contents of the Aerosol Retrieval Configuration File are shown in Table 6. The values shown correspond to the settings at the time this document was generated; however, the annotation text of the Level 2 Aerosol Product should be checked to determine the actual threshold values used in the retrievals. The column entitled "Section" indicates where in this ATB a description of the specific configuration parameter is found.

70

Table 6: Contents of the Aerosol Retrieval Configuration File

Parameter	Value	Section
Regional cosine of solar zenith angle threshold	0.2	3.3.1.2.1
Regional topographic complexity threshold	250 m	3.3.1.2.2
Regional cloudiness threshold (high confidence cloud fraction)	100%	3.3.1.2.3
Regional cloudiness threshold (low confidence cloud fraction)	100%	3.3.1.2.3
Maximum acceptable RDQI used in averaging data to appropriate resolution, $RDQI_1$	1	3.3.2.2
$RDQI_2$ [value of RDQI' in Eq. (3a) if $RDQI > RDQI_1$]	3	3.3.2.2
Value of c in Eq. (7)	34 K km^{-1}	3.3.6.2
Boltzmann constant, k	1.381×10^{-23} J/deg/ molecule	3.3.7.2
T_{STP}	288 K	3.3.7.2
P_{STP}	1.01325×10^5 N/m^2	3.3.7.2
Dobson to ozone optical depth conversion factor (band 1)	4.26×10^{-6}	3.3.7.2
Dobson to ozone optical depth conversion factor (band 2)	1.05×10^{-4}	3.3.7.2
Dobson to ozone optical depth conversion factor (band 3)	5.09×10^{-5}	3.3.7.2
Dobson to ozone optical depth conversion factor (band 4)	3.94×10^{-6}	3.3.7.2
Subregional topographic complexity threshold	250 m	3.3.8.2.5
Maximum allowable subregion average slope	20°	3.3.8.2.5
Cloud mask decision logic	See Table 5	3.3.8.2.6
Maximum acceptable RDQI for inclusion in retrieval, $RDQI_3$	0	3.3.8.2.8
Minimum scattering angle considered to be rainbow-influenced	110° dark water; 180° otherwise	3.3.8.2.9
Maximum scattering angle considered to be rainbow-influenced	160° dark water; 0° otherwise	3.3.8.2.9
Threshold for χ^2_{smooth}	4	3.3.8.2.9
Maximum acceptable RDQI for inclusion in angle-to-angle correlation test, $RDQI_4$	1	3.3.8.2.10
Angle-to-angle correlation threshold C_{thresh}	0.25	3.3.8.2.10
NDVI threshold, $NDVI_{thresh}$	0.75	3.4.2.2
Minimum number of common adjacent pixel differences required for correlation of two bands in band-differenced optical depth algorithm	100	3.4.4.2

Table 6: Contents of the Aerosol Retrieval Configuration File (continued)

Parameter	Value	Section
Minimum number of channels for dark water retrievals	1	3.5.1.2.1
Minimum number of channels for DDV retrievals	2	3.5.1.2.2
Minimum number of subregions for heterogeneous land retrievals	64	3.4.3.2
Adequate contrast threshold for heterogenous land retrieval	5	3.4.3.2
Minimum correlation coefficient for band-differenced optical depth	0.95	3.4.4.2
Maximum acceptable RDQI for inclusion in band-differenced optical depth algorithm, $RDQI_5$	0	3.4.4.2
Value of k in Eq. (39)	0.5	3.5.3.2.1
Value of g in Eq. (39)	-0.2	3.5.3.2.1
Constant α, vector A, and matrices $\hat{R}_0^{surf}$, $\hat{R}_1^{surf}$	Determined from k and g	3.5.3.2.1
Value of $r_{0,hot}$ to use in Eq. (38)	0.015	3.5.3.2.1
Value of $\{r_0\}$ to use in Eq. (58)	0.015	3.5.3.2.1
Maximum value of χ_{abs}^2 for successful dark water retrieval	4	3.5.5.2.1
Maximum value of χ_{geom}^2 for successful dark water retrieval	16	3.5.5.2.1
Maximum value of χ_{spec}^2 for successful dark water retrieval	4	3.5.5.2.1
Maximum value of χ_{maxdev}^2 for successful dark water retrieval	16	3.5.5.2.1
Maximum value of χ_{abs}^2 for successful DDV retrieval	3	3.5.5.2.2
Maximum value of χ_{geom}^2 for successful DDV retrieval	3	3.5.5.2.2
Maximum value of χ_{spec}^2 for successful DDV retrieval	3	3.5.5.2.2
Minimum value of r_0 to use in Eq. (67)	0	3.5.5.2.2
Maximum value of r_0 to use in Eq. (67)	0.03	3.5.5.2.2
Value of r_0 to use in Eq. (69a)	0.015	3.5.5.2.2
Variance of k to use in Eq. (69b)	0.02	3.5.5.2.2
Variance of g to use in Eq. (69b)	0.02	3.5.5.2.2
Maximum value of χ_{hetero} for successful heterogeneous land retrieval	10	3.5.5.2.3
Default value of σ_τ	2.0	3.5.6.2

3.6.3　Quality assessment and diagnostics

A number of parameters and indicators will be reported in the Aerosol/Surface Product as retrieval diagnostics. Maps or other summaries of these parameters will be reviewed by the MISR team for quality assessment. Included among these are retrieval residuals, sources of ancillary and external data, statistical information regarding the processing, etc. A tabulation of these indicators is provided in *[M-17]*, cross-referenced, where applicable, to the pertinent section of this ATB.

3.6.4　Exception handling

As discussed in §3.3.8, samples which do not pass through a variety of screens will not be processed for aerosol retrieval. In addition, it is possible that one or more of the 36 instrument channels could fail in flight. This situation will be handled as follows:

  (1) Over dark water, the maximum available number of channels in bands 3 and 4 will be used.

  (2) Over Dense Dark Vegetation, the maximum available number of channels in bands 1 and 3 will be used.

  (3) For the diffuse-field aerosol optical depth retrieval over heterogeneous land, the maximum available number of channels at all selected wavelengths will be used.

3.7　AEROSOL RETRIEVAL SENSITIVITIES

The MISR Aerosol/Surface Product reports two retrieved aerosol quantities: aerosol optical depth and aerosol type model number. Uncertainties in the reported optical depth arise from several sources, including instrument calibration errors, instrument noise, and selection of the wrong aerosol type. We deal first with the sensitivity of the MISR signatures to optical depth for individual aerosol types, and then examine the ability of MISR to distinguish among aerosol types.

The majority of the aerosol retrievals will occur either over dark water, large inland water bodies, or dense dark vegetation. Therefore we concentrate on the aerosol sensitivities resulting from the instrument characteristics for retrievals over dark surfaces. However, a case study dealing with a heterogeneous land surface is also presented. Estimation of uncertainties due to incorrect surface boundary conditions will be included in later versions of this document.

3.7.1　Dark surfaces

To quantify the MISR aerosol sensitivity, the distinguishability of "comparison" and "reference" models for various pure particle types were examined. Comparison and reference can refer, respectively, to two different optical depths for the same aerosol type, two different aerosol types, or model and observations. Formally, the MISR instrument provides three kinds of information: absolute radiance, spectrally varying relative radiance, and geometrically varying relative radi-

ance. Quantitative criteria for comparing the observations with SMART data account for each of these contributions. Goodness-of-fit criteria are based on the reduced chi-squared (χ^2) functions defined in Eqs. (61), (62), (64), and (66), with "comparison" and "reference" models replacing the "MISR" and "model" designations in these equations.

Depending on latitude and season, the nine MISR cameras sample scattering angles ranging from about 30° to nearly 180°. In this range, the medium-sized (accumulation mode) particles show distinct curvature, with factors of 10 or more between minimum and maximum values, and the largest spherical particles (sea salt coarse mode) have even more pronounced curvature as well as the "rainbow" feature between 135° and 155° degrees scattering angle.

3.7.1.1   Sensitivity to optical depth

Using the reduced χ^2 metrics defined above, Figure 7 illustrates the sensitivity of the MISR signatures to optical depth for pure aerosol type, as a function of aerosol optical depth. In Figure 7, the "accuracy" is determined by changing the optical depth of each model from the value shown on the abscissa until at least one of the χ^2 metrics changes by unity, since at this level the detectable signal is comparable to the instrumental uncertainty. For larger values of reduced χ^2, the models are considered distinguishable. Also shown on this figure is the optical depth accuracy requirement for MISR, which is 0.05 for optical depth less than 0.5, and 10% for larger optical depth values. All models meet the requirement except black carbon (soot), over a black surface. However, the candidate aerosol models to be included in MISR retrievals will not include cases in which the relative abundance of black carbon (as a fraction of total optical depth) exceeds 40%.
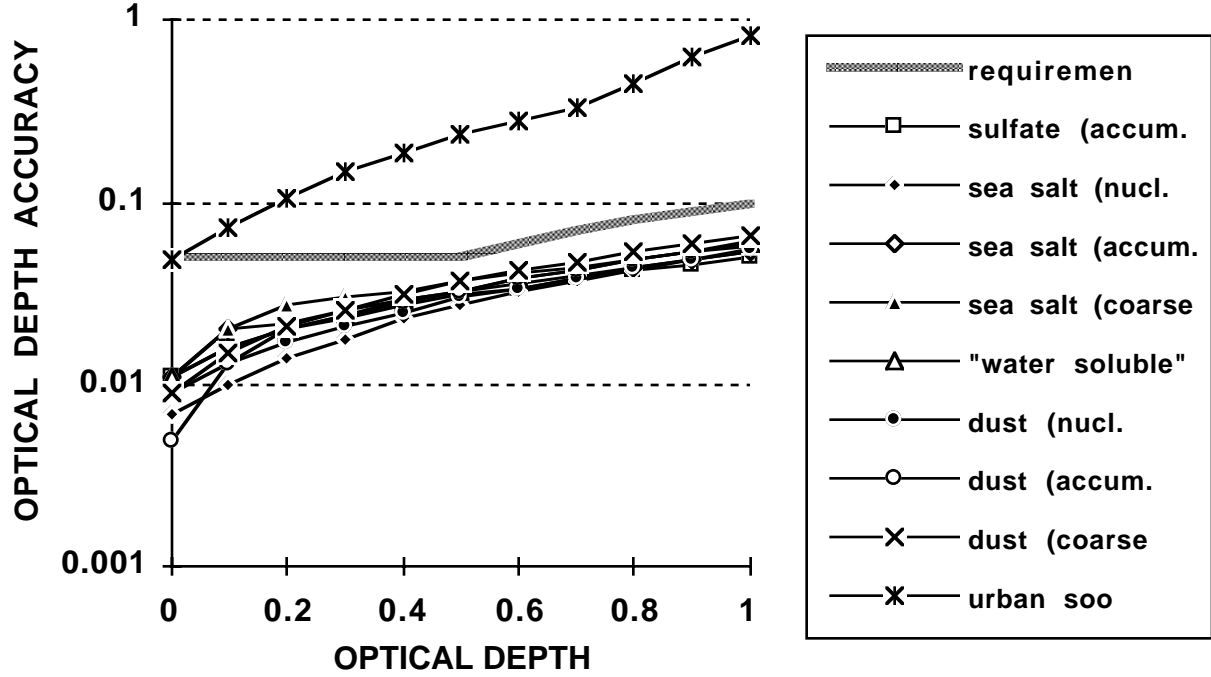
OPTICAL DEPTH ACCURACY

1

0.1

0.01

0.001

0   0.2   0.4   0.6   0.8   1

OPTICAL DEPTH

requiremen

sulfate (accum.

sea salt (nucl.

sea salt (accum.

sea salt (coarse

"water soluble"

dust (nucl.

dust (accum.

dust (coarse

urban soo

Figure 7. Optical depth accuracy for various pure aerosol types (black surface)

3.7.1.2   Sensitivity to particle size

Both particle size and composition vary among the aerosol types. In Figure 8, for example, particle size is varied while composition (sea salt) is fixed. The reference model consists of coarse mode particles, whereas the comparison model consists of accumulation mode particles. The top panel shows the values of three χ^2 criteria, as functions of the reference model optical depth. To make this an independent test of MISR sensitivity to particle size, the optical depth of the comparison model was varied to produce the best possible fit with the reference model, by minimizing the reduced χ^2 corresponding to the absolute radiances. The resulting difference in optical depth, a measure of the error that would be made if the wrong model were chosen, is given in the graph at the bottom of the figure. However, it is unlikely that the wrong model will be chosen in this case, since even for optical depth as small as 0.1, the reduced χ^2 values are all greater than 1. Note that in the figure legend, the curve labeled "multi-angle radiances" corresponds to χ^2_{abs}, "band ratio angular shape" corresponds to χ^2_{spec}, and "normalized angular shape" corresponds to χ^2_{geom}.

3.7.1.3   Sensitivity to particle composition

Figure 9 shows a case where composition is varied and size is approximately fixed. The reference model is accumulation mode sea salt, while the comparison model is accumulation mode

mineral dust. Again the models are easily distinguished in the simulation, reinforcing the conclusion that optical depth errors resulting from the wrong choice of compositional or size model are not expected to be realized due to MISR's use of the angular signature to distinguish between them.

For aerosol retrievals over dark water, the above discussion can be extended to include the Fresnel-reflecting properties of the surface. An approximate quantification of these error sources was performed by Wang and Gordon *[50]* who assumed an optically thin atmosphere with both molecular (Rayleigh) and aerosol scattering over a smooth Fresnel-reflecting water surface. Using a simple multi-angle algorithm to find best-fitting aerosol models, their simulations consisted of nine aerosol mixtures, denoted Maritime, Coastal, and Tropospheric, each with 70%, 90%, and 98% relative humidity. The Tropospheric aerosol is a mixture of 70% water soluble and 30% dust-like particles, where the mixing ratios are defined by Wang and Gordon in terms of numbers of particles. Its refractive index at 550 nm ranges from $1.53 - 0.0066i$ at RH = 0% to $1.369 - 0.0012i$ at RH = 98%. Thus, as the particles absorb more water, the real part of the refractive index approaches that of water and the imaginary part decreases. The modal diameter is < 0.1 μm for all relative humidities. The Maritime and Coastal aerosols are mixtures of the Tropospheric aerosol plus 1% Oceanic and 0.5% Oceanic, respectively, where the Oceanic aerosol is a sea salt-based component, whose modal diameter varies from about 0.3 to 1.2 μm as RH varies from 0 to 98%. Its index of refraction is essentially real, and ranges from 1.5 at RH = 0% to 1.35 at RH = 98%. Mie theory was used to calculate the scattering properties of these aerosol mixtures, based on size and optical constant data from Shettle and Fenn *[45]*. Wang and Gordon *[50]* then used these nine models to retrieve optical depth for simulated radiances produced by the Maritime, Coastal, and Tropospheric aerosols with RH = 80% (i.e., a value of RH *not* contained in the "climatology"). For aerosol optical depths of 0.2 and 0.4, the worst case optical depth retrieval errors, assuming no instrument calibration errors, were 0.019 and 0.025, respectively, assuming the viewing geometries obtained at the center of the MISR camera FOV's at about 30° latitude on June 21 and December 21. In each case, the model chosen by the algorithm was the correct aerosol type, and the algorithm chose RH of 90% for the best fit, which is close to the true value of 80%.

Wang and Gordon *[50]* extended the above retrievals to include calibration errors, using two examples. First, the actual optical depth was set to 0.2, and the simulated top-of-atmosphere reflectances were increased or decreased by 6%. The error in the retrieved optical depth was 0.035, a change of about 8% from the error obtained with no calibration error. Second, the mean calibration error was assumed to be zero and errors in the simulated equivalent reflectances were assumed to be normally distributed random variables with zero mean and standard deviation 0.02. Wang and Gordon then used the simulated reflectances at each angle for the Maritime aerosol (RH = 80%) applying calibration errors as a function of angle by assigning errors using a random number generator. Twenty realizations of the errors were used for each of the two MISR geometries investigated. Pooling the two geometry cases together, for 38 of the 40 realizations the same candidate model (Maritime with 90% RH) was chosen by the algorithm and in the other two cases the Coastal

model with 90% RH was chosen. The addition of a 2% random error changed the error-free estimates in optical depth by less than 2% and the correct model was chosen 95% of the time.
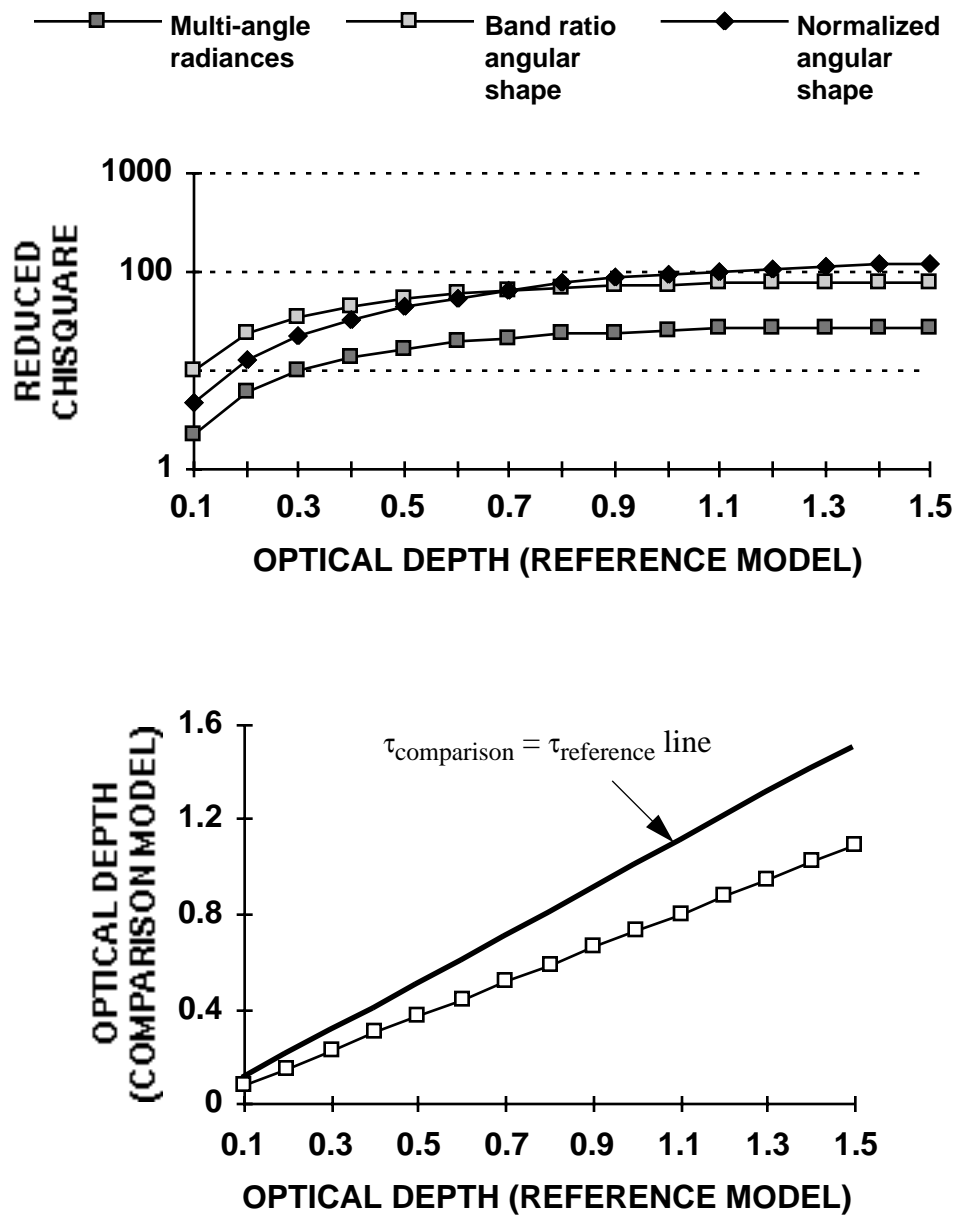
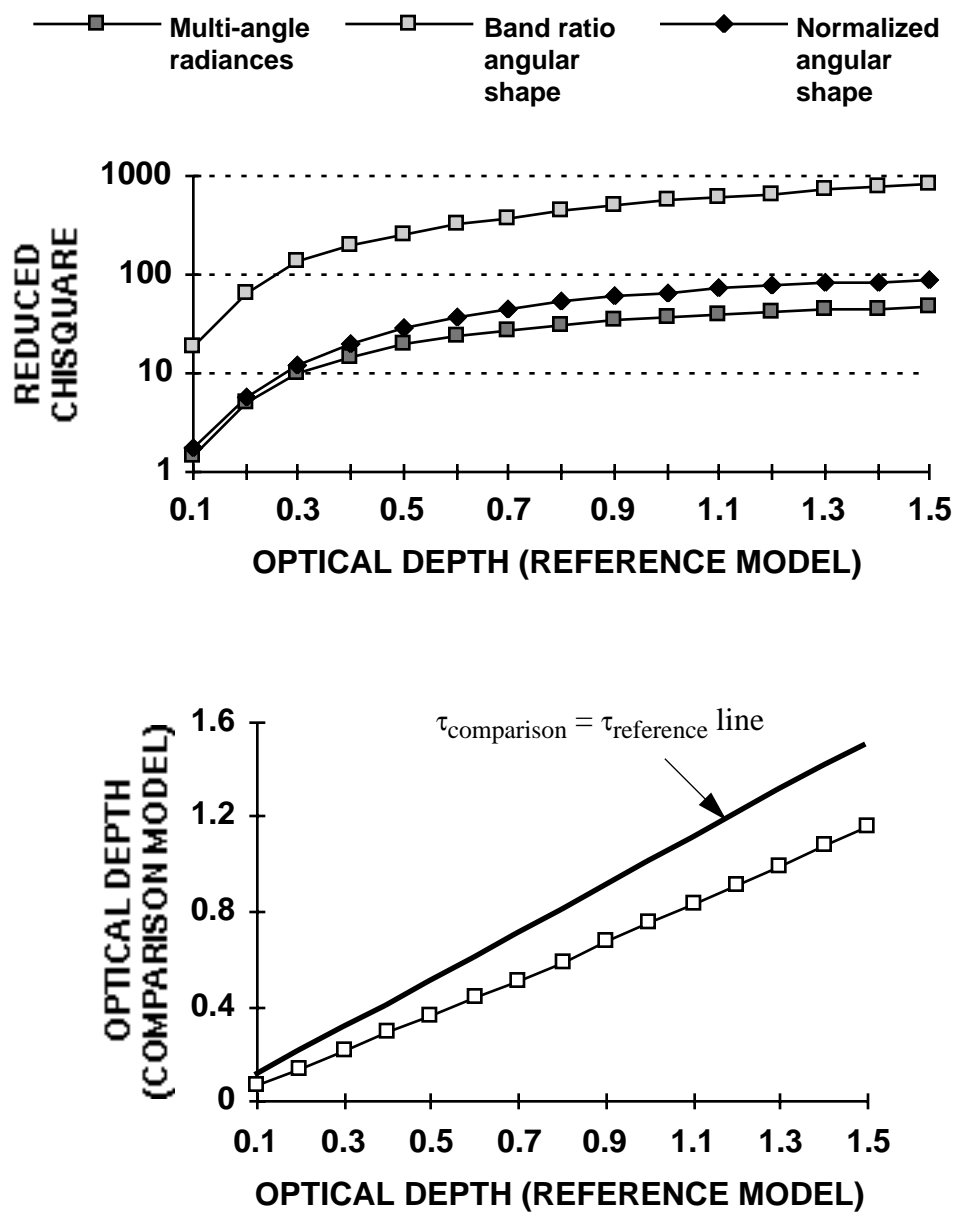**Figure 8. Distinguishability of coarse and accumulation mode sea salt aerosols**

Figure 9. Distinguishability of accumulation mode sea salt and dust aerosols

3.7.1.4   Sensitivity to particle shape

On a global scale, mineral dust makes an important contribution to the atmospheric aerosol budget. Of the major aerosol types, mineral dust is most likely to be non-spherical, non-hygroscopic, and large enough so the differences in scattering phase function can seriously affect our retrieval of aerosol optical depth. In a recent paper, Mishchenko et al. *[35]* studied the implications of assuming spherical particles in the retrieval of aerosol properties from remote sensing data, when non-spherical particles are present in the atmosphere. They demonstrate that for observations of dust-like aerosols over ocean, if a retrieval of total column optical depth is performed based on an assumption of spherical particles when in fact the particles are non-spherical, the results can be seriously in error. For the cases studied, the systematic error in total column optical depth is very sensitive to the geometry of the observation, and can be arbitrarily large, when simulated satellite measurements at a single view angle and single wavelength are used in the retrieval, even assuming noiseless data. The systematic errors demonstrated in *[35]* are unacceptably large for climate change studies.

To examine MISR's ability to distinguish between spherical and non-spherical aerosols, a sensitivity study was performed using single scattering phase functions and albedos for spherical and non-spherical particles similar to those generated by Mishchenko et al. *[35]*, *[36]*. The non-spherical particles were modeled as a mixture of polydisperse prolate and oblate spheroids with a uniform distribution of aspect ratios ranging between 1.4 and 2.2. Both spherical and non-spherical particle sizes were given by power law distributions, with $n(r) = C$ for $r \leq r_1$, $n(r) = C(r/r_1)^{-3}$ for $r_1 \leq r < r_2$, and $n(r) = 0$ for $r \geq r_2$. Here r is the particle radius for spherical particles and the radius of a sphere with equal surface area for non-spherical particles. C is a normalization constant for the distribution. The parameters r_1 and r_2 are selected so that the cross-section mean weighted radius of the distribution as a whole is r_{eff}, and the variance of the distribution is v_{eff} *[34]*. For all cases, v_{eff} is 0.2 and the particle index of refraction is 1.53 - 0.008i (representative of Sahara dust aerosol samples), independent of wavelength. The wavelength dependence of single scattering properties scales as $x = 2\pi r/\lambda$, and λ is the wavelength *[16]*. Simulations were performed for an atmosphere containing non-spherical particles with r_{eff} values of 0.1, 0.5, 1.0, and 2.0 μm, and optical depths of 0.05, 0.2, and 0.8.

The parameter χ^2_{geom} [see Eq. (62)] was then calculated for comparison models that assume distributions of spherical particles with column optical depth ranging from 0.05 to 1.0 in increments of 0.05, and effective radii ranging from 0.1 to 2.0 μm, in increments of 0.1. The results show that the χ^2_{geom} criterion is able to distinguish spherical from non-spherical particles for all cases chosen, except when the atmospheric particles are very small and the optical depth is low. We expect no discrimination for very small particles, since the corresponding spherical and non-spherical single scattering phase functions are indistinguishable. However, even for the very small particle case, the χ^2_{geom} criterion results in correct retrieval of effective particle radius, and optical depths within 0.05 of the correct values.

The optical depth uncertainty was within 0.05 for small and 10% for larger particle sizes, but is close to 50% using χ^2_{geom} alone. Also using χ^2_{abs} [see Eq. (61)] increased the retrieval sensitivity to optical depth to 10% or better over the entire parameter space. Combining the tests also improved slightly the retrieval sensitivity to particle size for larger particles. Size discrimination is poorest for low optical depth. Very similar results in terms of sensitivity to both optical depth and particle size were obtained at scattering geometries corresponding to high and low latitudes.

The conclusion of these simulations is that MISR measurements can distinguish spherical from non-spherical particles over calm dark water for mineral-dust-like particles the range of sizes and column amounts expected under natural conditions. In addition, column optical depth for non-spherical particles is retrievable to an accuracy of 0.05 or 10%, whichever is larger. Finally, three to four distinct size groups between 0.1 and 2.0 µm effective radius can be identified at latitudes greater than about 20° from the subsolar latitude. Further details are provided in Kahn et al. *[18]*.

3.7.2 Dense dark vegetation surfaces

The technique for retrieval of aerosol properties over dense dark vegetation (DDV) is described in §3.5.5.2.2. To test how well the algorithm can be expected to perform, a sensitivity study was done using simulated MISR datasets in which the atmospheric aerosol varied with both amount and type. The DDV detection algorithm, described in §3.4.2.2, was also exercised using the same datasets and the results used as input to the aerosol retrieval algorithm.

The aerosol type used to simulate the MISR measurements was Sulfate1 at RH 70%, a model contained in the Aerosol Physical and Optical Properties (APOP) file of the Aerosol Climatology Product (ACP). Three aerosol amounts were considered, characterized by optical depths of 0.1, 0.25, and 0.5 in MISR band 2 (green). The sun zenith angles were set at 25°, 45°, and 65° and the azimuth angles of the MISR views were set at values which are typical for that sun geometry. Eleven different surface types were used with directional reflectance properties based on field measurements (*[21], [22], [23]*). The multiple scattering calculations were performed using a matrix operator technique *[13]* where Rayleigh scattering was included in addition to the aerosol scattering and the bidirectional reflectance of the various surface types and all orders of surface-atmosphere reflections were taken into account. In Table 7 the surface types are listed along with their NDVI in the nadir view and the extrapolated NDVI for the case where the atmosphere is absent and also the extrapolated NDVI for the three aerosol amounts. The particular sun angle for Table 7 is 45°. Note that for those cases which are classified as DDV (extrapolated NDVI ≥ 0.75; therefore, cases 5, 6, 7, 8, and 10), the extrapolated NDVI (no atmosphere) is generally larger than the nadir view NDVI (no atmosphere), due to decreasing NDVI with increasing view angle. For the DDV cases the extrapolated NDVI (variable aerosol amount) is also quite consistent with the extrapolated NDVI (no atmosphere), illustrating the use of the extrapolated NDVI as an accurate indicator of DDV targets when aerosol is present. As input to the aerosol retrieval algorithm, the identified DDV target radiances are then averaged for both MISR bands 1 (blue) and 3 (red).

Table 7: Surface Type NDVI

Case	Surface Type	nadir NDVI no atmo.	extrap. NDVI no atmo.	extrap. NDVI $\tau_{aer} = 0.10$	extrap. NDVI $\tau_{aer} = 0.25$	extrap. NDVI $\tau_{aer} = 0.50$
1	Soil	0.088	0.089	0.122	0.133	0.128
2	Grassland	0.133	0.130	0.141	0.154	0.166
3	Steppe Grass	0.153	0.105	0.136	0.163	0.189
4	Hard Wheat	0.179	0.067	0.099	0.133	0.172
5	Irrigated Wheat	0.784	0.796	0.771	0.793	0.801
6	Hardwood forest	0.867	0.932	0.936	0.970	0.970
7	Pine Forest	0.782	0.862	0.864	0.893	0.872
8	Lawn Grass	0.763	0.777	0.750	0.772	0.775
9	Corn	0.520	0.439	0.464	0.508	0.539
10	Soybeans	0.896	0.946	0.949	0.981	1.000
11	Orchard Grass	0.555	0.511	0.534	0.576	0.589

In the aerosol retrieval sensitivity study the candidate aerosol models included the correct Sulfate1 at RH 70% model along with a selection of other aerosol possibilities, also contained in the APOP file. These additional models included Sulfate1 at RH 90%, Sea Salt (accumulation mode) at RH 70%, and Mineral Dust (both small and large particles). Using the averaged blue and red DDV radiances from the DDV detection algorithm, the aerosol retrieval results for the sun angle case of 45° are shown in Table 8. From the criteria that χ^2_{abs}, χ^2_{geom}, and χ^2_{spec} must each be less than or equal to 2 as an acceptable fit to the observations, both the correct aerosol type (RH 70% Sulfate1) and its heavily hydrated form (RH 90% Sulfate1) fulfill these conditions for the optical depth cases of 0.10 and 0.25, and only the correct aerosol type for the optical depth case of 0.5. In addition the correct aerosol type also produces a good retrieval of the optical depth for all optical depth cases. For the cases where the RH 90% Sulfate is acceptable, however, the corresponding retrieved optical depths are consistently larger by about 50% than the correct values. This emphasizes the fact that a reasonably correct aerosol model must be used if the correct optical depth is to be retrieved. Retrieval results of the DDV algorithm for the other sun angles and for a wider range of aerosol models can be found in Martonchik et al. *[32]*.

Table 8: DDV Aerosol Retrieval Summary

$\theta_0 = 45°$	Sulfate RH = 70% $\bar{r} = 0.10\ \mu m$	Sulfate RH = 90% $\bar{r} = 0.15\ \mu m$	Sea Salt RH = 70% $\bar{r} = 0.44\ \mu m$	Mineral Dust $\bar{r} = 0.1\ \mu m$	Mineral Dust $\bar{r} = 1.0\ \mu m$
Sulfate RH = 70% $\tau = 0.10$	$\tau = .10 \pm .04$ $\chi^2_{abs} = 0.4$ $\chi^2_{geom} = 1.8$ $\chi^2_{spec} = 0.9$	$\tau = .16 \pm .07$ $\chi^2_{abs} = 0.5$ $\chi^2_{geom} = 2.0$ $\chi^2_{spec} = 1.1$	$\tau = .11 \pm .07$ $\chi^2_{abs} = 1.2$ $\chi^2_{geom} = 5.9$ $\chi^2_{spec} = 4.5$	$\tau = .17 \pm .08$ $\chi^2_{abs} = 0.7$ $\chi^2_{geom} = 2.4$ $\chi^2_{spec} = 4.6$	$\tau = .37 \pm .20$ $\chi^2_{abs} = 2.3$ $\chi^2_{geom} = 7.6$ $\chi^2_{spec} = 112$
Sulfate RH = 70% $\tau = 0.25$	$\tau = .25 \pm .05$ $\chi^2_{abs} = 0.3$ $\chi^2_{geom} = 1.0$ $\chi^2_{spec} = 0.8$	$\tau = .36 \pm .08$ $\chi^2_{abs} = 0.5$ $\chi^2_{geom} = 1.6$ $\chi^2_{spec} = 1.6$	$\tau = .27 \pm .05$ $\chi^2_{abs} = 2.7$ $\chi^2_{geom} = 16.2$ $\chi^2_{spec} = 144$	$\tau = .36 \pm .07$ $\chi^2_{abs} = 2.3$ $\chi^2_{geom} = 6.3$ $\chi^2_{spec} = 320$	$\tau = .00 \pm 2.0$ $\chi^2_{abs} = 36.1$ $\chi^2_{geom} = 58.5$ $\chi^2_{spec} = 5.1$
Sulfate RH = 70% $\tau = 0.50$	$\tau = .49 \pm .07$ $\chi^2_{abs} = 0.2$ $\chi^2_{geom} = 1.4$ $\chi^2_{spec} = 1.3$	$\tau = .71 \pm .07$ $\chi^2_{abs} = 0.6$ $\chi^2_{geom} = 1.1$ $\chi^2_{spec} = 28.9$	$\tau = .40 \pm 2.0$ $\chi^2_{abs} = 46.0$ $\chi^2_{geom} = 24.5$ $\chi^2_{spec} = 130$	$\tau = .80 \pm 2.0$ $\chi^2_{abs} = 22.2$ $\chi^2_{geom} = 35.9$ $\chi^2_{spec} = 45.5$	$\tau = .00 \pm 2.0$ $\chi^2_{abs} = 254$ $\chi^2_{geom} = 102$ $\chi^2_{spec} = 8.4$

3.7.3 Heterogeneous land surfaces

The algorithm for retrieval of aerosol properties over heterogeneous land is described in §3.5.5.2.3. A sensitivity study, similar to that for the DDV algorithm, was performed for the same atmospheric conditions, surface BRF types, and sun geometries. However, a scene of the Wind River Basin in Wyoming from Landsat imagery was used to simulate MISR multiangle imagery. Two limiting cases relating pixel brightness to BRF type were considered. One case (random) had randomly assigned BRF types (from the list of eleven types) to the pixels in the scene. The other case (correlated) assigned a particular BRF type to a pixel, depending on the pixel brightness. It is expected that a real scene would exhibit albedo-BRF characteristics which fall somewhere within these limiting cases. Each MISR camera view image was 256x256 pixels in size which were subsequently subdivided into 16x16 subimages, each 16x16 pixels in size. Each of these resulting 256 multiangle subimages were then analyzed using the heterogeneous land retrieval algorithm. For the

random surface property case, an aerosol optical depth of 0.5 and a sun angle of 45°, the set of eigenvalues for a typical subimage are listed in Table 9.

Table 9: Subimage Eigenvalues

1	2	3	4	5	6	7	8	9
5.84E-1	1.56E-1	5.25E-2	3.93E-4	1.23E-4	8.53E-5	8.22E-5	6.98E-5	6.40E-5

The criterion for selecting the number of eigenvectors to be use in the analysis of a given sub-image is described in Eq. (75). For the eigenvalues in Table 9, the number of eigenvectors is five and for the other associated 255 subimages, the number of eigenvectors ranged from three to six. The results of the subsequent retrieval for a sun angle of 45° is shown in Table 10 where the optical depths τ and χ^2_{hetero} are averages of the 256 subimages. Applying the criterion that χ^2_{hetero} be less than or equal to 3 as an acceptable fit to the observations, the results are similar to those for the DDV algorithm. Again, the results of a more complete study can be found in Martonchik et al. *[32]*.

Table 10: EOF Aerosol Retrieval Summary

$\theta_0 = 45°$	Sulfate RH = 70% $\bar{\bar{r}} = 0.10$ μm	Sulfate RH=90% $\bar{\bar{r}} = 0.15$ μm	Sea Salt RH=70% $\bar{\bar{r}} = 0.44$ μm	Mineral Dust $\bar{\bar{r}} = 0.1$ μm	Mineral Dust $\bar{\bar{r}} = 1.0$ μm
Sulfate RH = 70% $\tau = 0.10$	$\tau = .11 \pm .04$ $\chi^2_{hetero} = 1.4$	$\tau = .14 \pm .05$ $\chi^2_{hetero} = 1.2$	$\tau = .06 \pm .04$ $\chi^2_{hetero} = 3.9$	$\tau = .14 \pm .04$ $\chi^2_{hetero} = 2.9$	$\tau = .30 \pm .09$ $\chi^2_{hetero} = 3.9$
Sulfate RH = 70% $\tau = 0.25$	$\tau = .26 \pm .03$ $\chi^2_{hetero} = 1.0$	$\tau = .33 \pm .04$ $\chi^2_{hetero} = 2.1$	$\tau = .16 \pm .04$ $\chi^2_{hetero} = 21$	$\tau = .37 \pm .07$ $\chi^2_{hetero} = 8.7$	$\tau = .31 \pm .11$ $\chi^2_{hetero} = 19$
Sulfate RH = 70% $\tau = 0.50$	$\tau = .51 \pm .04$ $\chi^2_{hetero} = 1.6$	$\tau = .64 \pm .04$ $\chi^2_{hetero} = 12$	$\tau = .40 \pm .08$ $\chi^2_{hetero} = 140$	$\tau = .76 \pm .14$ $\chi^2_{hetero} = 67$	$\tau = .93 \pm .18$ $\chi^2_{hetero} = 322$

A rigorous sensitivity analysis for the heterogeneous land surface retrieval algorithm is difficult to make due to the wide range of surface boundary conditions that occur naturally. An evaluation of the uncertainties to be expected over land surfaces can alternatively be obtained using

case studies. We present here a case study involving data from the Advanced Solid-state Array Spectroradiometer (ASAS) airborne multi-angle instrument *[17]*. ASAS made a series of multi-angle images of Bowman Lake in Glacier National Park on 26 February 1992. The lake is at an elevation of 1.25 km and the aircraft flew at an altitude of 4.45 km ASL with a heading of 235° from true north. The sun was in the west at a zenith angle of 63.4° and an azimuth angle of 214° from true north. Thus, the aircraft was flying into the sun, only about 20° azimuth angle off the principal plane. The 10 view angles were 70, 60, 45, 30 and 15° in the forward direction, nadir, and 15, 30, 45, 55° in the aftward direction. The images show the tip of snow and ice-covered Bowman Lake surrounded by a conifer forest. Although the data set contains 29 spectral bands, only those four bands closest to MISR bands 1 - 4 were analyzed. The averaged image signal-to-noise ratio in the middle two bands was quite good (>100) but that in the blue and near-infrared bands were markedly less due to lower detector sensitivity. Additionally, data in the near-infrared had a coherent noise problem and a large uncertainty in the instrument calibration.

Heterogeneous land aerosol retrieval algorithms were applied to the ASAS data *[29]*, *[31]*. One difference in the algorithms used to analyze the ASAS data is that the 3-D radiative transfer regime is appropriate, given the high resolution of the imagery. The aerosol retrieval results in MISR bands 1 - 3 are shown in Figure 10 for two techniques, one similar to that described in §3.5.5.2.3 and the other designed to identify pixels in the ASAS imagery with similar angular shapes. For this case study, an aerosol type was assumed and only the optical depth was retrieved. The aerosol was assumed to be clean-continental, composed mainly of water soluble sulfates and nitrates and a minute part of dust *[2]*. Both techniques give essentially the same optical depth results, about 0.03 in the green band with an uncertainty of about ±0.01. The low optical depth retrieved is consistent with the low radiances observed in the darkest pixels of the image set.

Using the same set of ASAS data, the band-differenced aerosol optical depth $\Delta\tau_{aerosol}$ was also retrieved using the algorithm described in §3.4.3.2 *[6]*. The reference wavelength was taken to be the green band and values for $\Delta\tau_{aerosol}$ were obtained in the blue and red relative to the reference wavelength. These values were determined by retrieving the total column spectral optical depth difference, given by $\Delta\tau_{aerosol} + \Delta\tau_{Rayleigh}$, then subtracting the Rayleigh contribution which was calculated using its well-known spectral dependence, assuming a standard atmosphere, and taking into account the terrain and aircraft altitudes. The retrieved values, using the method of establishing uncertainty as provided in the algorithm description, are $\Delta\tau_{aerosol}$(blue - green) = 0.014 ± 0.029 and $\Delta\tau_{aerosol}$(red - green) = -0.028 ± 0.013. The small values of $\Delta\tau_{aerosol}$ indicate either that the aerosol is spectrally "gray", or that its optical depth is low. This result is consistent with the conclusions obtained from independent application of the EOF algorithms, as described above. For further discussion, see Martonchik *[31]*.
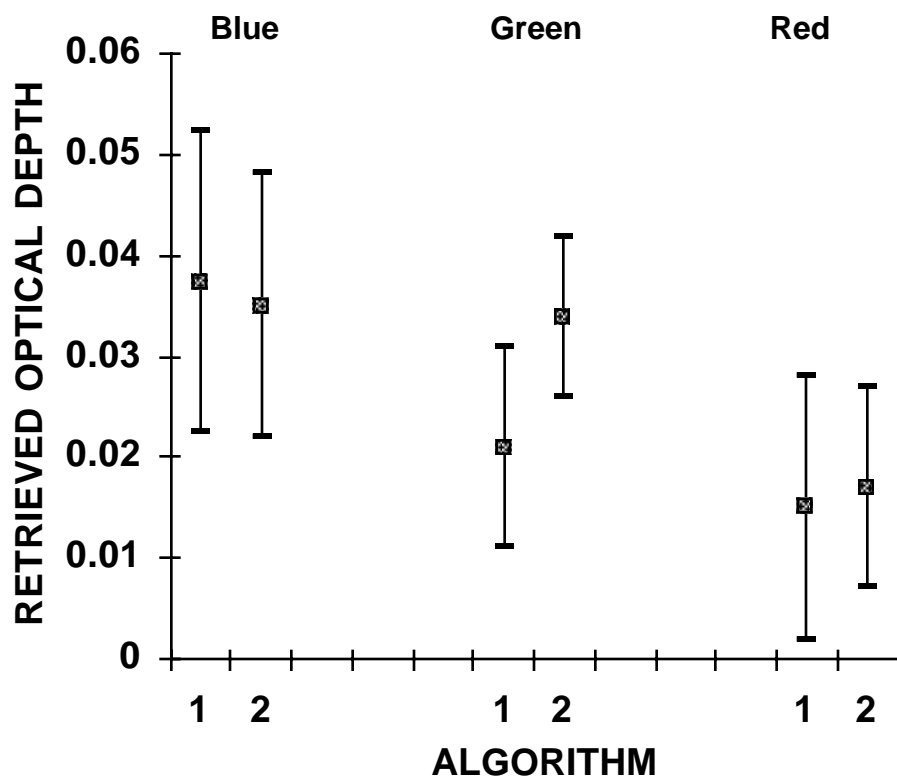
Figure 10. Optical depth retrievals using ASAS data and two EOF algorithms

3.8   ALGORITHM VALIDATION

Validation of the aerosol retrieval algorithms will rely on several sources of data including aircraft observations, together with field observations of downwelling diffuse sky spectral radiance and irradiance, the direct solar irradiance component and the surface spectral bidirectional reflectance factor (BRF).

In contrast to MISR or aircraft observations of the upwelling radiation field at the top or middle of the atmosphere, ground-based deployments obtain downwelling measurements of sky spectral diffuse radiance and irradiance together with the directly transmitted solar irradiance. The validation approach adopted for MISR consists of comparing geophysical parameters generated using MISR algorithms adapted to use with aircraft, MISR algorithms adapted to retrievals using the downwelling radiation field at the bottom-of-the-atmosphere, and using independent algorithms on ground-based observations in order to secure ground-based estimates of aerosol spectral optical depth, effective size distribution, phase function, and single scattering albedo. Thus, retrievals will be carried out, where applicable, both by forward calculations with radiative transfer models based on the MISR Aerosol Climatology Product, and according to formal inversion procedures involving the governing integral equations.

Details on planned field campaigns, experimental methodologies, and instrument calibration and data reduction procedures are documented in *[M-15]*. In addition, *[M-12]* provides the theoretical basis behind the algorithms to be used as part of the validation activity. For this information, the reader is referred to those sources.

4. ASSUMPTIONS AND LIMITATIONS

4.1 ASSUMPTIONS

The following assumptions are made with respect to the aerosol retrievals described in this document:

(1) Hydrated aerosol particles are modeled as homogenous spheres.

(2) Nonspherical dust particles are modeled as randomly oriented prolate and oblate spheroids with a distribution of aspect ratios.

(3) Nonspherical thin cirrus particles are modeled using a fractal approach.

(4) Natural mixtures of atmospheric aerosols are homogeneous, external mixes of pure particles types contained in the ACP.

(5) The aerosol mixtures specified by the ACP span the range of natural conditions for the duration of the EOS mission.

(6) Hydration is the only effect which causes evolution of dry particle sizes.

(7) Estimates of boundary-layer relative humidity will be available and the theory relating particle properties to RH is valid.

(8) Measurements corresponding to each 17.6 km x 17.6 km region upon which an aerosol retrieval is performed are assumed to be acquired through a locally horizontally homogeneous atmosphere.

(9) The EOS Project will insure that assimilated meteorological fields from the EOS Data Assimilation Office (DAO) are available to the MISR data processing system at the DAAC in a timely fashion.

(10) Selected MODIS data will be available to the MISR data processing system at the DAAC in a timely fashion.

(11) A "standard" accumulation mode sulfate aerosol model (denoted mode 2) is sufficient to specify the single scattering properties of the stratospheric aerosol, except during extreme volcanic events.

(12) MISR bands 1, 2, and 3 are assumed to be unaffected by water vapor in the atmosphere. Water vapor column abundance will be taken into account in MISR band 4 during calculation of the SMART Dataset, using a standard atmospheric profile. The water vapor optical depth in band 4 is small enough that this procedure leads to negligible errors.

(13) Ozone column abundance will be obtained from the DAO; otherwise climatological values will be used. Corrections for ozone absorption will be made to all MISR channels.

(14) NO_2 absorption affects MISR bands 1 and 2. However, over most of the globe,

the maximum column optical depth of NO_2 is small enough (i.e., < 0.002), to be neglected.

4.2 LIMITATIONS

The following limitations apply to the at-launch aerosol retrievals described in this document:

(1) Retrievals will not be performed when the cosine of the solar zenith angle is less than 0.2.

(2) Retrievals will not be performed over topographically complex terrain.

(3) Retrievals will not include samples that are not clear of clouds.

(4) Retrievals will not include samples containing shadows due to topography or clouds.

(5) Retrievals will only be performed over regions that are dark water, DDV, or for which the spatial contrast exceeds a certain threshold.

5. REFERENCES

[1] Bevington, P.R. (1969). *Data reduction and error analysis for the physical sciences*. McGraw-Hill, Inc., 336 pp.

[2] d'Almeida, G. A., P. Koepke, and E. P. Shettle (1991). *Atmospheric Aerosols: Global climatology and radiative characteristics*. Deepak Publishing.

[3] Deering, D.W. and P. Leone (1986). A sphere-scanning radiometer for rapid directional measurements of sky and ground radiance. *Rem. Sens. Environ.* **19**, 1-24.

[4] Diner, D. J. and J. V. Martonchik (1985a). Influence of aerosol scattering on atmospheric blurring of surface features. *IEEE Trans. Geosci. and Rem. Sens.* **GE-23**, 618-624.

[5] Diner, D. J. and J. V. Martonchik (1985b). Atmospheric transmittance from spacecraft using multiple view angle imagery. *Appl. Opt.* **24**, 3503.

[6] Diner, D.J., S.R. Paradise, and J.V. Martonchik (1994). Development of an aerosol opacity retrieval algorithm for use with multi-angle land surface images. *Proceedings of the IGARSS'94 Symposium* (Pasadena, CA).

[7] Engelsen, O., B. D. Pinty, and M. M. Verstraete (1996). Parametric Bidirectional Reflectance Factor (BRF) models: I. Evaluation. Internal report, Institute for Remote Sensing Applications, Joint Research Centre, Ispra, Italy.

[8] Fraser, R. S. (1976). Satellite measurement of mass of Sahara dust in the atmosphere. *Appl. Opt.* **15**, 2471.

[9] Gordon, H. R. and D. K. Clark (1981). Clear water radiances for atmospheric correction of Coastal Zone Color Scanner imagery. *Appl. Opt.* **20**, 4175.

[10] Gordon H. R. (1984). Some studies of atmospheric optical variability in relation to CZCS atmospheric correction (NOAA National Environmental Satellite and Data Information Service, Final Report Contract No. NA-79-SAC-00714).

[11] Gordon, H. R. (1994). Presentation to the MISR Science Team, Pasadena, CA, March.

[12] Govaerts, Y. and M. M. Verstraete (1994). Applications of the L-systems to canopy reflectance modelling in a Monte Carlo Ray Tracing technique. In *Multispectral and Microwave Sensing of Forestry, Hydrology, and Natural Resources*, SPIE, Rome.

[13] Grant, I.P. and G.E. Hunt (1968). Solution of radiative transfer problems using the invariant S_n method. *Mon. Not. Roy. Astron. Soc.* **141**, 27-41.

[14] Griggs, M. (1975). Measurements of atmospheric aerosol optical thickness over water using ERTS-1 data. *J. Air Pollut. Control Assoc.* **25**, 622.

[15] Griggs, M. (1983). Satellite measurements of tropospheric aerosols. *Adv. Space Res.* **2**, 109.

[16] Hansen, J.E., and L.D. Travis (1974). Light scattering in planetary atmospheres. *Space Sci. Rev.* **16**, 527-610.

[17] Irons, J. R., K. J. Ranson, D. L. Williams, R. R. Irish, and F. G. Huegel (1991). An off-nadir-pointing imaging spectroradiometer for terrestrial ecosystem studies. *IEEE. Trans. Geosci. Rem. Sens.* **GE-29**, 66.

[18] Kahn, R., R. West, D. McDonald, B. Rheingans, and M.I. Mishchenko (1997). Sensitivity of multi-angle remote sensing observations to aerosol sphericity. *J. Geophys. Res.* **102**, 16,861-16,870

[19] Kaufman, Y. J., and C. Sendra (1988). Algorithm for atmospheric corrections. *Int. J. Remote Sens.* **9**, 1357-1381.

[20] Kaufman, Y.J. and D.Tanre (1992). Atmospherically Resistant Vegetation Index (ARVI) for EOS-MODIS. *IEEE Trans. Geosci. Rem. Sens.* **30**, 261-270.

[21] Kimes, D. S. (1983). Dynamics of directional reflectance factor distributions for vegetation canopies. *Appl. Opt.* **22**, 1364.

[22] Kimes, D.S., W. Newcomb, C. Tucker, I. Zonneveld, W. van Wijngaarden, J. de Leeuw, and G. Epema (1985). Directional reflectance factor distributions for cover types of northern Africa in NOAA 7/8 AVHRR bands 1 and 2. *Rem. Sens. Environ.* **18**, 1-19.

[23] Kimes, D. S., W. W. Newcomb, R. F. Nelson, and J. B. Schutt (1986). Directional reflectance distributions of a hardwood and pine forest canopy. *IEEE Trans. Geosci. Rem. Sens.* **GE-24**, 281.

[24] Kimes, D.S. and W.W. Newcomb (1987). Directional scattering properties of a wintering deciduous hardwood canopy. *IEEE Trans. Geosci. Rem. Sens.* **25**, 510-515.

[25] King, M. D., Y. J. Kaufman, W. P. Menzel, and D. Tanre (1992). Remote sensing of cloud, aerosol, and water vapor properties from the Moderate resolution Imaging Spectrometer (MODIS). *IEEE Trans. Geosci. Remote Sens.* **30**, 2-27.

[26] Krekov, G. M. (1993). Models of atmospheric aerosols, in *Aerosol Effects on Climate*, S. G. Jennings, ed., University of Arizona Press, 304 pp.

[27] Long, C. S., and L. L. Stowe (1993). Using the NOAA/AVHRR to study stratospheric aerosol optical thickness following the Mt. Pinatubo eruption. *Geophys. Res. Lett.*, submitted.

[28] Martonchik, J. V., and D. J. Diner (1992). Retrieval of aerosol optical properties from multi-angle satellite imagery. *IEEE Trans. Geosci. Rem. Sens.* **GE-30**, 223.

[29] Martonchik, J.V. and J.E. Conel (1994). Retrieval of surface reflectance and atmospheric properties using ASAS imagery. *Proceedings of the IGARSS'94 Symposium* (Pasadena, CA).

[30] Martonchik, J.V. (1995). Atmospheric correction of vegetation index using multi-angle measurements. *Proceedings of the IGARSS'95 Symposium* (Firenze, Italy).

[31] Martonchik, J.V. (1996). Determination of aerosol optical depth and land surface directional reflectances using multi-angle imagery. Submitted to *J. Geophys. Res.*

[32] Martonchik, J.V., D.J. Diner, R. Kahn, M. M. Verstraete, B. Pinty, H. Gordon, and T. Ackerman (1998). Techniques for retrieval of aerosol properties over land and ocean using multi-angle imagery. *IEEE Trans. Geosci. Rem. Sens.* In preparation.

[33] Minnis, P., P.W. Heck, and D.F. Young (1993). Inference of cirrus cloud properties using satellite-observed visible and Infrared radiances. Part II: Verification of theoretical cirrus radiative properties. *J. Atmos. Sci.* **50**, 1305-1322.

[34] Mishchenko, M.I., and L.D. Travis (1994). Light scattering by polydisperse, rotationally symmetric nonspherical particles: Linear polarization. *J. Quant. Spectrosc. Radiat. Transfer* **51**, 759-778.

[35] Mishchenko, M.I., A.A. Lacis, B.E. Carlson, and L.D. Travis (1995). Nonsphericity of dust-like tropospheric aerosols: Implications for aerosol remote sensing and climate modeling, *Geophys. Res. Lett.* **22**, 1077-1080.

[36] Mishchenko, M.I., L.D. Travis, R.A. Kahn, and R.A. West (1997). Modeling phase functions for dust-like tropospheric aerosols using a shape mixture of randomly oriented polydisperse spheroids. *J. Geophys. Res.* **102**, 16,831-16,847

[37] Mishchenko, M. I., W. B. Rossow, A. Mache, and A. Lacis (1996). Sensitivity of cirrus cloud albedo, bidirectional reflectance, and optical thickness retrieval accuracy to ice particle shape. *J. Geophys. Res.* **101**, 16,973-16,985.

[38] Myneni, R.B. and G. Asrar (1993). Radiative transfer in three-dimensional atmosphere-vegetation media. *J. Quant. Spectrosc. Radiat. Transfer* **49**, 585-598.

[39] Nicodemus, F. E., J. C. Richmond, J. J. Hsia, I. W. Ginsberg, and T. Limperis (1977).

Geometrical Considerations and Nomenclature for Reflectance, NBS Monograph **160**, National Bureau of Standards, U.S. Department of Commerce, Washington, D.C.

[40] Pinty, B. and M. M. Verstraete (1992). GEMI: A non-linear index to monitor global vegetation from satellites. *Vegetatio* **101**, 15-20.

[41] Preisendorfer, R.W. (1988). *Principal component analysis is meteorology and ocean-ography*. Elsevier, NY, 425 pp.

[42] Rao, C. R. N., L. L. Stowe, and E. P. McClain (1989). Remote sensing of aerosols over the oceans using AVHRR data: Theory, practice and applications. *Int. J. Remote Sensing* **10**, 743.

[43] Rahman, H., B.Pinty, and M.M. Verstraete (1993). Coupled Surface-Atmosphere Reflectance (CSAR) model. 2. Semiempirical surface model usable with NOAA Advanced Very High Resolution Radiometer data. *J. Geophys. Res.* **98**, 20,791-20,801.

[44] Sassen, K., D. Starr, and T. Uttal (1989). Mesoscale and microscale structure of cirrus clouds: Three case studies. *J. Atmos. Sci.* **46**, 371-396.

[45] Shettle, E.P., and R.W. Fenn, (1979). Models for the aerosols of the lower atmosphere and the effects of humidity variations on their optical properties. AFGL-TR-79-0214, Air Force Geophysics Laboratory, pp. 94.

[46] Stowe, L. L., R. M. Carey, and P. P. Pellegrino (1992). Monitoring the Mt. Pinatubo aerosol layer with NOAA/11 AVHRR data. *Geophys. Res. Lett.* **19**, 159-162.

[47] Stowe, L.L., A.M. Ignatov, and R.R. Singh (1997). Development, validation, and potential enhancements to the second-generation operational aerosol product. *J. Geophys. Res.* **102**, 16,923-16,934.

[48] Takano, Y., and K-N Liou (1989). Solar radiative transfer in cirrus clouds. Part I: Single-scattering properties of hexagonal ice crystals. *J. Atmos. Sci.* **46**, 3-19.

[49] Verstraete, M. M., B. Pinty, and R.E. Dickinson (1990). A physical model of the bidirectional reflectance of vegetation canopies. 1. Theory. *J. Geophys. Res.* **95**, 11,775-11,765.

[50] Wang, M. and H. R. Gordon (1994). Estimating aerosol optical properties over the oceans with MISR: Some preliminary studies. *Appl. Opt.* **33**, 4042-4057.

[51] Williamson, S. J. (1972). *Fundamentals of Air Pollution*. Addison-Wesley, MA.

[52] World Meteorological Organization (WMO) (1988). Report of the International Ozone Trends Panel, Global Ozone Research and Monitoring Project -- Report No. 18.

[53] World Climate Programme WCP-112 (1984). A Preliminary Cloudless Standard Atmosphere for Radiation Computation. IAMAP (International Association for Meteorology and Atmospheric Physics), Boulder, CO, pp.53.